UPRATED FINE GUIDANCE SENSOR STUDY

Kodak

ABOUT THE COVER: One of the great achievements of recent years has been the understanding that stars form in dense obscured regions of interstellar space, these regions being embedded in very much larger diffuse clouds, the giant molecular clouds. Regions such as the Rosette Nebula have been shown to be the seat of much greater activity than had been previously expected with the discovery of bipolar outflows of hot molecular hydrogen. There are many questions we do not, however, have clear answers. To help answer these questions astronomical telescopes in space with fine pointing control will be required. Pointing errors as small as a few percent of a star image diameter must be measured and corrected to prevent the resulting image motion from significantly degrading image quality.

UPRATED FINE GUIDANCE SENSOR STUDY

Final Report
Contract No. NAS8-35504

17 October 1984

prepared by

Eastman Kodak Company
U.S. Apparatus Division
901 Elmgrove Road
Rochester, New York 14650

for

George C. Marshall Space Flight Center
National Aeronautics and Space Administration
Marshall Space Flight Center, Alabama 35812

TABLE OF CONTENTS

LIST OF FIGURES

LIST OF FIGURES

LIST OF FIGURES

LIST OF FIGURES

LIST OF TABLES

1.0 INTRODUCTION

Future orbital observatories will require star trackers of extremely high precision. These new sensors must maintain high pointing accuracy and pointing stability simultaneously with a low light level signal from a guide star. The star tracking system (Fine Guidance Sensor) is one of the most demanding components of the Space Telescope. The Space Telescope must be able to track an object within a pointing stability error of 0.007 arcsecond with a time constant of much less than one second. The only way to reach this level is to use images formed by the Space Telescope itself. Rather than risk interference with the portion of the field of view being used for observation, images at the edge must be used. The Ritchey-Chretien optical design gives astigmatic images at the edge of the field of view. The tracking system must accommodate this.

Improved image quality will be a major goal for any future astronomical telescope. A traditional image quality "figure of merit" for astronomical imaging is the diameter of the point spread function. The angular subtense of this image diameter is directly proportional to the operational wavelength and inversely proportional to the diameter of the collecting aperture. For the perfect system with 84% of the energy to the first maximum of the image diameter the proportionality constant is 2.44. (This image diameter has the special name ---- Airy disk.) Therefore, improved image quality (i.e., smaller "Airy disks") will occur as future telescopes operate either at shorter wavelengths or with larger collecting diameters. Assuming a pointing stability requirement of 1/30 of the Airy disk yields the results shown in Figures 1.0-1 and Figure 1.0-2.
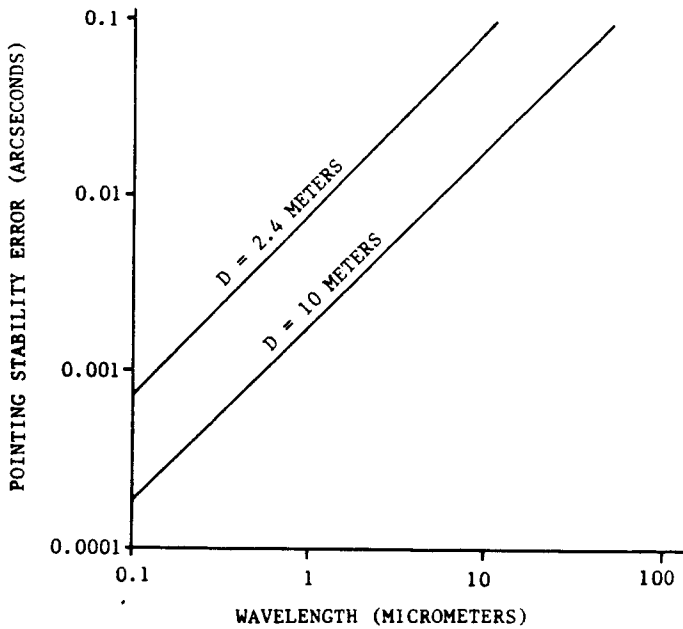
POINTING STABILITY REQUIREMENT
(AIRY DISK/30)
Figure 1.0-1
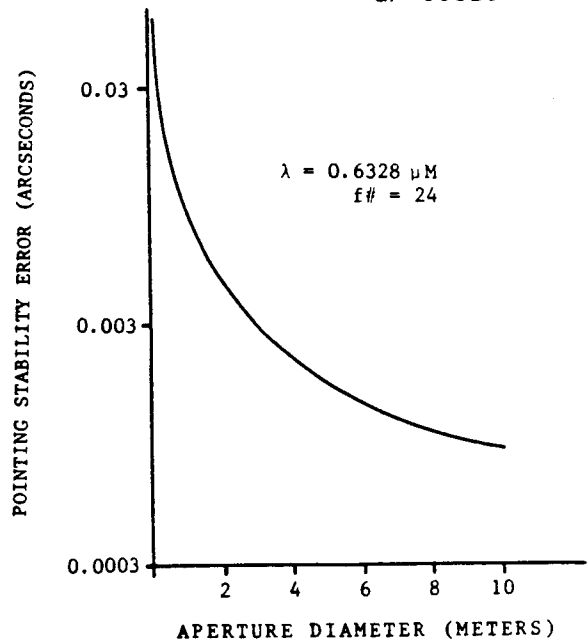
POINTING STABILITY REQUIREMENT
(AIRY DISK/30)
Figure 1.0-2

From these figures it can be seen that pointing stability errors even less than the Space Telescope value (0.007 arcsecond) will be required for future systems. Pointing errors as small as a few percent of the star image diameter must be measured and corrected to prevent the resulting image motion from significantly degrading image quality. These small pointing errors will also be required for imaging extended objects.

To illustrate this point the effect of the pointing stability error on the resolved distance on Mars and Venus using the Space Telescope Planetary Camera is shown in Figure 1.0-3.
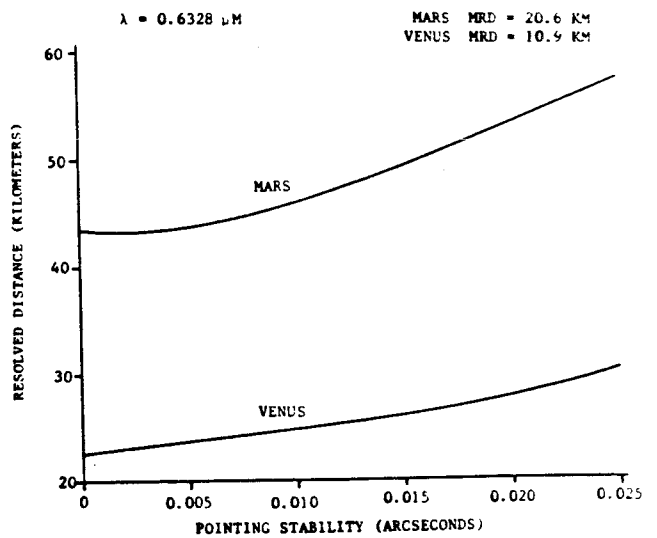
RESOLVED DISTANCE
Figure 1.0-3

Assuming a pointing stability error of 0.021 arcsecond (3X Space Telescope limit), the resolved distance on Venus would be increased to 28 kilometers from a resolved distance of 22 kilometers with no pointing stability error.

The system requirements for this study are summarized in Table 1.0-1.

Table 1.0-1
SYSTEM REQUIREMENTS
• NOISE EQUIVALENT ANGLE   0.005 SEC
• SIGNAL LEVEL $9 \leq M_v \leq 14.5$
• BANDWIDTH   40 HERTZ
• PROBABILITY OF TWO OR MORE STARS IN GUIDE FIELD AREA   85%

In addition, new approaches to off-axis stellar tracking have been investigated taking into account advances in detectors, optical fabrication, structures and control technologies. Emphasis was placed on concepts with no moving parts, high throughput efficiencies, and modularity.

2.0 REQUIREMENTS REVIEW

To establish the fine guidance sensing requirements and to evaluate candidate fine guidance sensing concepts, the Space Telescope Optical Telescope Assembly has been used as the reference optical system. Our requirements review has been separated into three areas: Optical Telescope Assembly (OTA), Fine Guidance Sensing, and Science (astrometry).

In order to first understand the fine guidance sensing problem (an angular error of 0.005 arcsecond is analogous to hitting a dime at 325 miles) a four quadrant system engineering approach was utilized. In this approach all parameters are first considered variables. Secondly, the fixed parameters are identified, thereby identifying the "real" variables. It is these variables which establish the options which can be used to solve the problem. Shown in Figure 2.0-1 is the first 4 quadrant diagram. The parameters in the 4 quadrants are guide star area, visual star magnitude, irradiance, aperture diameter, number of photons per second, integration time and the number of photons. The fixed parameters are visual star magnitude, aperture diameter and integration time. The "route-of-the-arrow" indicates the number of available photons. Shown in Figure 2.0-2 is the second 4 quadrant diagram (8 quadrants were required to completely define all the parameters). The parameters in the 4 quadrants are available photons, signal to noise ratio, subimage resolution, system focal ratio, knowledge of image location, system focal length and knowledge of line of sight error. The fixed parameters are system focal ratio and system focal length. Starting with the number of available photons from the previous 4 quadrant diagram the "route-of-the-arrow" indicates the line of sight error that could be achieved under these conditions. For this example the value is 0.015 arcsecond. This is 3 times the required value. What are the options to achieve 0.005 arcsecond? To answer this question the 4 quadrant diagrams can be used in reverse. The "route-of-the-arrow" in Figure 2.0-3 indicates more photons are needed. The "route-of-the-arrow" in Figure 2.0-4 indicates that a brighter threshold visual magnitude is required. What are the options? The

first option is to increase integration time (25 milliseconds ----▶ 500 milli-
seconds). The second option is to decrease threshold visual magnitude (14.5
M_v ----▶ 13 M_v). This can be accomplished by increasing the guide field area
(60 square arcminutes --▶ 140 square arcminutes). The third option is to
increase subimage resolution (1/30 ---▶ 1/150). The state-of-the-art in sub-
image resolution is considered to be approximately 1/50. The third option may
be difficult to implement. Therefore, the fine guidance sensing problem comes
down to the correct handling of the only "real" variables; -- integration time
and guide field area.

Many assumptions and approximations have been used in the utilization of the 4
quadrant approach. The validity of these assumptions, and approximations will
be analyzed in this section.

IRRADIANCE LEVELS OF VISUAL
MAGNITUDE STARS

GUIDE STAR AREA REQUIRED
FOR P = 0.85
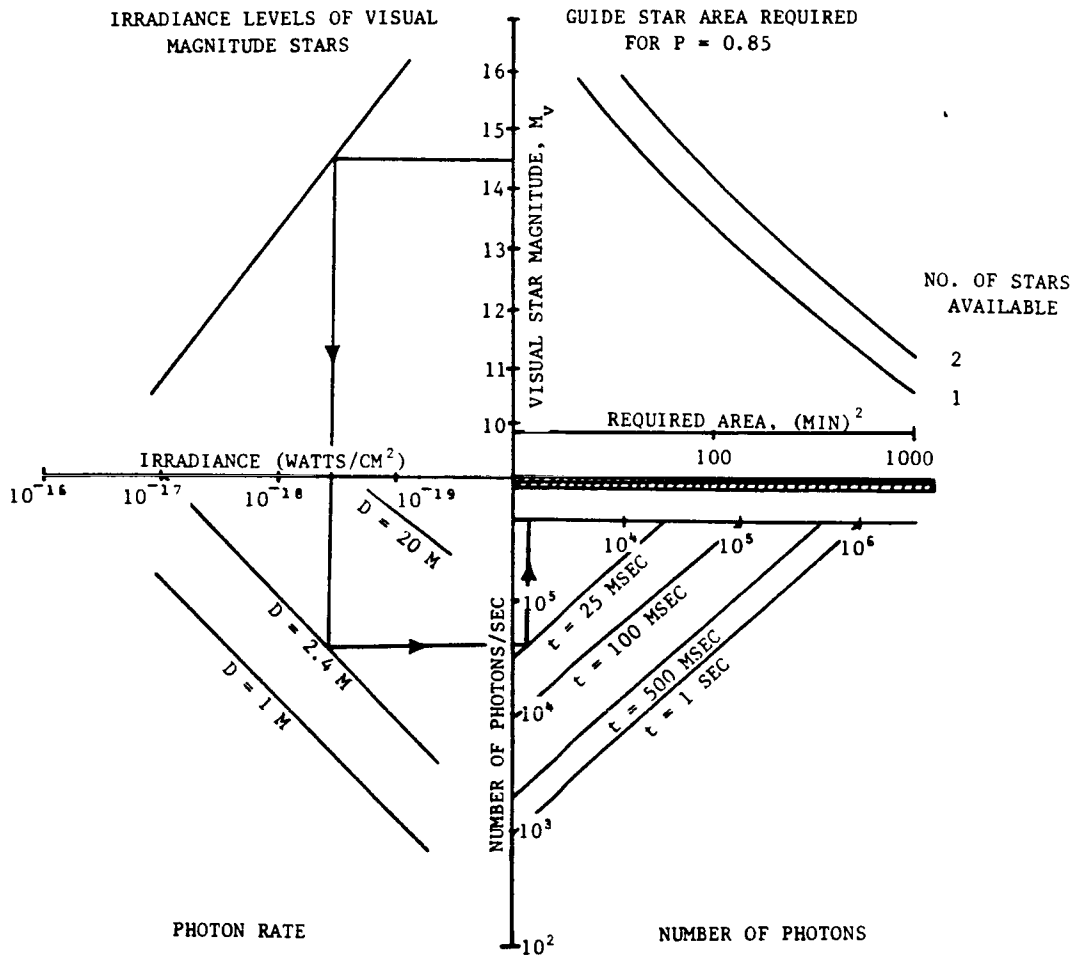
NUMBERS OF AVAILABLE PHOTONS
Figure 2.0-1

2-3
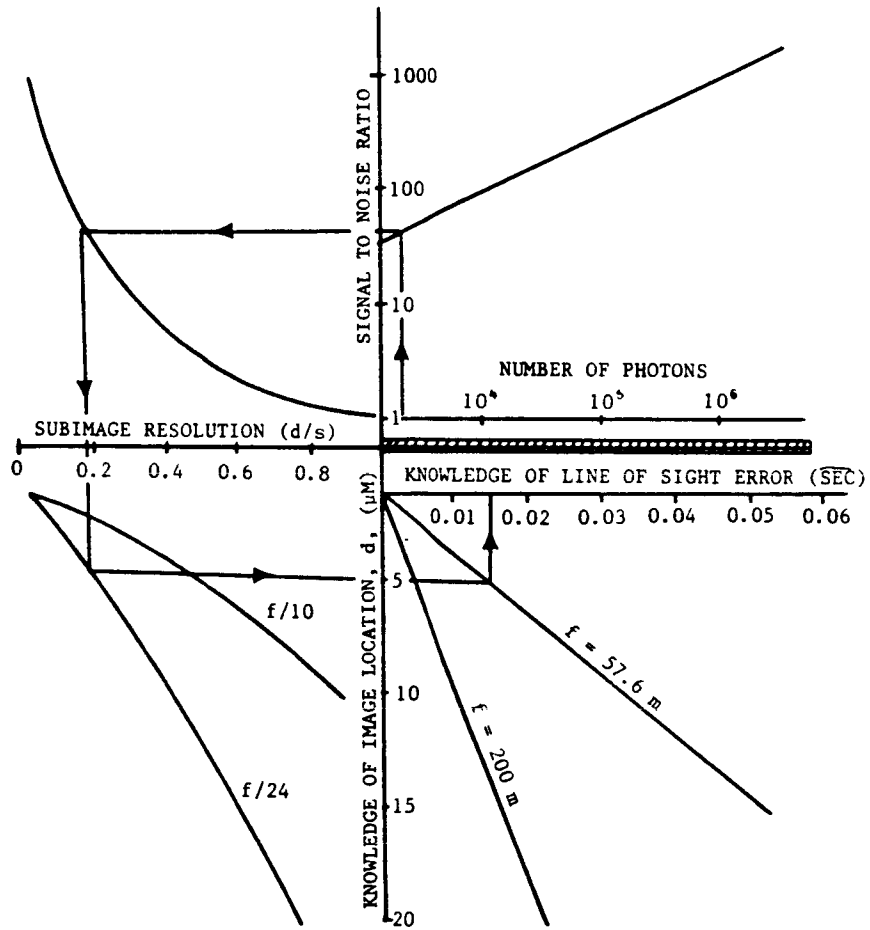
KNOWLEDGE OF LINE OF SIGHT ERROR
Figure 2.0-2
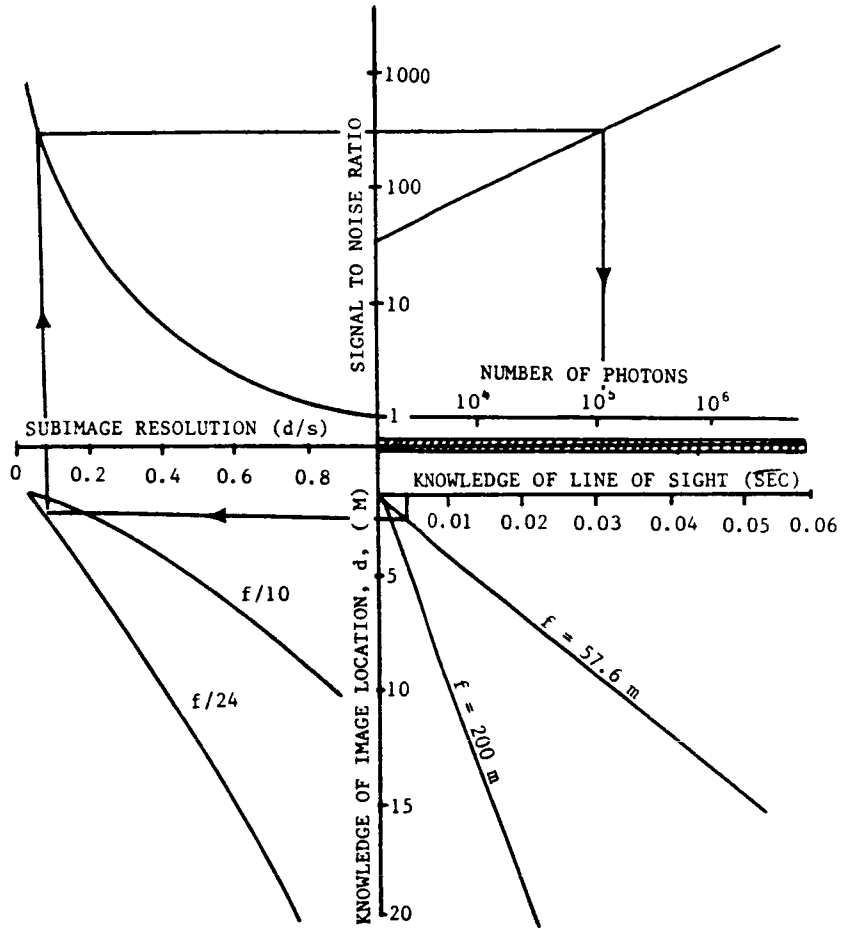
$\Delta \theta = 0.005 \ SEC \longrightarrow \dfrac{d}{s} = 0.54$

$\longrightarrow \dfrac{S}{N} = 343 \longrightarrow \boxed{N_p = 118,000}$

KNOWLEDGE OF LINE OF SIGHT ERROR
Figure 2.0-3

2-5

IRRADIANCE LEVELS OF VISUAL
MAGNITUDE STARS

GUIDE STAR AREA REQUIRED
FOR P = 0.85

$Np = 118,000; \quad t = 500 \text{ MSEC} \longrightarrow Rp = 236,000 \text{ PHOTONS/SEC}$

$\longrightarrow M_v = 13 \longrightarrow A = 140 \text{ MIN}^2$
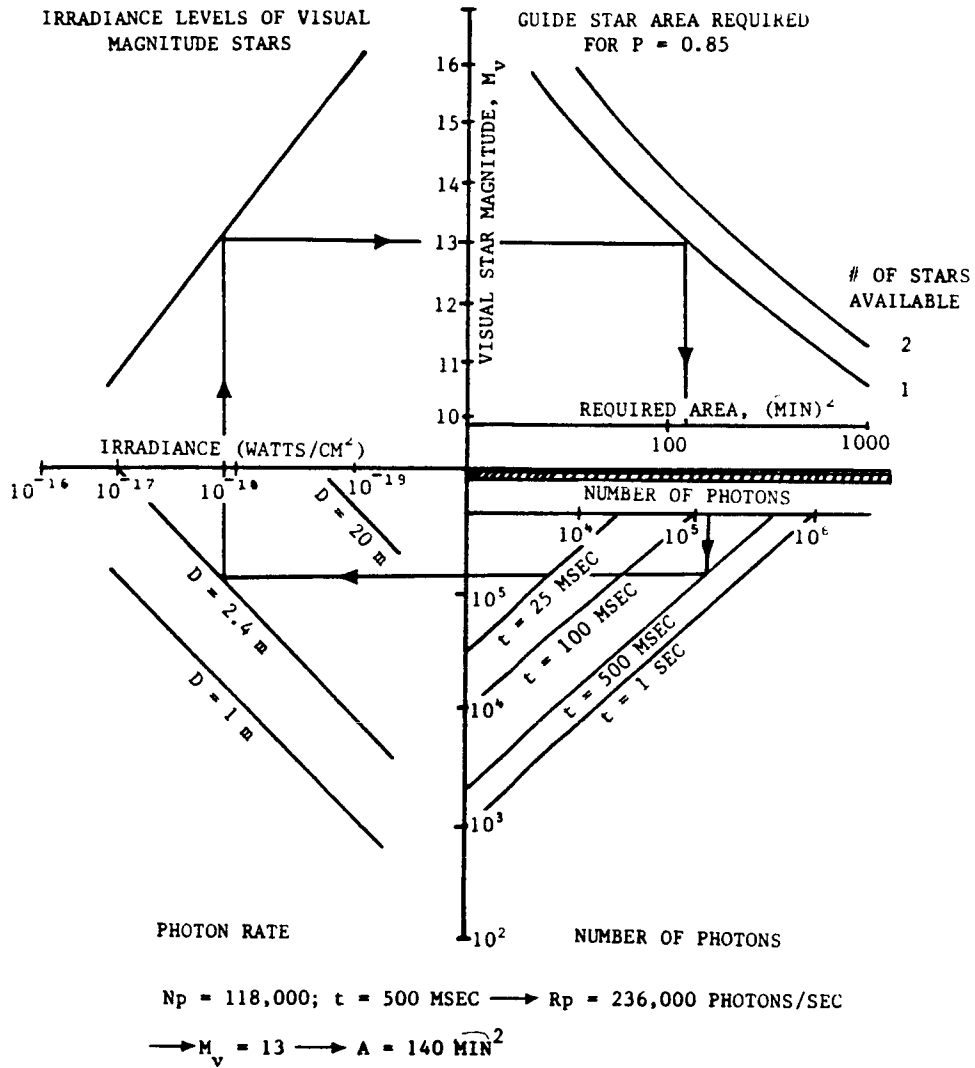
NUMBER OF AVAILABLE PHOTONS
Figure 2.0-4

2-6

2.1 OPTICAL TELESCOPE ASSEMBLY (OTA)

The OTA optical configuration is a catoptric Ritchey-Chretien version of the Cassegrain telescope (Figure 2.1-1). The configuration consists of hyperbolic primary and secondary mirrors. The conic shapes have been chosen to simultaneously correct spherical aberration and coma. The aberrations of astigmatism, field curvature, and distortion are present off-axis in predictable amounts. Field curvature and astigmatism appear as two well-defined curved focal surfaces (two concave prolate spheroids), shown in Figure 2.1-2. At a semi-field angle of 14.0 arcminutes (edge of tracking field of fine guidance sensor), the primary astigmatism is 0.6 λrms (λ = 6328 Angstroms) with a residual coma of 0.2 λrms. At a semi-field angle of 7.8 arcminutes (inside data field of axial scientific instrument) the primary astigmatism is 0.18 λ rms with a residual coma on the order of 0.002 λrms.

An optical control subsystem is provided on the OTA. Its purpose is to (1) sense the condition of primary mirror position, (2) sense the condition of secondary mirror optical axis to primary mirror optical axis alignment, (3) sense the condition of focus, (4) define the relative positions of the OTA focal surfaces mounted on the focal plane structure, (5) provide the means for primary mirror position adjustment and, (6) provide means by which alignment and focus can be adjusted.

Under orbital operational conditions for up to ten hours of observation, the optical control subsystem will be used to maintain the on-axis static wave front error to be less than 0.075 λrms. However, it is anticipated that the on-axis static wave front error should be less than 0.05 λrms. Coupled with a worst case image stability requirement of 0.007 arcsecond (overall Space Telescope), 70 percent of the encircled energy in the star image will occur in a radius of 0.1 arcsecond.

In Figure 2.1-3 is shown the designed, static, on-axis geometric mean MTF for the OTA. The geometric mean is an average of the sagittal and tangential MTF's which are independently calculated.

2-7
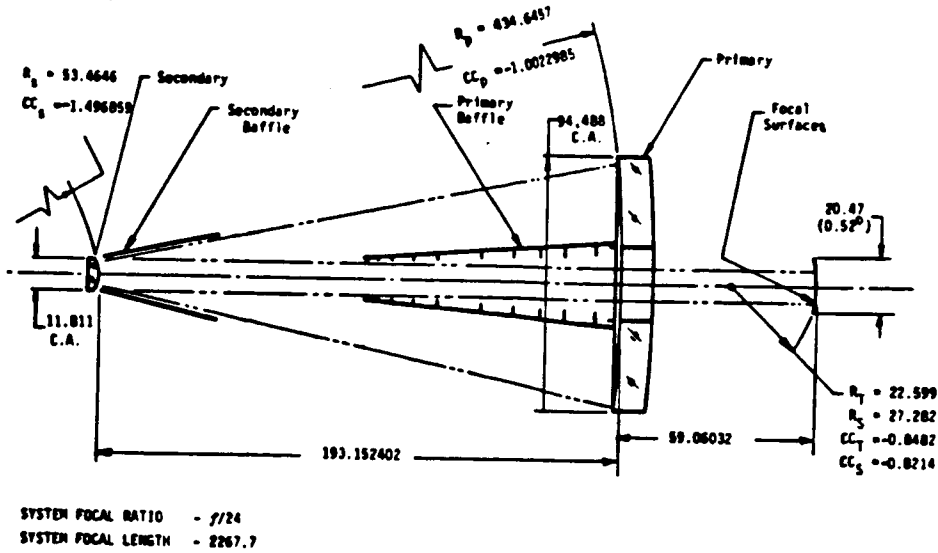
OTA OPTICAL CONFIGURATION *MARCH 1979
Figure 2.1-1

$$X_S = (1.833 \times 10^{-2}) Y^2 + (1.099 \times 10^{-6}) Y^4 + (1.318 \times 10^{-10}) Y^6 + (1.977 \times 10^{-14}) Y^8$$

$$X_T = (2.212 \times 10^{-2}) Y^2 + (1.644 \times 10^{-6}) Y^4 + (2.443 \times 10^{-10}) Y^6 + (4.539 \times 10^{-14}) Y^8$$
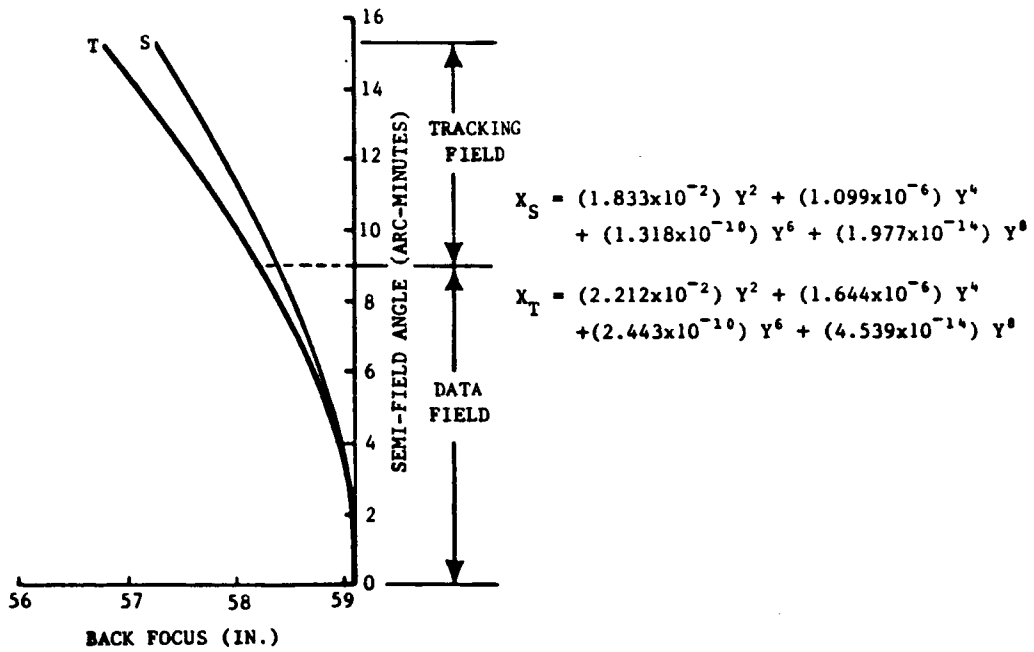
FOCAL PLANE TOPOGRAPHY
Figure 2.1-2

2-8
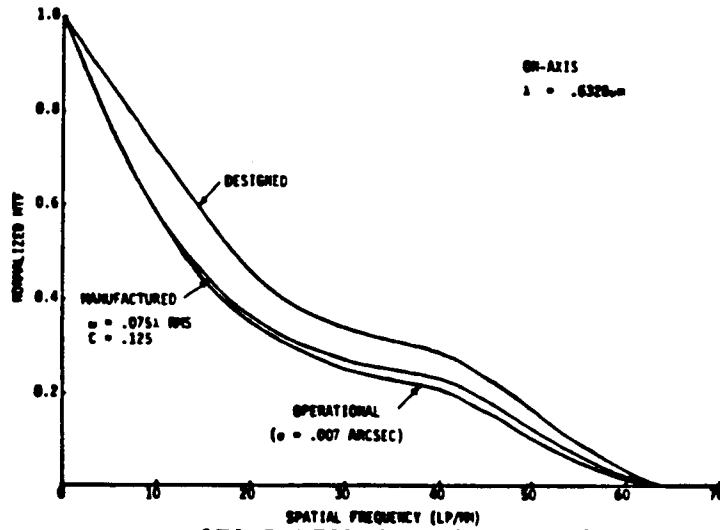
OTA PERFORMANCE PREDICTION
Figure 2.1-3

In an operational (dynamic) condition, the designed MTF will be reduced by manufacturing, alignment, and focus errors as well as pointing stability error. As noted, the OTA is designed to have an on-axis, static wave front error of no more than 0.05 λrms (λ=6328 Angstroms) with an autocorrelation length of 0.125. The predicted "manufactured" on axis, static MTF is shown in Figure 2.1-3. The overall system is designed to have a pointing stability error of no greater than 0.007 arcsecond. Also shown in Figure 2.1-3 is the predicted on-axis, operational MTF performance.

The Space Telescope is expected to make exposures on the day side of the orbit when stray light from the sun or the earth could limit the sensitivity of its instruments. Therefore, an extensive system of light shields and baffles to protect the focal surface from stray light has been specified for the OTA.

One of the principal advantages of a space telescope is that ultraviolet measurements can be made without detriment due to absorption or turbulent effects from an intervening atmosphere. (Of special astronomical interest is the Lyman Alpha line at 1215 Å.) To meet the overall wavelength requirements, a coating of aluminum with a protective overcoating of magnesium fluoride has been specified for the mirror surfaces.

2-9

2.1.1 Paraxial Evaluation of OTA Optics

The locations of optical images are calculated by paraxial ray trace equations. These equations are:

$$y_i = y_{i-1} + (nu)_{i-1} (t/n)_{i-1}$$
$$(nu)_i = (nu)_{i-1} + y_i (n_{i-1} - n_i) r_i$$

Where:

y_i = ray height on i-th surface

u_i = ray slope following i-th surface

n_i = refractive index following i-th surface

t_i = thickness between i-th surface and next surface

r_i = vertex radius of curvature of i-th surface

Thickness and index are positive (+) in the region where the ray travels from left to right and the vertex radius of curvature is positive (+) if its center of curvature lies to the right of the vertex.

2.1.1.1 OTA Focal Surface Location, Focal Length and f-number - For the OTA, the following surface subscripts will be used:

0 - object surface

1 - entrance pupil/primary mirror

2 - secondary mirror

3 - exit pupil

4 - image surface

The OTA lens prescription is:

$r_1 = -1104.0$ cm $t_1 = -490.6071$ cm $n_1 = -1.0$

$r_2 = -135.8$ cm $(t_2 + t_3) = 640.61992$ cm $n_2 = n_3 = +1.0$

2-10

Let an axial reference ray, parallel to the optical axis ($u_0 = 0$) be incident upon the primary mirror. The height of this incoming ray, traveling left to right, is 100 units ($y_0 = y_1 = 100$). After reflection from the primary mirror, the ray slope is:

$$(nu)_1 = 0 + (100) \ (1 + 1)/(-1104.0) = -0.18115942$$

At the secondary mirror, the ray height is:

$$y_2 = 100 + (-0.18115942)(-490.6071/-1) = 11.121902 \ \text{units}$$

And after reflection from the secondary mirror, the ray slope is:

$$(nu)_2 = (-0.18115942) + (11.121902) \ (-1 \ -1) \ (-135.8) = -0.017361156$$

At this point in the analysis, the location of the exit pupil is unknown; however, because it is a dummy surface causing no reflection or refraction of the ray, it can be neglected and the ray can be traced directly to the image surface. At the image surface, the ray height is:

$$y_4 = (11.121902) + (-0.017361156) \ (640.61992/1.0) = 0.000000 \ \text{units}$$

A ray height of zero at the OTA image surface shows that incoming on-axis rays are brought to a focus at the prescribed image surface. The focal length (f) of the OTA can also be easily checked by the formula:

$$f = y_1 \ /u_R$$

Where:

Surface 1 is the entrance pupil
Surface R is the exit pupil

Then, the calculated OTA focal length is:

$$f = -100/(-0.017361156) = 5760 \text{ cm}$$

The OTA system f-number is the ratio of system focal length divided by entrance pupil diameter. This diameter, 240 cm, is also the clear aperture diameter of the primary mirror. Thus 5760/240 = 24 and the system f-number is f/24.

2.1.1.2 <u>OTA Exit Pupil</u> - The exit pupil of the OTA is the image of its entrance pupil. The location of the exit pupil is found by tracing a chief ray through the optical system. Chief rays, by definition, pass through the centers of both the entrance and exit pupils. Thus, the height of a chief ray in the entrance pupil is zero ($\bar{y}_1 = 0$). Let the slope for an incoming reference chief ray be unity ($\bar{u}_0 = 1.0$).

Then, the slope for the chief ray after reflection from the primary mirror is:

$$(n\bar{u})_1 = 1.0 + (0)\ (1 + 1)/(-1104.0) = 1.0$$

The ray height of the chief ray at the secondary mirror is:

$$\bar{y}_2 = 0 + (1.0)(-490.6071/1) = 490.6071 \text{ units}$$

After reflection from the secondary mirror, the slope of the chief ray is:

$$(n\bar{u})_2 = 1.0 + (490.6071)(-1 - 1)/(-135.8) = 8.225436$$

The height of the chief ray on the next surface is then calculated. This next surface is the exit pupil and the chief ray height is, by definition, zero at that surface ($\overline{y}_3 = 0$). Thus, equation (1) is written:

$$0 = 490.6071 + (8.225436)(t_2/1)$$

Solving for the unknown distance t_2:

$$t2 = -(490.6071)/(8.225436) = -59.645118 \text{ cm}$$

The exit pupil, therefore, is located 59.645118 cm from the secondary mirror vertex. The minus sign means that this exit pupil is a virtual image of the entrance pupil and is located to the left of the secondary mirror.

Finally, the spacing t_3 between the exit pupil and the image surface is solved:

$$t_3 = (t_2 + t_3) - t_2 = (640.61992) - (-59.64512) = 700.26504 \text{ cm}$$

Now that t_2 and t_3 are known, the height (y_3) of the axial ray on the exit pupil can be calculated. Using equation (1):

$$y_3 = 11.121902 + (-0.017361156)(-59.645118/1) = 12.15741 \text{ units}$$

The actual diameter (Dep') of the OTA exit pupil in centimeters is found by scaling y_3 by the ratio of actual entrance pupil diameter (240 cm) divided by axial ray height (100 units) used at the entrance pupil:

$$\text{Dep'} = (12.15741)(240/100) = 29.17778 \text{ cm}$$

In summary, the above paraxial evaluation of the OTA verified the location of the OTA focal surface and the values of OTA focal length and f-number with respect to the OTA lens prescription. Also, the above evaluation determined the location and diameter of the OTA exit pupil.

2.1.1.3 <u>OTA Conic Constants</u> - The OTA is a two-mirror Ritchey-Chretien (RC) optical system. An RC system is corrected for third-order spherical aberration and coma by adjustment of the conic constants for the two mirrors. The following sets of equations are used to calculate these conic constants (K). Subscript 1 refers to the first mirror (primary) and subscript 2 refers to the second mirror (secondary).

$$B_1 = (nu)_0 + y_1/r_1$$

$$B_2 = (nu)_2 + y_2/r_2$$

$$A_1 = (nu)_0 + \bar{y}_1/r_1$$

$$A_2 = (nu)_2 + \bar{y}_2/r_2$$

$$B_1 = (nu)_1 - (nu)_0$$

$$B_2 = (nu)_2 - (nu)_1$$

$$C_1 = +2\,(y_1/r_1)^3$$

$$C_2 = -2\,(y_2/r_2)^3$$

$$E = B_1{}^2 B_1{}' y_1 + B_2{}^2 B_2{}' y_2 + R_s$$

$$F = A_1 B_1 B_1{}' y_1 + A_2 B_2 B_2{}' y_2 + R_c$$

$$K_1 = (F y_2 - E \bar{y}_2)\,/C_1\,(y_1 \bar{y}_2 - \bar{y}_1 y_2)$$

$$K_2 = (F y_1 - E \bar{y}_1)\,/C_2\,(y_2 \bar{y}_1 - \bar{y}_2 y_1)$$

The application of these equations will be illustrated by calculating the conic constants for the OTA. The paraxial ray trace data generated in the preceding sections will be used. For those data, the subscripts coincide with those used in the above equation set.

$B_1 = 0 + 100/(-1104) = 0.0905797101$

$B_2 = (-0.017361156 + 11.121902/(-135.8) = -0.0992602871$

$A_1 = 1 + 0/(-1104) = 1$

$A_2 = (8.225436) + 490.6071/(-135.8) = 4.612718032$

$B_1 = (-0.17361156) - (-0.18115942$

$B_2 = (0.18115942) - 0 = 0.18115942) = 0.163798264$

$C_1 = 2 [100/(-1104)]^3 = -0.0014863558$

$C_2 = -2 [11.121902/(-135.8)]^3 = 0.0010986715$

The quantities R_s and R_c are residual spherical aberration and residual coma, respectively. For the OTA, these two aberrations are corrected exactly. Hence, $R_s = 0$ and $R_c = 0$. Then:

E = -0.1306866124
F = 0.8068316434

And:

K_1 = -1.0022985
K_2 = -1.4968601

These conic constants agree exactly with those specified in the OTA lens prescription.

2.1.2 Scientific Instrument Surface Location

The compliment of scientific instruments includes, the Wide Field/Planetary Camera (WF/PC), the Faint Object Camera (FOC), the Faint Object Spectrograph (FOS), the High Resolution Spectrograph (HRS), the High Speed Photometer (HSP), and three Fine Guidance Sensors (FGS).

The design philosophy of the scientific instruments is to introduce the least possible degradation to the image provided by the OTA. Ideally, all of the scientific instruments would be designed with their detector surfaces at the OTA image surface. However, there are three basic reasons for optics in the scientific instruments. The first is to correct the astigmatism in the OTA data field. The Space Telescope optical system (OTA + scientific instrument) can then be considered field curvature limited (one well-defined image surface). In this case the field curvature can be "accommodated" by a similarly curved detector surface. The second reason is to change the OTA system focal ratio (f/24). This will change the angular resolution and the field of view. The third reason is to relay the OTA image to a different location for ease of access.

The four axial scientific instruments are located in off-axis locations in the focal plane structure (Figure 2.1-4). A mirror will be provided to fold the on-axis light beam 90 degrees into the radial scientific instrument. Under the philosophy of Space Telescope operation, the image at a single scientific instrument will be optimally focused utilizing the optical control subsystem. Other scientific instruments could be used simultaneously (serendipity mode). Since focal control is not required in the scientific instrument, the OTA condition will not be optimum for the other scientific instruments in the serendipity mode.

ORIGINAL PAGE IS
OF POOR QUALITY.
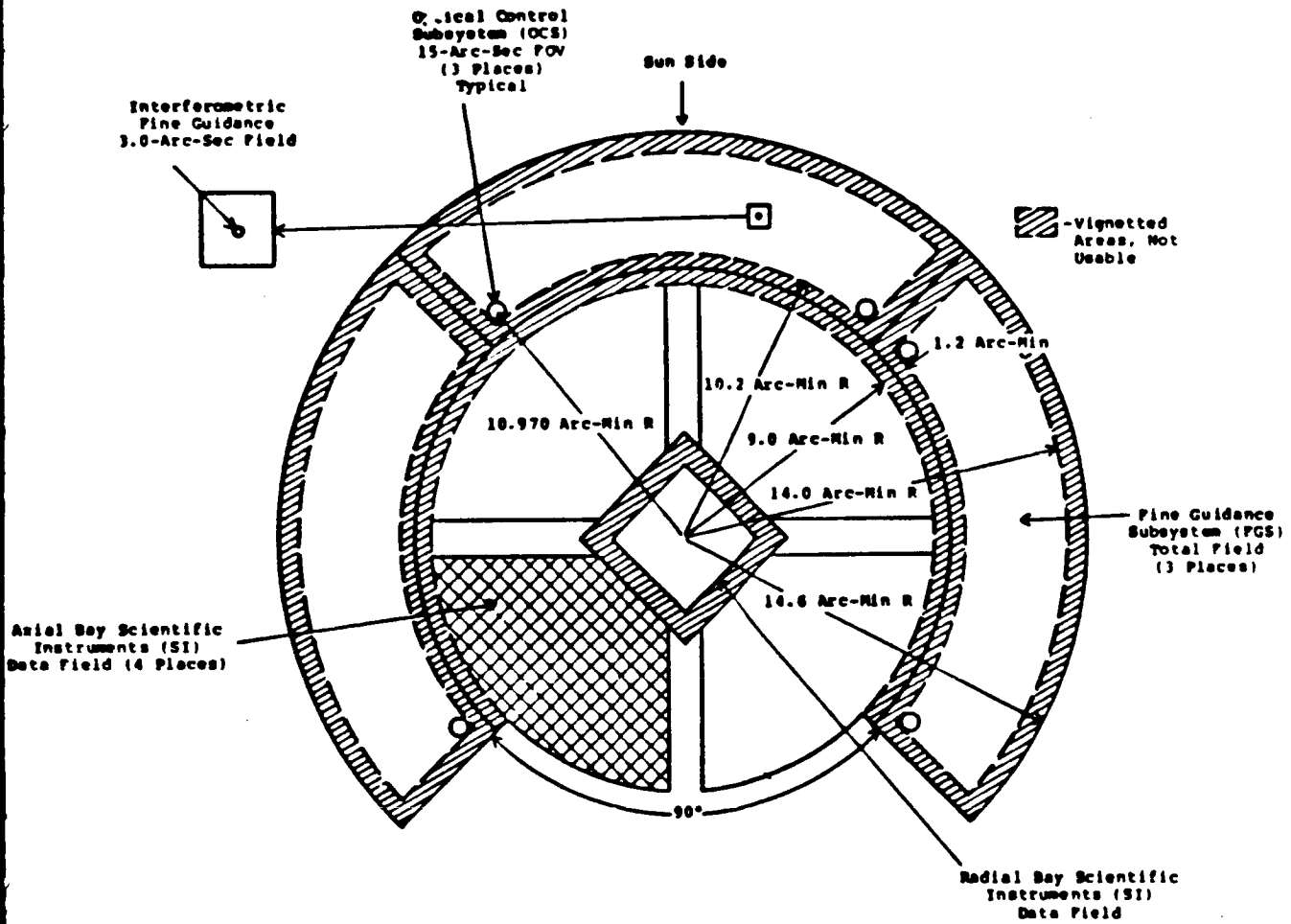
SPACE TELESCOPE FIELD OF VIEW

Figure 2.1-4

2-17

The scientific instruments are mounted to the focal plane structure and require tight alignment and pointing tolerances. The Fine Guidance Sensor (FGS) position must be measured with respect to the OTA reference axis to an accuracy of 0.002 inch in translation within the V_2, V_3 plane. Each scientific instrument will be aligned to the focal surface reference to within the following tolerances.

- axial V_1 axis $\pm$0.003 inch
- lateral $V_2 - V_3$ axis $\pm$0.019 inch
- angular   rotation about V_1 axis $\pm$10 arcseconds

The pointing requirements imposed on OTA are of two types, initialization and dynamic. For initialization (Figure 2.1-5) the calibration focal plane accuracy must be such that any scientific instrument aperture can be positioned with respect to a guide star to 0.01 arcsecond to a probability of 0.9974. Under Space Telescope operation excitation during fine pointing due to relative motion of OTA structure to Support Systems Module (SSM) or between optical elements, the relative dynamic displacement between the OTA image and any scientific instrument aperture must not exceed 0.003 arcsecond (Figure 2.1-6).

IN IMAGE SPACE:
5 ±110 MICROINCHES

IN OBJECT SPACE
θ ±0.01 ARCSECOND
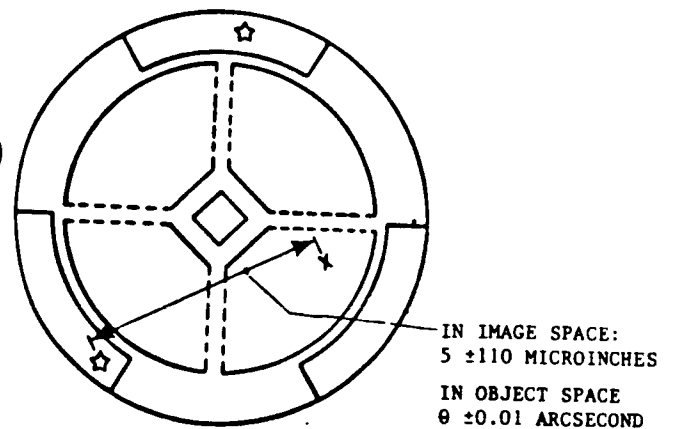
INITIALIZATION
POINTING REQUIREMENT
Figure 2.1-5

IMAGE SURFACE PRESENTED TO SI

SI ENTRANCE APERTURE

SI ENTRANCE APERTURE POINT

≤ 0.03 ARCSECOND

OTA IMAGE POINT
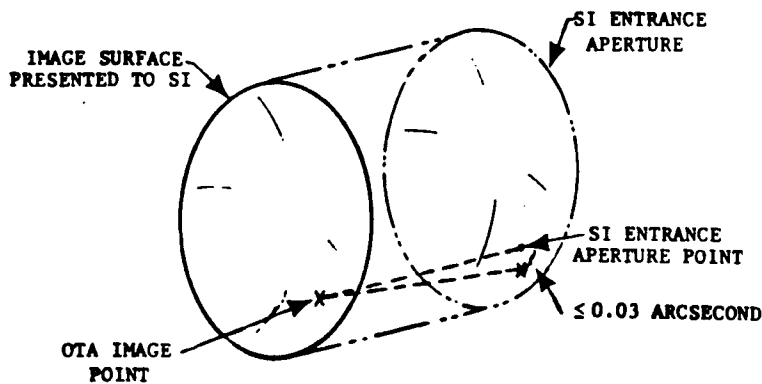
DYNAMIC POINTING REQUIREMENT
Figure 2.1-6

2-18

2.1.3 Sensitivity Analysis

An optical subsystem will deviate from its idealized design configuration during buildup due to assembly errors and during operation due to thermal/ structural changes. Rigid-body misalignments in the optical subsystem can introduce wave front degradation and pointing error (via image motion and change in the image scale).

This analysis assumes that the optical subsystem is: (1) a two mirror Cassegrain telescope, (2) the mirrors are monolithic (single piece) and passive (no active figure control), and (3) the misalignments induced in the system are of the "rigid-body motion" type. Two orthogonal coordinate systems, which are established at the vertices of the mirrors, are shown in Figure 2.1-7. Six degrees of freedom are allowed without constraints (three translations along the orthogonal axes and three rotations about the orthogonal axes) in each coordinate system. If it is assumed that the six degrees of freedom rigid-body motions of the primary mirror are constrained to be zero within allowable manufacturing error budgets, the primary mirror coordinate system can be assumed to be a fixed reference against which the positions of all other elements are measured.

MISALIGNMENTS OF
PASSIVE MONOLITHIC
SECONDARY MIRROR:
$\delta_x, \delta_y, \delta_z, \tau_x, \tau_y, \tau_z$

MISALIGNMENTS OF
PASSIVE MONOLITHIC
PRIMARY MIRROR:
$\delta_x', \delta_y', \delta_z',$
$\tau_x', \tau_y', \tau_z'$
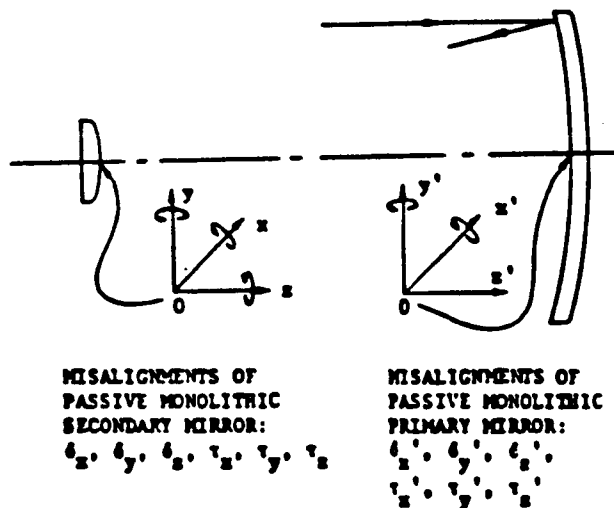
TWO MIRROR TELESCOPE - MONOLITHIC SM; MONOLITHIC PM

Figure 2.1-7

2-19

This implies that from a hardware standpoint, the primary mirror must be constructed of a carefully selected material, such as ultra low expansion (ULE™) titanium silicate, and that the primary mirror must be isolated from mechanical and thermal stresses during all phases of assembly, launch of a space telescope, and operations.

Of the six remaining degrees of freedom, rotation about the z-axis has no effect for rotationally symmetrical mirrors. Under this philosophy, two tilts, two decenters and despace of the secondary mirror, with respect to the primary mirror, therefore constitute the five unconstrained rigid-body motions which are of interest.

If the optical axes remain coincident but there is a longitudinal misalignment between mirrors (traditionally called despace) the wave front error will show up as a focus error in the image. Large longitudinal displacements can introduce spherical aberration.

The second form of rigid-body misalignment is pure lateral misalignment in which the mirror separation remains at its nominal value but the optical axes fall out of coincidence. (The orthogonal translations are traditionally called decenter and the orthogonal rotations are traditionally called tilt.) Lateral misalignment of the secondary mirror with respect to the primary mirror can cause the image to shift laterally away from its nominal position, or it can introduce wave front error in the form of axial coma (coma whose magnitude is not a function of field height) or both.

Assuming that the only aberration resultant from longitudinal displacement is power error and the only aberration resultant from lateral displacement is axial coma, the following "closed-form" expressions for the wave front degradation can be derived:

Decenter

$$W_{\delta_{x,y}}(rms) = S_{\delta_{x,y}} \delta_{x,y} = \frac{3.7 \times 10^{-3}}{\lambda f_p^{\#3}} (1.0 + 0.5\varepsilon^2 - 2.5\varepsilon^4)\delta_{x,y}$$

Tilt

$$W_{\tau_{x,y}}(\text{rms}) = S_{\tau_{x,y}}\tau_{x,y} = \frac{3.7 \times 10^{-3}D}{\lambda(m+1)f_p^{\#2}}(1.0 + 0.5\epsilon^2 - 2.5\epsilon^4)\tau_{x,y}$$

Despace

$$W_{\delta_z}(\text{rms}) = S_{\delta_z}\delta_z = \frac{3.6 \times 10^{-2}}{\lambda f_p^{\#}}(1.0 - \epsilon^2)\delta_z$$

where

$W \sim$ rms wavefront error

$\delta_{x,y} \sim$ decenter of secondary mirror vertex in micrometers

$\tau_{x,y} \sim$ tilt of secondary mirror vertex in radians

$\delta_z \sim$ despace of secondary mirror vertex in micrometers

$f_p^{\#} \sim$ primary mirror focal ratio

$D \sim$ primary mirror diameter in meters

$\epsilon \sim$ linear obscuration ratio

$\lambda \sim$ operational wavelength in micrometers

$m \sim$ secondary mirror magnification

Shown in Table 2.1-1 is the resultant rigid-body misalignment sensitivities for the OTA.

Table 2.1-1		
DEGRADATION IN IMAGE QUALITY DUE TO RIGID BODY MISALIGNMENTS		
MISALIGNMENT	ALIGNMENT SENSITIVITY
SM DECENTER (δ_x, δ_y)	0.0005 λ/MICROMETER
SM TILT (τ_x, τ_y)	0.0014 λ/ARCSECOND
SM DESPACE (δ_z)	0.011 λ/MICROMETER
*PRIMARY MIRROR IS A FIXED REFERENCE FOR THE TELESCOPE $\Longrightarrow \delta_x' = \delta_x' = \delta_z' = \tau_x' = \tau_y' = \tau_z' = 0$	

Error contributors are defined and toleranced based on the predicted "manufactured" system performance, sensitivity analysis, and assembly buildup philosophy. For an imaging system the rms wave front error is usually used as the tolerancing denominator (Figures 2.1-8, 2.1-9, and 2.1-10). The rms wave front error is related to a single point merit function for a manufacturing optical subsystem--the optical quality factor (OQF). The value indicates how close the manufactured optical subsystem is to the "ideal" optical formula (100 percent indicates perfection). The optical quality factor can be separated into two parts: the lens quality factor (LQF) and the metering quality factor (MQF). The LQF is a single point merit function for the optics. The value indicates how close to perfect the manufactured optics have to be. The MQF is a single point merit function for the optical support structure.
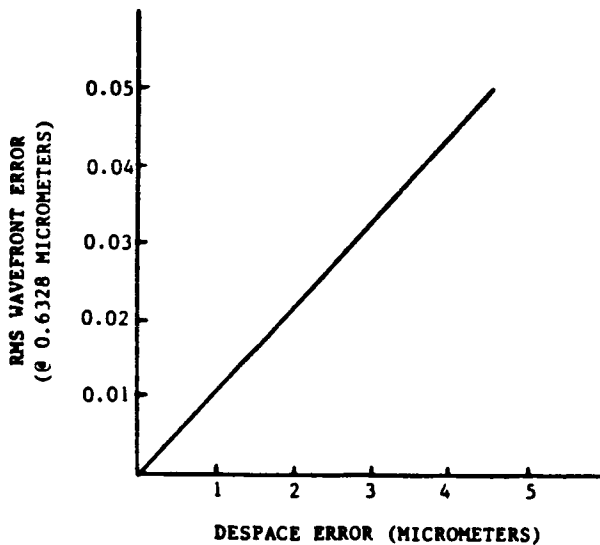
WAVE FRONT DEGRADATION DUE TO
SECONDARY MIRROR DESPACE ERROR

Figure 2.1-8
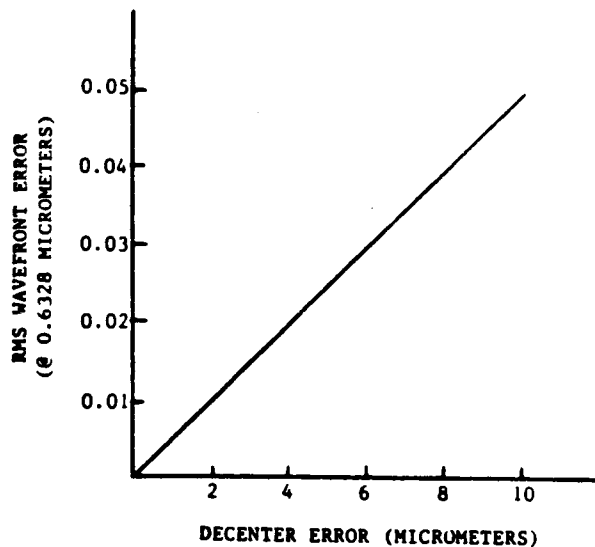
WAVE FRONT DEGRADATION DUE TO
SECONDARY MIRROR DECENTER ERROR

Figure 2.1-9

2-22
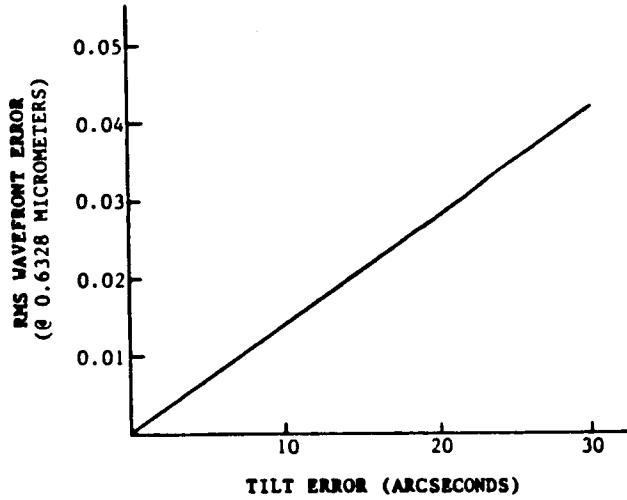
WAVE FRONT DEGRADATION DUE TO
SECONDARY MIRROR TILT ERROR
Figure 2.1-10

The value indicates how close to perfect the optical support structure has to be. Shown in Figure 2.1-11 is "an" allocated tolerance budget for the OTA.
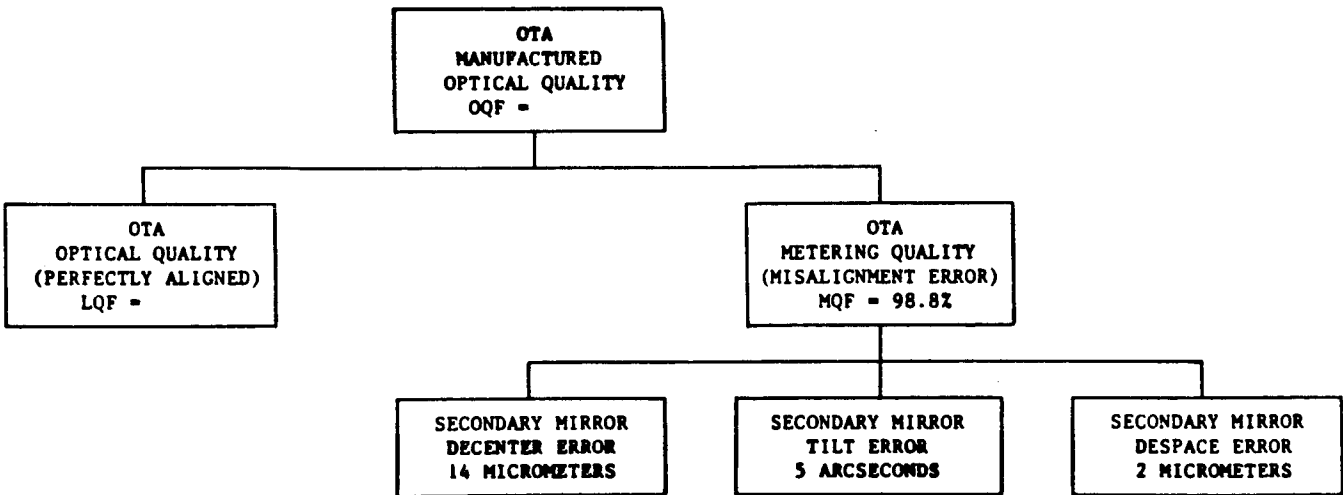
OTA RIGID-BODY MISALIGNMENT ERROR
Figure 2.1-11

Closed form expressions for image shift (the second affect of rigid-body motion misalignments) can be derived based on paraxial ray tracing:

2-23

Decenter

$$\Delta y = S_{\delta_{x, y}} \quad \delta_{x, y} = -(m - 1) \, \delta_{x, y}$$

Using the pointing error equation with $\Delta f = 0$

$$\Delta y \approx f \Delta \phi$$

Where $f \sim$ system focal length.

The change in the optical subsystem line of sight, if the secondary mirror is decentered is, therefore given by the following expression:

$$\Delta \phi = - \frac{(m - 1)}{f} \, \delta_{x, y}$$

Tilt

$$\Delta y = S_{\tau_{x, y}} \quad \tau_{x, y} = \frac{2(f + mB)}{(m + 1)} \, \tau_{x, y}$$

Where $B \sim$ back focus relative to primary mirror vertex

if $mB \ll f$

$$\Delta y = \frac{2f}{(m + 1)} \, \tau_{x, y}$$

Using the pointing error equation with $\Delta f = 0$

$$\Delta y \approx f \, \Delta \phi$$

The change in the optical subsystem line of sight, if the secondary mirror is tilted, is therefore given by the following expression:

$$\Delta \phi = \frac{2\tau_{x, y}}{(m + 1)}$$

2-24

Figures 2.1-12 and 2.1-13 show the closed form expressions for image shifts graphed for the OTA parameters. Under Space Telescope operation excitation during fine pointing due to relative motion of OTA structure to Support Systems Module (SSM) or between optical elements, the relative dynamic displacement between the OTA image and any scientific instrument aperture must not exceed 0.003 arcsecond (set at a fraction of the Airy disk diameter).

The resultant effects of rigid-body misalignment (wave front degradation and image motion) can be categorized as static and dynamic. (Note: The static case is the limit of the dynamic case with zero pointing stability error.) Comparing the static misalignment case (Figures 2.1-9 and 2.1-10) with the dynamic misalignment case (Figures 2.1-12 and 2.1-13) it can be seen that the misalignment required to produce the maximum acceptable wave front error is much larger than that required to produce the maximum acceptable image motion.
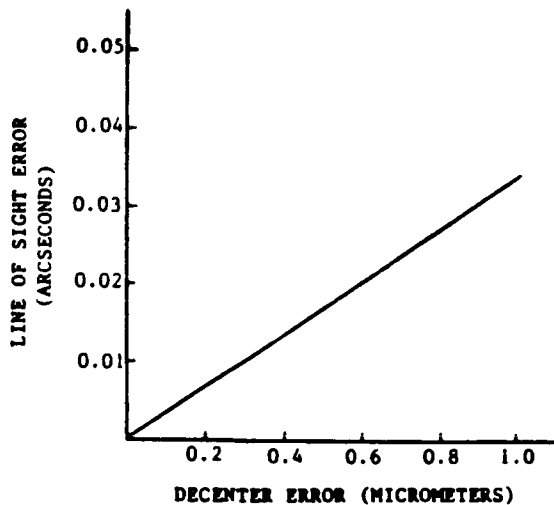
CHANGE IN THE LINE OF SIGHT ANGLE DUE
TO SECONDARY MIRROR DECENTER ERROR

Figure 2.1-12
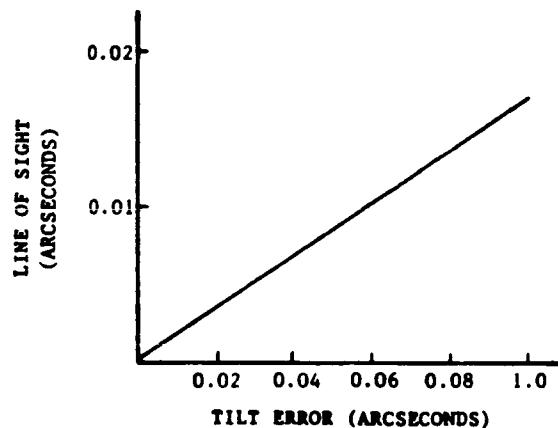
CHANGE IN THE LINE OF SIGHT ANGLE
DUE TO SECONDARY MIRROR TILT ERROR

Figure 2.1-13

This means that only image motion need be considered in establishing dynamic lateral misalignment limits. Conversely if the lateral image motion is "slow" enough to be compensated for by the tracking system then wave front error forms the limit on lateral misalignment. If the optical subsystem cannot be designed and manufactured for factory "set-and-forget", the rigid-body

2-25

misalignments due to wave front degradation would be periodically controlled in six degrees of freedom using linear actuators.

The dynamic lateral misalignment errors are very difficult to meet. The optical support structure is not as rigid as along the orthogonal despace direction and there are a number of sources of vibration that can feed lateral oscillations at a fast rate into the position of the secondary mirror. These include elements of tracking system, such as the control moment gyros and other elements of the spacecraft, such as solar panels. Dynamic longitudinal misalignment errors which cause a dynamic defocus error must also be considered. It is specified as a percentage of the static longitudinal error (Figure 2.1-8) and is set by the "dither" in the focus mechanism. Dynamic longitudinal misalignments are due to oscillations of the metering structure between the primary and secondary mirrors. The structure can usually be designed rigid enough in this direction so that only static longitudinal control is required.

2.2 FINE GUIDANCE SENSING

The primary function of a Fine Guidance Sensor (FGS) is to detect misalignment of the Line Of Sight (LOS) vector. In the Space Telescope this is accomplished by measuring the positions of auxiliary or guide star images in the telescope focal plane. The measurement is converted to an electrical error signal for use of the Support System Module (SSM) in correcting the pointing direction.

A telescope represented as a simple lens is shown in Figure 2.2-1. A lens from a physical optics standpoint transforms a diverging spherical wave front from a point source (i.e., plane wave front for a star at infinity) to a converging spherical wave front. The lens can also be looked at as transforming object angular information ($\varphi \pm_{\Delta\phi}$) into image displacement information ($y \pm \Delta y$) through the scale factor of focal length. Figure 2.2-2 shows schematically the geometry involved in pointing. Every point in the image plane is associated with a unique direction, a Line Of Sight (LOS), in object space. This direction is most easily found from the ray passing through the specific focal point in the field and the center of the principal plane of the telescope, the ray called the principal ray. The principal ray which strikes the center of this image plane may be regarded as the LOS of the telescope. In Figure 2.2-2, OP corresponds to the telescope LOS. A field point Q would then have an angle:

$$\phi = \text{Tan}^{-1}\left(\frac{y}{f}\right) \quad ,$$

with respect to the telescope LOS. This simple expression is called the pointing equation.

OBJECT SPACE $\Longrightarrow$ IMAGE SPACE

$\phi \pm \Delta\phi$ $y \pm \Delta y$
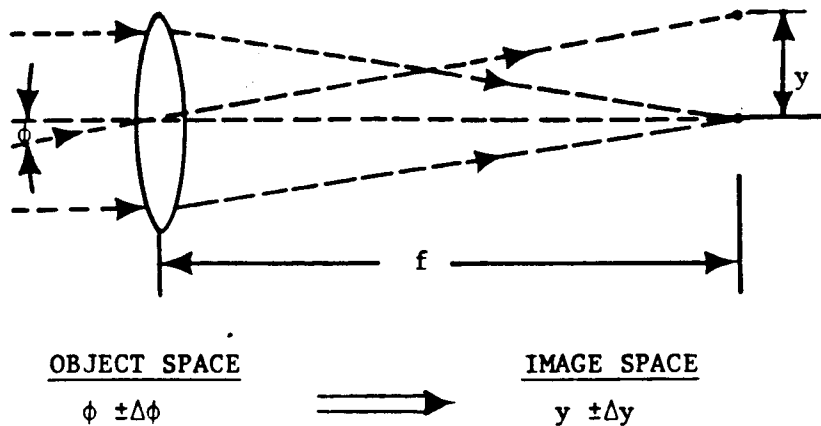
CONCEPT OF OPTICAL POINTING

Figure 2.2-1
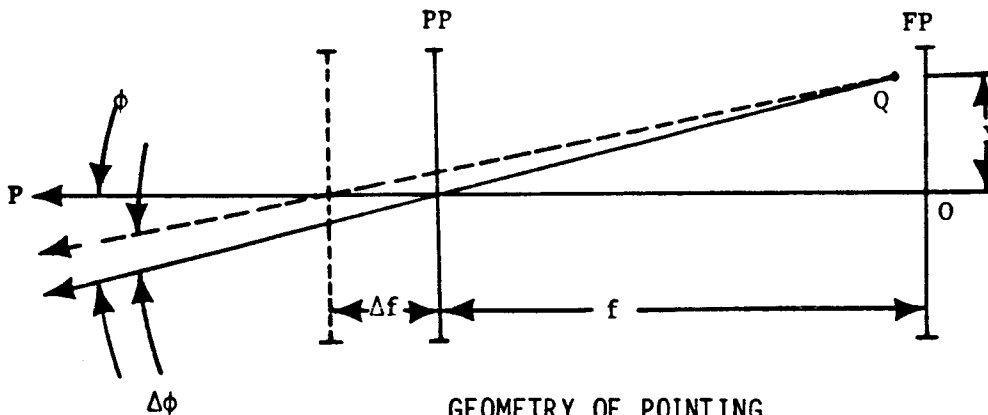
GEOMETRY OF POINTING

Figure 2.2-2

If the principal plane moves longitudinally along the optical axis the telescope focal length changes. The LOS of the telescope would not change but the LOS of any point in the field would change. In a similar manner, if the image displacement changes, the LOS of the telescope would not change but the LOS of any point in the field would.

To determine the fundamental pointing error expression let be the LOS field angle before the perturbation and be the LOS field angle after the perturbation.

2-28

Let $y' = y + \Delta y$ and $f' = f + \Delta f$.

$$\text{Tan } \phi' = \frac{y'}{f'}$$

Alternately using the finite difference method the pointing equation can be expressed as:

$$\text{Tan } [\phi + \Delta \phi] = \frac{y + \Delta y}{f + \Delta f}$$

or,

$$\Delta \phi = \text{Tan}^{-1} \left[\frac{\Delta y}{(f - \Delta f)} - \frac{\Delta f \text{ Tan } \phi}{(f - \Delta f)} \right]$$

This expression is called the pointing error equation, and serves as the mathematical basis for fine guidance sensing.

2.2.1 Fine Guidance Sensing (On-Axis)

Shown in Figure 2.2-3 is a graph of the OTA image diameter (on-axis). The manufacturing error is expressed as the rms wavefront error at a wavelength of 0.6328 micrometer. Assuming a static wavefront error of 0.05 wave rms, the circular image diameter will be approximately 0.14 arcsecond (encircled energy of 70%).

This image is re-imaged by the optics in the Wide Field/Planetary Camera. The wide field mode and the planetary camera mode correspond to focal ratios of f/12.9 and f/30, respectively.
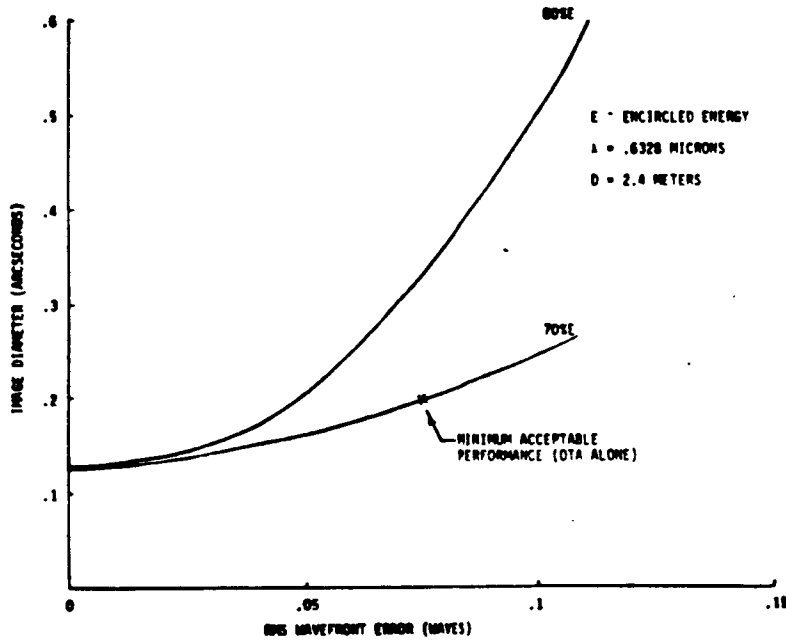
STAR SPOT SIZE WITH MANUFACTURING ABERRATIONS IN OPTICS

Figure 2.2-3

To meet the field of view requirement (2.7 arcminutes x 2.7 arcminutes for the WFC and 68.7 arcseconds x 68.7 arcseconds for the PC) with state-of-the-art CCD technology (800 x 800 array), the total field (1600 x 1600 array) is split into four fields via a four faceted reflective pyramid. The OTA focal ratio is changed and re-imaged at a second focal surface via a finite conjugate Cassegrain relay. One of the four optical paths is shown in Figure 2.2-4. The Cassegrain relays have been corrected for third order spherical aberration, coma and astigmatism. There is some residual astigmatism and field curvature.

However, for the planetary camera, the effect of these aberrations on image quality is negligible because it operates at a higher f-number and has a smaller angular field. Figures 2.2-5 and 2.2-6 show spot diagrams for the f/12.9 and f/30 relays, respectively. A 20 x 20 array of rays entered the lens. The intercepts of these rays at the focal surface were plotted as individual spots. These spot diagrams show the effect of geometric aberrations of image quality, but ignore diffraction effects. For the high f-number Planetary Camera, the Airy disk is much larger than the geometric spot diagrams. This relay, has near diffraction limited performance.
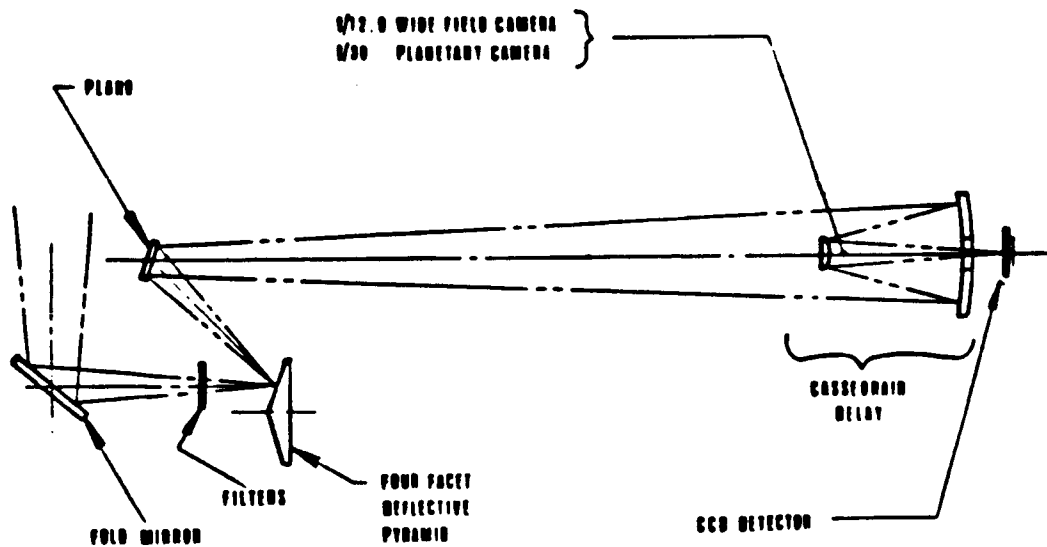
WF/PC OPTICAL CONFIGURATION

Figure 2.2-4

A

A'

AIRY DISK DIAMETER

B

$D = 2.44 \, \lambda \, F* = (2.44)(0.6328 \times 10^{-3} MM)(12.88)$
$= 0.020 \, MM$

C

F

G

D

0.00   0.03   0.06
SCALE - MM

E
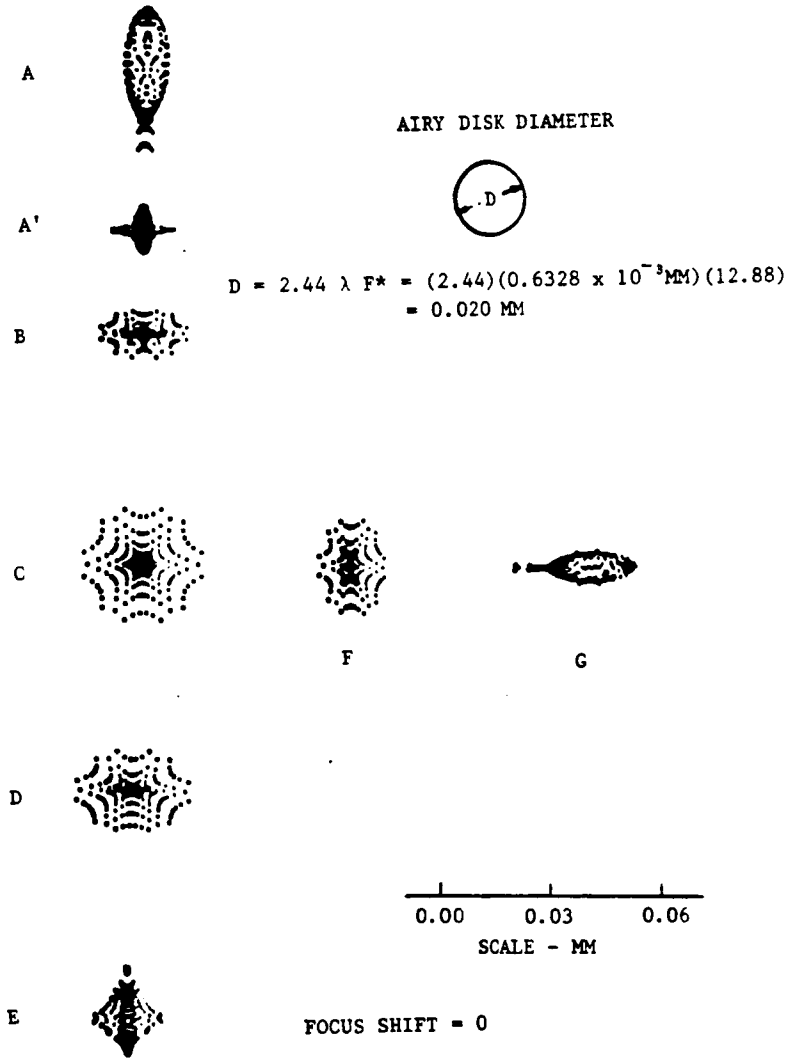
FOCUS SHIFT = 0

f/12.88 SPOT DIAGRAMS

Figure 2.2-5

2-32

A

AIRY DISK DIAMETER

D

B
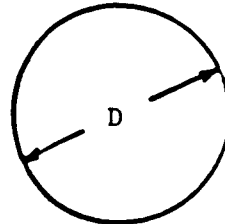
$$D = 2.44 \; \lambda \; F* = (2.44)(0.6328 \times 10^{-3} \; \text{MM})(30)$$
$$= 0.046 \; \text{MM}$$

C

F

G

D

| 0.00 | 0.03 | 0.06 |

SCALE — MM

FOCUS SHIFT = 0

E
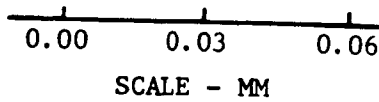
f/30 SPOT DIAGRAMS
Figure 2.2-6

2-33

Therefore, the Wide Field/Planetary Cameras have geometric distortion as the limiting aberration. Computation of geometric distortion is based upon the expression:

$$\% \ D = \frac{100 \ (Y - y)}{y}$$

where:

% D is distortion expressed as a percent of the paraxial image height y. This image height is the radial distance between a specified image point on the relay optics focal plane and the on-axis point on that plane. The change in chief ray intercept height, y, is derived by exact trigonometric ray trace.

The effect of image distortion is angular pointing error. A star at a field angle of ϕ will appear to be at an angle $\phi + \Delta \phi$. By using the pointing error equation, the angular error can be expressed as follows:

$$\text{Tan} \ \Delta \ \phi = \frac{y}{f} \left(\frac{D}{1 + D} \right)$$

The geometric distortion calculations for the Wide Field/Planetary Camera are summarized in Tables 2.2-1 and 2.2-2. Knowledge of the focal plane topography (geometric distortion), if calibratable, can be backed out as a line of sight bias on a point-by-point basis.

Table 2.2-1 GEOMETRIC DISTORTION - f/12.88 RELAY (f = 3091.0 CM)				
ϕ (DEGREE)	Ψ (CM)	y (CM)	DST (%)	$\Delta\phi$ (ARCSECOND)
0.015816	0.854896	0.853244	+0.194	0.110
0.007908	0.426959	0.426622	+0.079	0.022
0	0	0	--	--
0.007908	0.426596	0.426622	-0.006	-0.002
0.015816	0.853436	0.853244	+0.023	0.013
0.007908	0.426780	0.426622	+0.037	0.010
0.015816	0.854191	0.853244	+0.111	0.063

Table 2.2-2

GEOMETRIC DISTORTION - f/30 RELAY
(f = 7200.6 CM)

φ (DEGREE)	Ψ (CM)	Y (CM)	DST (%)	Δφ (ARCSECOND)
0.0067556	0.849387	0.849005	+0.045	0.011
0.0033778	0.424548	0.424502	+0.011	0.001
0	0	0	--	--
0.0033778	0.424392	0.424502	-0.026	-0.003
0.0067556	0.848761	0.849005	-0.029	-0.007
0.0033778	0.424470	0.424502	-0.008	-0.001
0.0067556	0.849078	0.849005	+0.009	0.002

Inherent in the manufacture of a combined OTA with WF/PC is a maximum rms wave front error 0.075 λ due to the OTA alone. The addition of an independent WF/PC optical system to the OTA will increase this inherent wave front error. Shown in Figure 2.2-7 is the system static wave front error allocation for the combined OTA with WF/PC. From Figure 2.2-3 this implies that the image diameter will be approximately 0.25 arcsecond (encircled energy is 70%). Shown in Figure 2.2-8 are the subimage resolution requirements to implement optical pointing using the on-axis image. A resolution of a fiftieth of the spot diameter corresponds to 0.005 arcsecond. This corresponds to resolving an image plane displacement of 0.7 micrometer and 2 micrometers in the Wide Field Camera and the Planetary Cameras, respectively.

SYSTEM STATIC
WAVEFRONT ERROR
0.108 λ

OTA STATIC
WAVEFRONT ERROR
0.075 λ

WF/PC OPTICS SUBSYSTEM
STATIC WAVEFRONT ERROR
0.078 λ
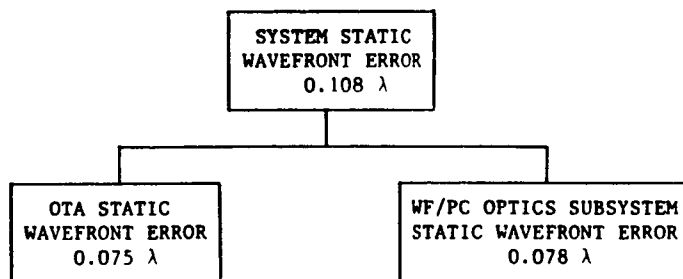
SYSTEM WAVE FRONT ERROR (RMS ERROR AT 0.6328 μ M)
Figure 2.2-7

θ = 0.25 ARCSECOND
Δφ = 0.005 ARCSECOND

IMAGE PLANE DISPLACEMENT (MICROMETERS)

SUBIMAGE RESOLUTION REQUIREMENT
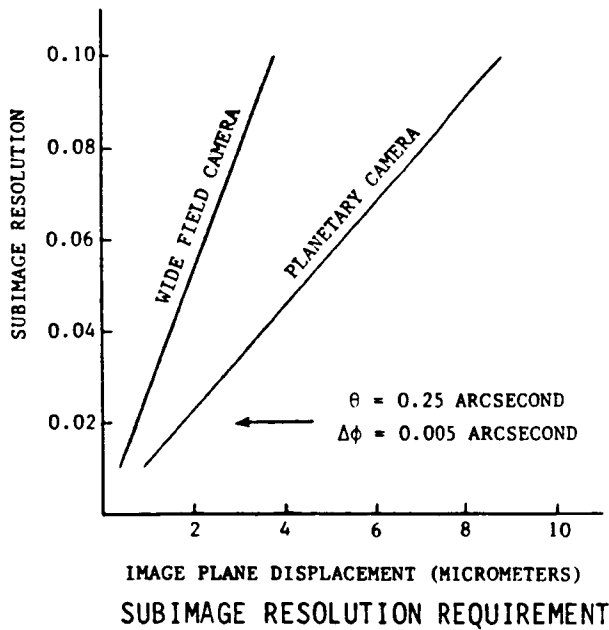
Figure 2.2-8

2.2.2 Fine Guidance Sensing (Off-Axis)

In the Space Telescope the image field near the optical axis is used for
scientific purposes. The available fine guidance sensing field is an annulus
as shown in Figure 2.2-9 (9 arcminutes $\leq$ R $\leq$ 14.6 arcminutes). Since the
optical pointing concept involves locating of the centroid of the image, the
shape and size of the image in this annulus becomes extremely important.
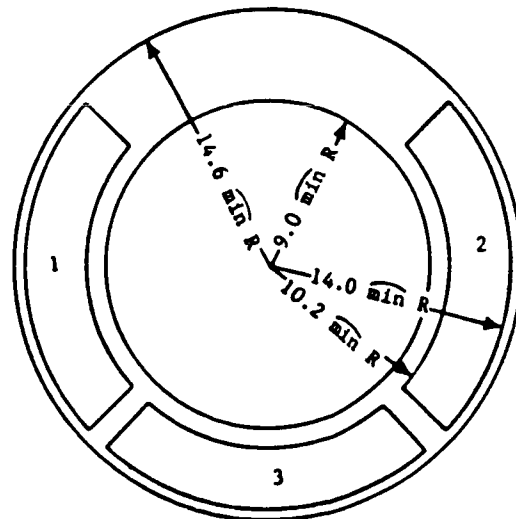
SPACE TELESCOPE GUIDE FIELD AREA

Figure 2.2-9

2-36

To optimize theoretical design performance of the optical subsystem the lens designer has several "degrees of freedom" available. They include the radii of curvature of the surfaces, the thicknesses and airspaces, the refractive indices and dispersive powers of the glasses used for the separate lens elements, and the position of the stop. The ultimate goal is that all rays in all the wavelengths originating at a given object point should be made to pass accurately through the image of that object point, and the image of a plane object should be a plane, without any appearance of distortion in the images of straight lines. Therefore, the lens designer has the capability to theoretically obtain the same image quality off-axis in the annulus as on-axis. (Note: Within the limits of geometrical distortion which, if calibratable, can be "backed-out".) The OTA optical configuration is a catoptric Ritchey-Chretien version of the Cassegrain telescope. This limits the "degrees of freedom" to those of two mirrors and therefore, the resultant aberration correction.

The configuration consists of hyperbolic primary and secondary mirrors. The conic shapes have been chosen to simultaneously correct spherical aberration and coma. The aberrations of astigmatism, field curvature, and distortion are present off-axis in predictable amounts (Figures 2.5-10 and 2.6-11). Field curvature and astigmatism appear as two well-defined curved focal surfaces. At a semi-field angle of 14.6 arcminutes (edge of tracking field of fine guidance sensor), the primary astigmatism is 0.6 wave rms ($\lambda = 0.6328 \mu$m) with a residual coma of 0.2 wave rms. At a semi-field angle of 7.8 arcminutes (inside data field of axial scientific instrument) the primary astigmatism is 0.18 wave rms with a residual coma on the order of 0.002 wave rms. The magnitude of the astigmatism in the data field of the scientific instrument is small enough to be corrected by the scientific instrument if required. Alternately, these two curved focal surfaces can be matched by two similarly curved scientific instrument surfaces. If this is to be done, the astigmatism is accommodated, and distortion is the limiting aberration.
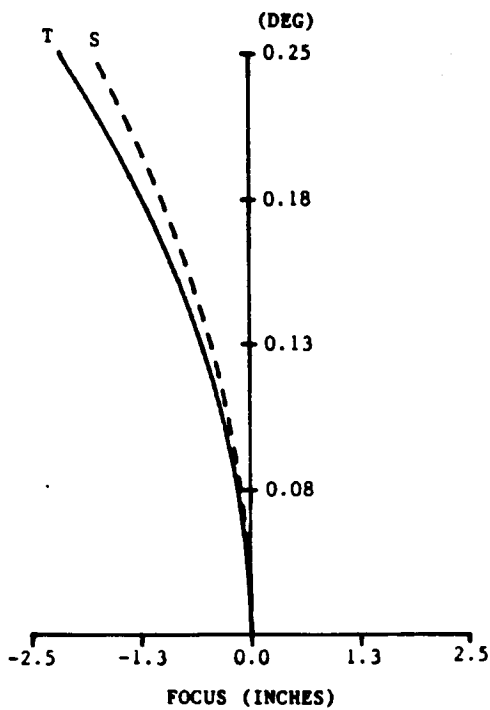
ASTIGMATIC FIELD CURVES

Figure 2.2-10
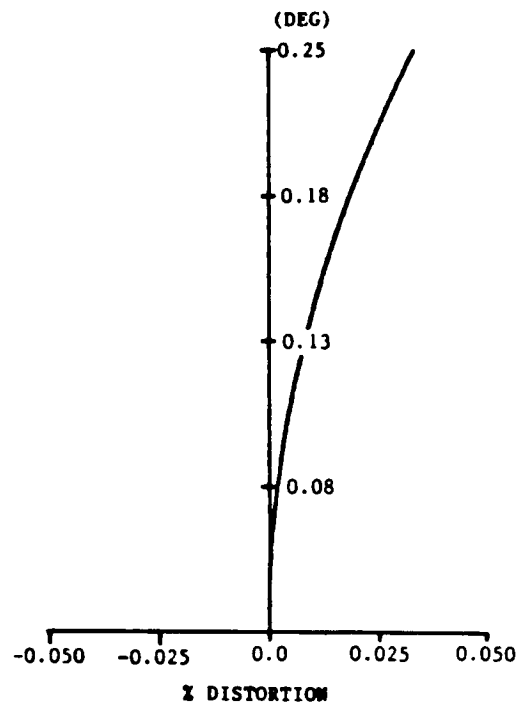
DISTORTION

Figure 2.2-11

The effect of image distortion is angular pointing error. A star at a field angle of ϕ will appear to be at an angle $\phi + \Delta\phi$. By using the pointing error equation, the angular error can be expressed as follows:

$$\text{Tan } \Delta\phi = \frac{y}{f}\left(\frac{D}{1 + D}\right)$$

The geometric distortion calculations for the OTA image are shown in Table 2.2-3. Knowledge of the focal plane topography (geometric distortion), if calibratable, can be backed out as a line of sight bias on a point-by-point basis.

2-38

Table 2.2-3
GEOMETRIC DISTORTION - f/24 IMAGE
(f = 57.6 M)

φ (ARCMINUTE)	y (METERS)	y (METERS)	DST (%)	Δφ (ARCSECONDS)
9	0.150813	0.150797	0.011	0.059
11	0.184338	0.184307	0.017	0.112
13	0.217864	0.217818	0.021	0.164
14.6	0.244705	0.244627	0.032	0.280

Inherent in the assembly and operation of the fine guidance sensor is the ability to install and retain the detector surface onto the image surface as presented by the optical subsystem. For this analysis it is assumed that the detector surface is planar. In the case of an optical subsystem with a flat field, matching between the image plane and the detector plane becomes relatively simple. However, since in the OTA the field curvature and astigmatism appear as two well-defined curved surfaces (two concave prolate spheroids), alternate choices for the detector surface location occur.

Shown in Figure 2.2-12 are alternate well-defined curved surfaces as presented by the optical subsystem. Cross sections of these images are shown in Figure 2.2-13.
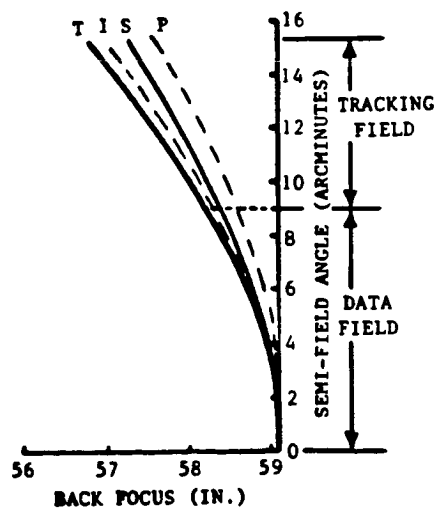
FOCAL PLANE TOPOGRAPHY
Figure 2.2-12

2-39
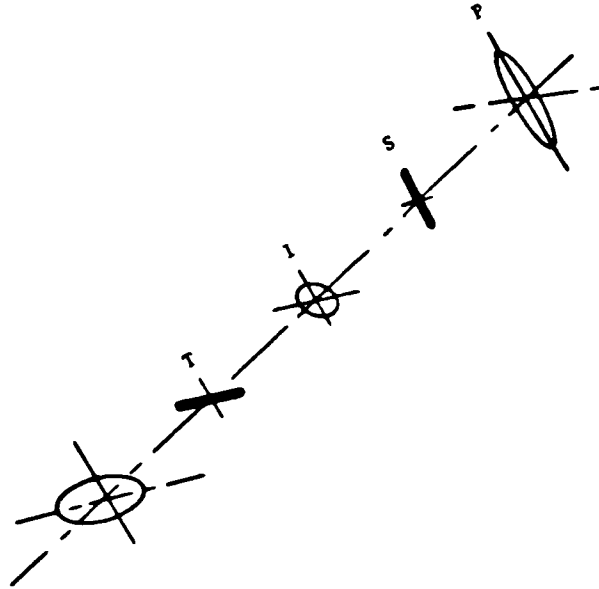
ASTIGMATIC FOCAL LINES
Figure 2.2-13

At the sagittal image surface (S) the image is a line which is radial to the field and points toward the optical axis.

At the tangential image surface (T) the image is a line which is tangential to the field. Both focal lines are perpendicular to the principal ray which establishes the line of sight. At the Petzval image surface (P) the image has

an elliptical cross section. The ratio of line length to line width is 3:1.
At small field angles the longitudinal distance from the Petzval surface to
the tangential focal line (tangential astigmatism), is three times as great as
the longitudinal distance from the Petzval surface to the sagittal focal line
(sagittal astigmatism). If the astigmatism can be made zero the two focal
lines will coalesce on the Petzval surface. At the image surface (I) midway
between the tangential and sagittal images surfaces the image has a circular
cross section (circle of least confusion). Shown in Figure 2.2-14 is the
image size at a semi-field angle of 9 arcminutes. A circle with a diameter of
51 micrometers contains 70 percent of the energy, and a circle with a diameter
of 58 micrometers contains 80 percent of the energy. Shown in Figure 2.2-15
is the image size at a semi-field angle of 14.6 arcminutes. A circle with a
diameter of 146 micrometers contains 70 percent of the energy and a circle
with a diameter of 162 micrometers contains 80 percent of the energy. Shown
in Figure 2.2-16 is the resultant OTA image diameter as a function of the
field angle. This data includes the effects of design residuals, static
manufacturing and assembly errors, and anticipated residual image motion
during operation.

OTA OPTICAL SYSTEM

Figure 2.2-14

2-41

OTA OPTICAL SYSTEM
Figure 2.2-15

D = 2.4 METERS
f = 57.6 METERS
ε = 0.34
λ = 0.6328 μ
w = 0.075 λ RMS
σ = 0.007 SEC
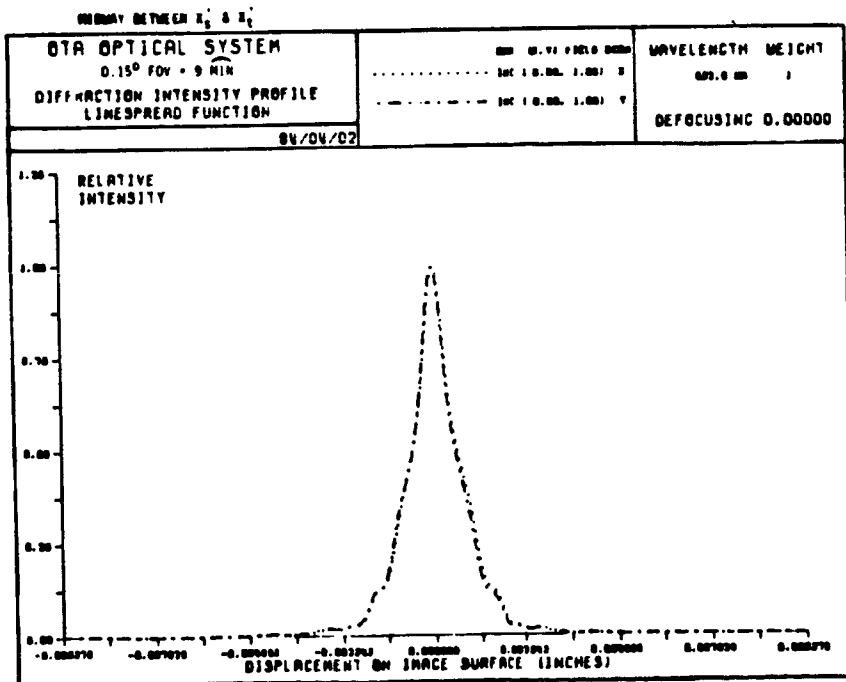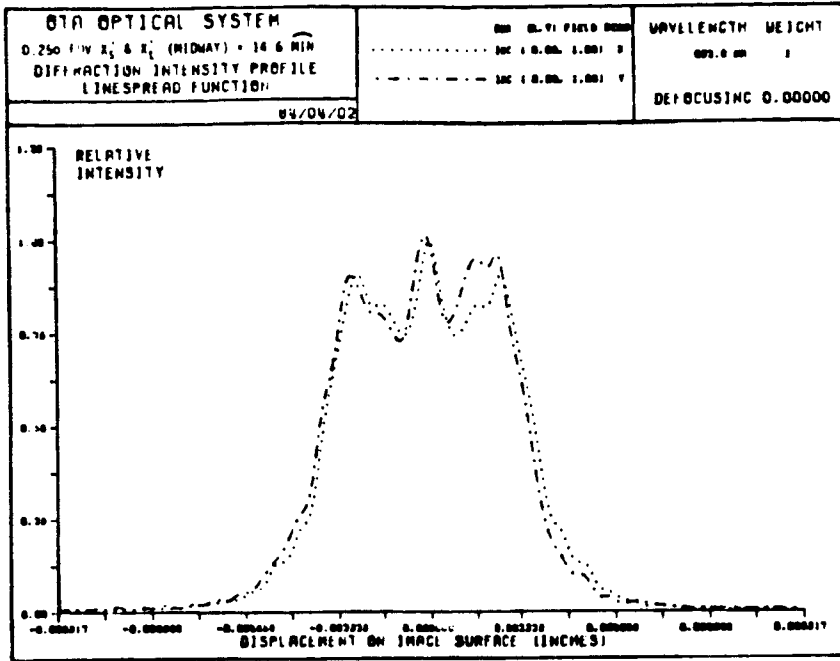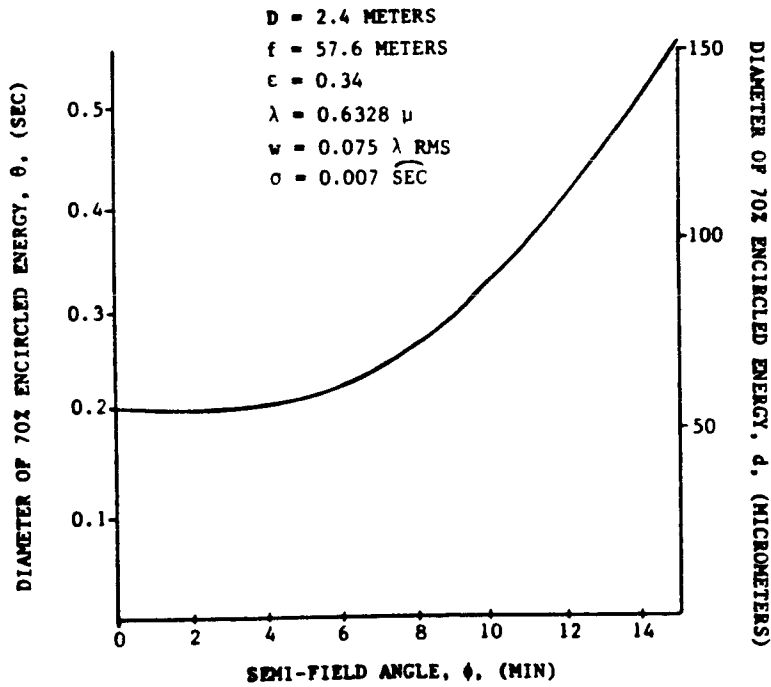
OTA IMAGE DIAMETER (@ CIRCLE OF LEAST CONFUSION)
Figure 2.2-16

2-42

Residual wave front error and residual image motion increase the diffraction image size near the optical axis. The design residual (astigmatism) increases the diffraction image size and dominates over the effects of residual wave front error and residual image motion in the field.

From Figure 2.2-16 the resultant image diameter will be approximately 0.55 arcsecond (under the following conditions: edge of field, circle of least confusion, and encircled energy is 70 percent).

Shown in Figure 2.2-17 are the subimage resolution (centroid determination) requirements to implement optical pointing using the off-axis image at the circle of least confusion. A subimage resolution of 1 part in 110 of the spot diameter corresponds to a line of sight error in object space of 0.005 arcsecond. This corresponds to resolving an image plane displacement of 1.3 micrometers.
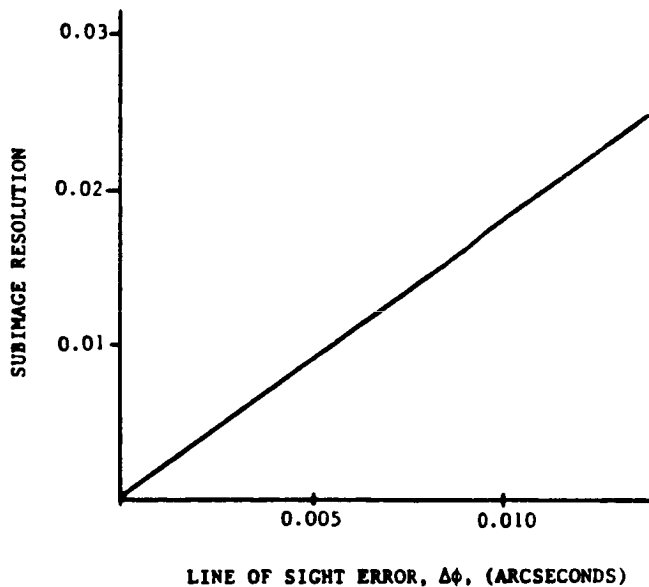
SUBIMAGE RESOLUTION REQUIREMENTS

(0 = 0.55 ARCSECOND)

Figure 2.2-17

Shown in Figures 2.2-18 and 2.2-19 is the geometrical size at the sagittal focus for semi-field angles of 9 arcminutes and 14.6 arcminutes, respectively. As can be seen from these curves the line width retains its on-axis diffraction limited performance at the expense of an increase in line length. At tangential focus the line width and line length would be reversed. The resultant image sizes are summarized in Table 2.2-4.
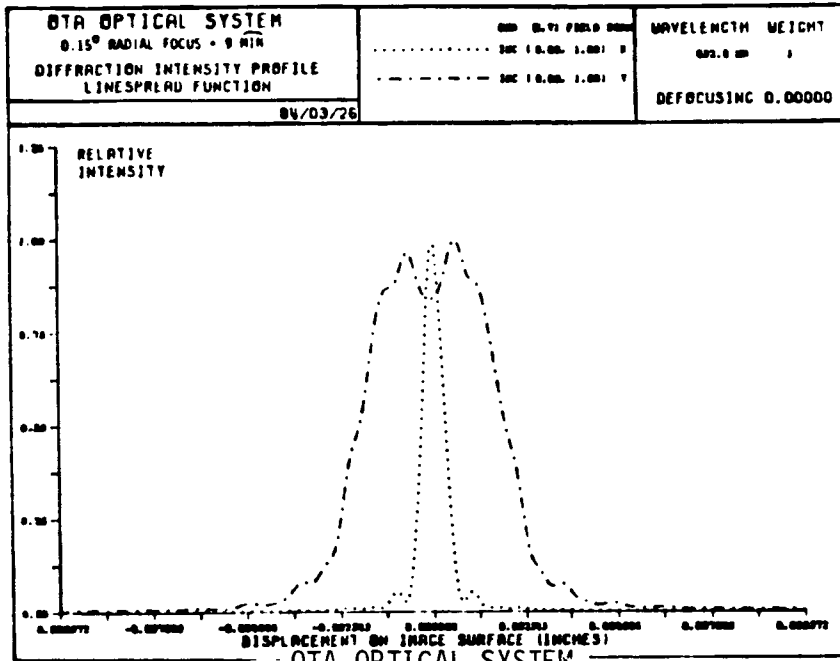
Figure 2.2-18

Figure 2.2-19

2-44
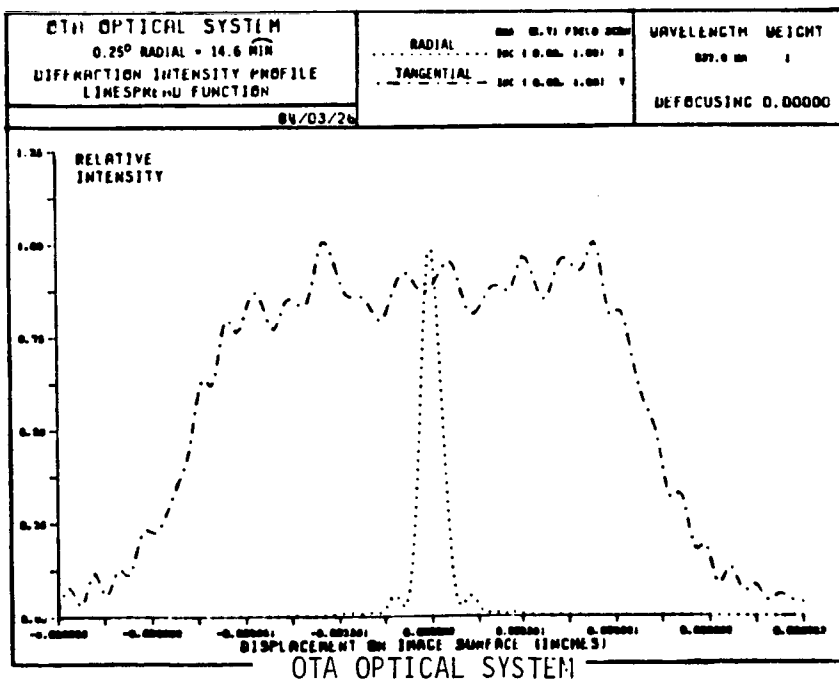
Table 2.2-4 RESULTANT IMAGE DIAMETERS				
	IMAGE DIAMETER (70% E)		IMAGE DIAMETER (80% E)	
	@9 MIN	@14.6 MIN	@9 MIN	@14.6 MIN
LINE WIDTH	32 μ	32 μ	44 μ	44 μ
LINE LENGTH	114 μ	310 μ	123 μ	330 μ

Shown in Figure 2.2-20 is the resultant image diameter at the sagittal or tangential image surface including the effects of residual design, wave front and image motion errors.

D = 2.4 METERS
f = 57.6 METERS
ε = 0.34
λ = 0.6328 μ
w = 0.075 λ RMS
σ = 0.007 SEC
E = 70%
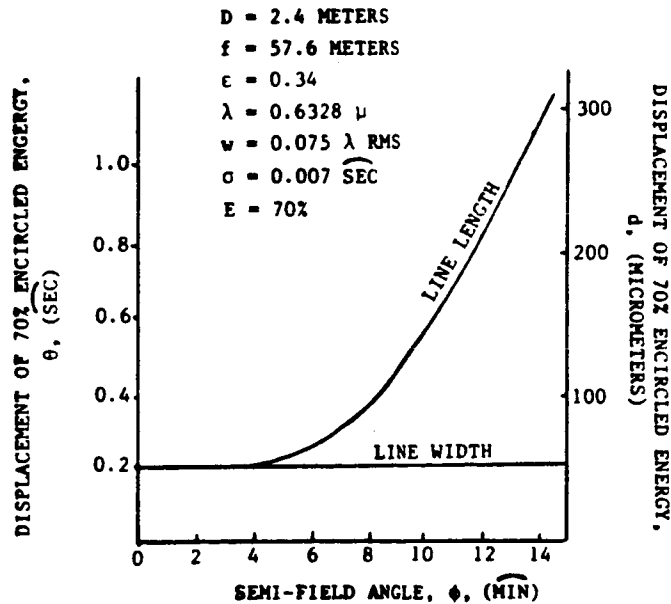
OTA IMAGE DIAMETER (@ SAGITTAL OR
TANGENTIAL IMAGE SURFACE)

Figure 2.2-20

2-45

Shown in Figure 2.2-21 are the subimage resolution (centroid determination) requirements to implement optical pointing using the off-axis image at either the sagittal or tangential image surface. A subimage resolution of 1 part in 40 utilizing the line width, corresponds to a line of sight error in object space of 0.005 arcsecond.
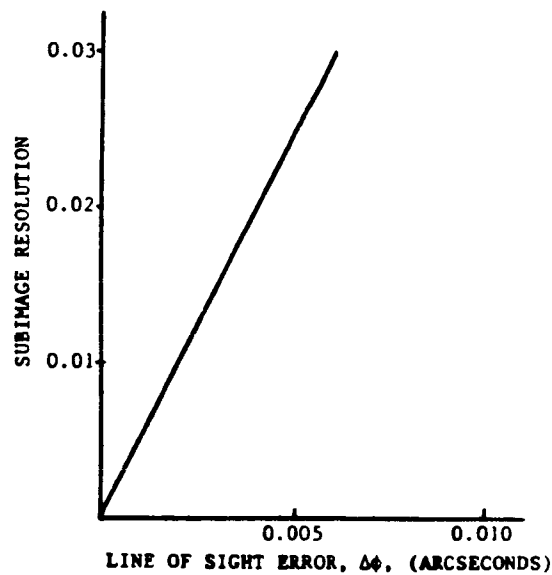
SUBIMAGE RESOLUTION REQUIREMENT

(0 = 0.20 ARCSECOND)

FIGURE 2.2-21

2.2.3 Signal Level

Stars and galaxies appear as faint sources. The light gathering power of a telescope is used to increase their detectability. Detection of a point source against a background (continuum) involves "by definition" determining that it is present and where it is located. Only those image points whose signal to noise ratio exceeds some threshold value will be detected. A threshold value of SNRp = 2.0 traditionally has been set for detection of the presence of a point object. A SNRp = 10 is considered to be the minimum allowable limit for photometric measurements. Once this value is set, the detector is integrated over the required time, t, to bring a star up to that threshold.

Astronomers denote stellar brightness (signal level) by star magnitudes. Assume two stars with brightness levels I_1 and I_2. By definition their "magnitude difference" is the quantity:

$$m_1 - m_2 = -2.5 \log (I_1/I_2)$$

Therefore to a difference of magnitude there corresponds a certain ratio of stellar brightness. More generally, a magnitude difference of -2.5n corresponds to a ratio of 10^n to 1. The brightness of a first magnitude star is 100 times greater than that of a star of magnitude (n = 2) and 10,000 times greater than that of a star of magnitude 11.0 (n = 4). In order to have a particular magnitude correspond to each stellar brightness, the magnitude of some star is arbitrarily set to determine the zero point of the scale. To each selective receiver there corresponds a particular magnitude system. In each of these the zero point of the scale is fixed by special convention.

For the eye as a detector the visual magnitude is designated m_ν. The brightness of a star of visual magnitude is given by the expression:

$$I \text{ (lumens/m}^2) = 10^{-(5.68+0.4 \, m_\nu)}$$

The brightness produced by stars of magnitudes 1.0 and 6.0 will be 8.3×10^{-7} and 8.3×10^{-9} lumens/m^2, respectively.

2-47

The standard reference for photometric astronomy is the Johnson and Morgan catalog published in 1953. Measurements were made with a 1P21 tube and three color filters: ultraviolet (U), blue (B), and yellow (V). Care has to be made in making the transition to other detectors and filters using this catalog. By convention an attempt is always made to reduce all photometric measurements to the U-B-V system of Johnson and Morgan. Luckily the magnitudes (m_v) determined with the yellow filter coincide almost exactly with those of the photovisual magnitudes (m_v).

For a star with $m_v = 0$ (above the atmosphere) the star irradiance is 3.1 x 10^{-13} watts/cm^2 (Note: Since the time of the Johnson and Morgan catalog the data has been redefined in radiometric units rather than photometric units). Therefore, the irradiance of a star of visual magnitude is given by the expression:

$$I(watts/cm^2) = 3.1 \times 10^{-(13+0.4 m_v)}$$

This is shown graphically in Figure 2.2-22. A star of 14.5 visual magnitude yields an irradiance of 4.91 x 10^{-19} watts/cm^2. From "Astrophysical quantities" by Allen there are 4.11 x 10^{15} photons per second per lumen at a wavelength of 555 nanometers. Assuming 680 lumens/watt, the following expression for the photon irradiance is derived:

$$I_p (photon/cm^2\text{-}sec) = 8.65 \times 10^{(5-0.4 m_v)}$$

These levels are also graphically shown in Figure 2.2-22
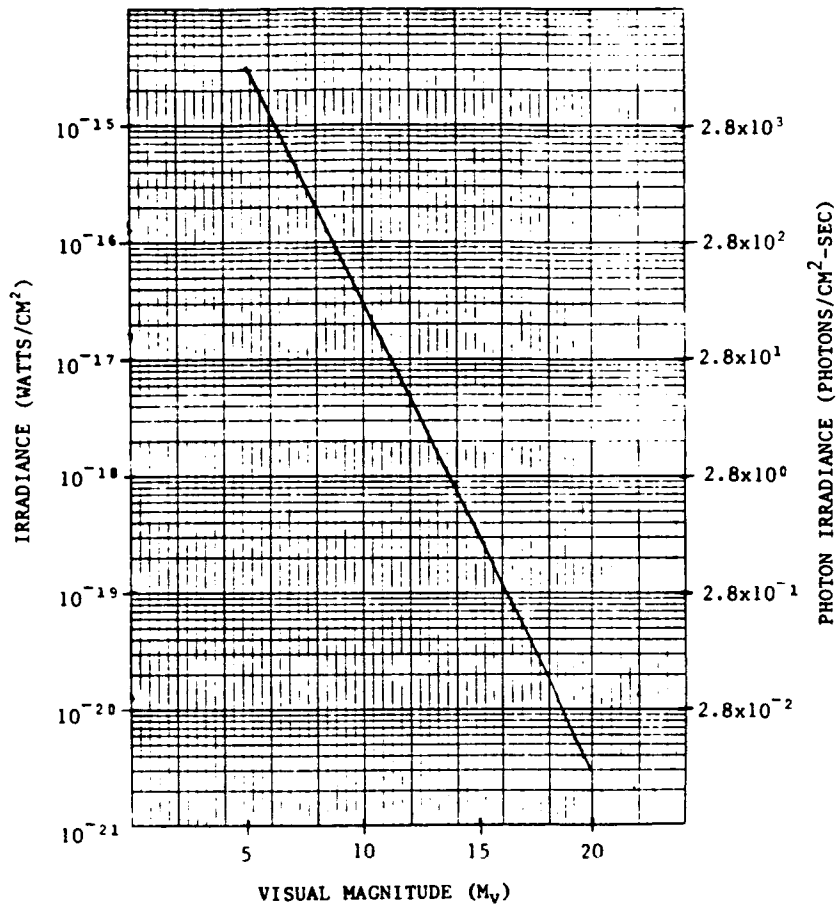
IRRADIANCE LEVELS OF VISUAL MAGNITUDE STARS

Figure 2.2-22

Shown in Figure 2.2-23 is a schematic of a telescope. The telescope is separated into two sections: the optical subsystem and the detector subsystem. The optical subsystem portion forms an image and focuses the image onto the detector. The image is regarded as the input signal which is applied to the detector. The detector may be regarded as a device which converts this input signal into some recordable form. The output signal from the detector may be the blackening of a photographic emulsion, the current from a photomultiplier or television, or numbers stored on a magnetic tape. Inherent in the assembly of the telescope is the ability to accurately determine the image plane topography as presented by the optical subsystem and the ability to match the detector surface onto this topography.

IMAGE SURFACE

DETECTOR SURFACE

θ

f

OPTICAL SUBSYSTEM

DETECTOR SUBSYSTEM

$$N_e = \left(\frac{I_p \pi D_p^2 \tau}{4} \right) \quad X \quad \left(\frac{A_d}{A_i} t \, Q \right)$$
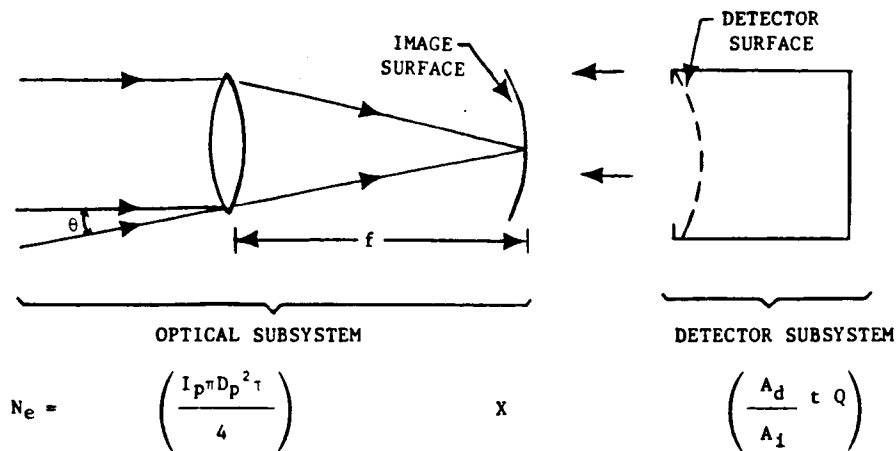
SIGNAL LEVEL OF A TELESCOPE

Figure 2.2-23

The signal is the number of photons reaching the image surface from the point source. A fraction of the image will be intercepted by the detector and converted into signal electrons. The quantum efficiency of the detector will determine the number of electrons produced. It is defined as the number of photons recorded by the detector divided by the number of photons that would have been recorded by a perfect detector under the same conditions. The quantum efficiency figure of merit is most often used in comparing the performances of detectors of the same type. (For example, the sensitivity of various photocathodes as a function of wavelength.) The concept of quantum efficiency does not allow for any photons which may have been recorded and subsequently lost. It is, therefore, not very useful in comparing photographic emulsions or other detectors where it is difficult to quantify the number of photons detected.

The change from the number of signal photons to the number of signal electrons can be expressed as follows:

$$Ne = \left(\frac{AD \; TQ}{A_i} \right) Np$$

$$= k_1 N_p$$

where: N_e - number of signal electrons

N_p - number of signal photons

A_d - detector area

A_i - image area

τ - optical subsystem transmittance

Q - quantum efficiency

k_1 - reduction factor

In the limit for the ideal telescope (100% transmittance of the optical subsystem and 100% quantum efficiency of the detector) the reduction factor is simply the ratio of the area of the detector to the area of the image.

$$N_e = R_p \left(\frac{A_d}{A_i} \right) \tau \, t \, Q$$

where: R_p - number of photons/sec

t - integration time

$$N_e = (I_p \, A_p) \left(\frac{A_d}{A_i} \right) \tau \, t \, Q$$

where: I_p - photon irradiance

A_p - optical subsystem collecting area

assuming a circular aperture with diameter Dp:

$$A_p = \frac{\pi D_p^2}{4}$$

and rearranging terms:

$$N_e = \left(\frac{\pi I_p D_p^2 \tau}{4} \right) \left(\frac{A_d}{A_i} \, t \, Q \right)$$

The first term in parentheses is called the optical subsystem signal factor. It is a function of parameters of the optical subsystem only. Shown in Figure 2.2-24 is a graph of the ideal optical subsystem signal factor (assumes 100% transmittance). It should be noted that the optical subsystem signal factor is equivalent to the number of photons/sec. In order to exceed the irradiance threshold (i.e., detect) the photon rate should be maximized by having as large an aperture as possible. Assuming an arbitrary threshold of 10,000 photons/second the limiting magnitude achievable can be obtained from the figure. (Dp = 1.0 m → $m_v \leq 14.5$; Dp = 2.4 m → $m_v \leq 16$; Dp = 20m → $m_v \leq 21$). The optical subsystem signal factor will be reduced by the optical subsystem transmittance. For a two mirror Cassegrain optical subsystem the transmittance is given by the following expression:

OPTICAL SUBSYSTEM SIGNAL FACTOR
Figure 2.2-24

$$T = \rho^2 (1 - \epsilon^2)$$

where: $\rho \sim$ mirror reflectance
$\epsilon \sim$ linear obstruction ratio

For the OTA the value for T is approximately 0.77 at a wavelength of 500 nanometers. Shown in Figure 2.2-25 is the optical subsystem signal factor taking into account this reduction in transmittance. From the graph, a star of 14.5 visual magnitude incident on a 2.4-meter diameter aperture will produce a signal of approximately 50,000 photons/second. It is important to note that once the diameter is set and the transmittance is achieved through manufacturing, the optical subsystem signal factor becomes a fixed quantity for a given limiting magnitude (i.e., signal).
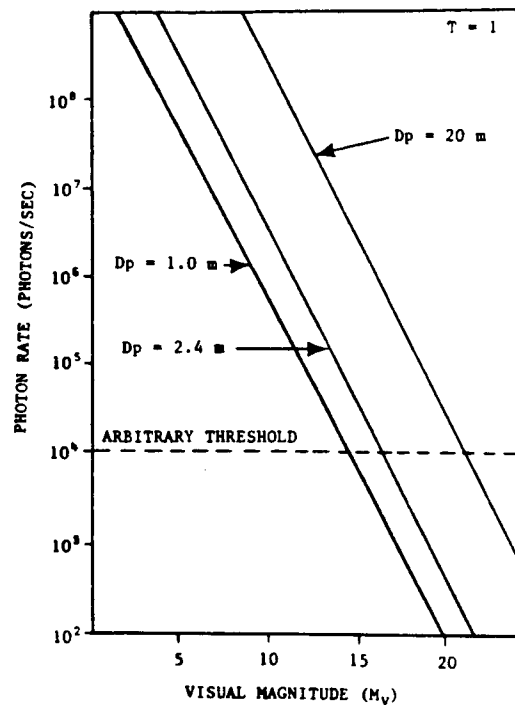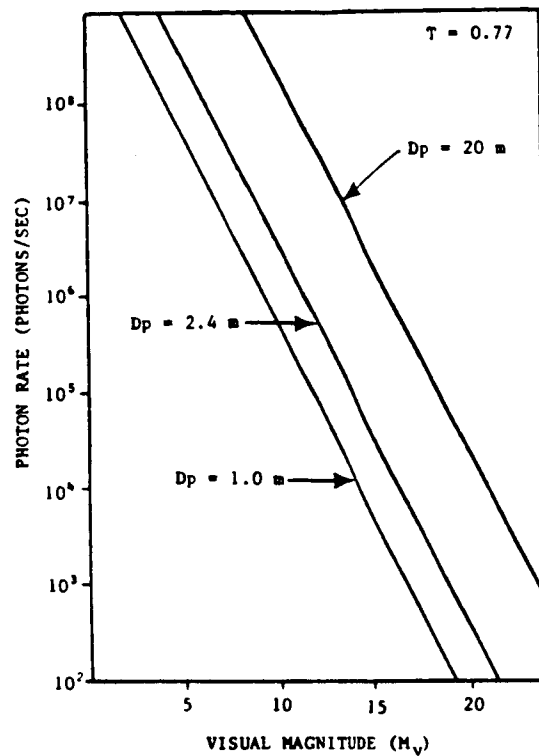
OPTICAL SUBSYSTEM SIGNAL FACTOR

Figure 2.2-25

The transformation from photons to electrons produced in the detector occurs in the detector signal factor. Shown in Figure 2.2-26 is the number of signal electrons produced to reach star magnitude threshold as a function of integration time. The ratio of the area of one detector to the area of the image is a critical factor in optimizing the detector signal factor. Some linear array alignment schemes which have been engineered in the past have had ratios as low as 1/300. A minimum value of 1/25 is probably required for a low light level application due to spot centroiding requirements.

Once this ratio is set the only variable to reach star magnitude threshold is integration time. The number of electrons for the ideal telescope case can be expressed as follows:

$$Ne = 1.57 \times 10^{(9-0.4 \, m_v)} t$$
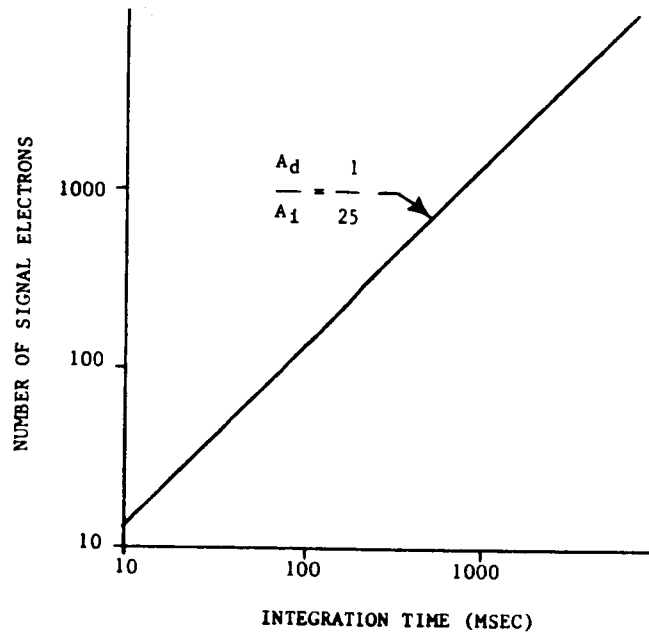
NUMBER OF SIGNAL ELECTRONS
$(m_v = 14.5)$
Figure 2.2-26

Shown in Figure 2.2-27 is the integration time required to reach star magnitude threshold (as defined by the number of electrons) for the ideal telescope case ($T = 1$; $Q = 1$). The number of electrons for a more realistic telescope ($T = 0.77$; $Q = 0.7$) can be expressed as follows:

$$Ne = 8.43 \times 10^{(8-0.4 m_v)} t$$

This is shown in Figure 2.2-28. To reach a star magnitude threshold of 14.5, there will be only 134 electrons for a millisecond integration time.
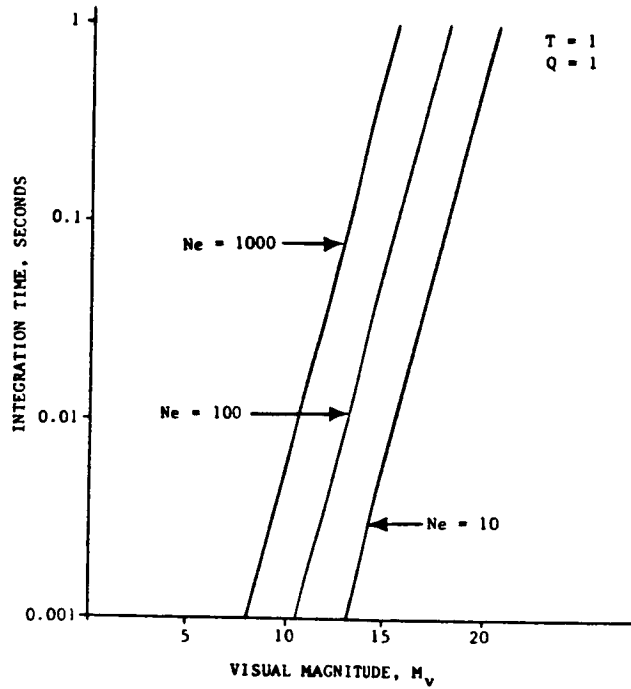
INTEGRATION TIME REQUIREMENT

Figure 2.2-27
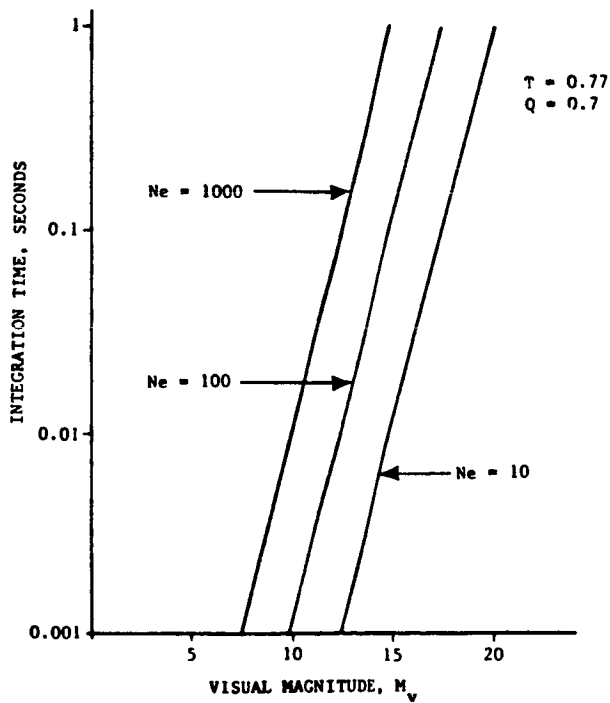
INTEGRATION TIME REQUIREMENT

Figure 2.2-28

2-55

The dark current for a room temperature, high quality, linear array is about 100 electrons for a 1.5 millisecond integration time. Since dark current scales linearly with integration time, the dark current will be about 6700 electrons for a 100 millisecond integration time. Obviously this is unacceptable. Dark current decreases, however, with temperature in a nonlinear fashion. The dark current can be decreased 67 times by lowering the temperature about 30°C. Consequently, 100 electrons of noise can be obtained with an array operated at -7°C and 100 millisecond integration time. A preliminary signal-to-noise ratio of three had been set for detection. Obviously, if a linear array was used it should be cooled as much as possible. There is, however, a lower bound at 120°K. At temperatures below this value silicon ceases to operate as a semi-conductor. Because dark current is a strong function of temperature, the temperature must be very accurately controlled. In addition to the dark current there are other noise sources which also must be minimized.

2.2.3.1 <u>Spectral Class</u> - The Harvard classification is the standard for the classification of stellar spectra. It is associated with the Henry Draper catalog which contains the spectra of more than 225,000 stars. The stars are divided into 13 classes, each being arbitrarily designated by one of the following capital letters:

Q, P, W, O, B, A, F, G, K, M, S, R, N.

Each class is divided into 10 groups (spectral types) designated by a digit from 0 to 9 placed after the capital letter of the class. The Harvard classification establishes the stars in the order of decreasing temperature (Note: The temperature is associated with the layers of the stellar atmosphere where the lines are produced). As can be seen from Table 2.2-5 the spectral class, color and temperature are related with the 0 stars being bluer and hotter than the M stars.

Johnson and Morgan made precise measurements in three colors with a 1P21 photomultiplier tube and three color filters: ultraviolet (U), blue (B), and yellow (V). Color indices are defined as the differences between the values. By convention, the color index B-V is set equal to zero for an AO star.

The detector signal is given by the following expression:

$$I = A \int F(\lambda) R(\lambda) T(\lambda) \, d\lambda$$

where:

I ~ current (amperes)

A ~ collecting area (cm^2)

F(λ) ~ spectral irradiance (watts/cm^2 - Å)

R(λ) ~ detector responsivity (amperes/watt - Å)

T(λ) ~ spectral transmittance

The instrumental magnitude, m_I can be expressed in terms of the detector signal.

$$m_I = 2.5 \log (B-V)$$

where I(0,0) is the detector response for a V = 0, B-V = 0 star and I (V,B-V) is the detector response for any star. Shown in Figure 2.2-29 is the calculated instrumental magnitude for the twenty brightest stars of the Henry Draper Catalog, using an S-20 photocathode. Assuming that the instrumental magnitude is a linear combination of the visual magnitude and the star's color the instrumental magnitude can be expressed as follows:

$$m_I = m_V + m_C$$

where:

m_V visual magnitude

m_C color correction magnitude

Table 2.2-5 HARVARD CLASSIFICATION		
SPECTRAL TYPE	SURFACE TEMPERATURE (°K)	PEAK WAVELENGTH (Å)
Oo	30,000	966
Bo	20,000	1,449
Ao	11,000	2,634
Fo	7,500	3,864
Go	6,000	4,830
Ko	5,000	5,796
Mo	3,500	8,280

*FORBES AND MITCHELL, COMMUNICATIONS OF THE LUNAR AND PLANETARY LABORATORY,
UNIVERSITY OF ARIZONA, NO. 141 (1968)

INSTRUMENTAL MAGNITUDE (m_I) VERSUS
COLOR INDEX (B-V)* (S-20 PHOTOCATHODE)
Figure 2.2-29

Using a linear regression curve fit to the data of Figure 2.2-29 yields:

$$m_I = m_V + 0.45 \ (B-V)$$

The correction magnitude is shown in Figure 2.2-30. The S-20 photocathode
with its strong response at the blue wavelengths (Figure 2.2-31) is less
sensitive to red stars and more sensitive to blue stars than the eye. In
comparison CCD spectral sensitivity curves which are red sensitive are shown
in Figure 2.2-32.
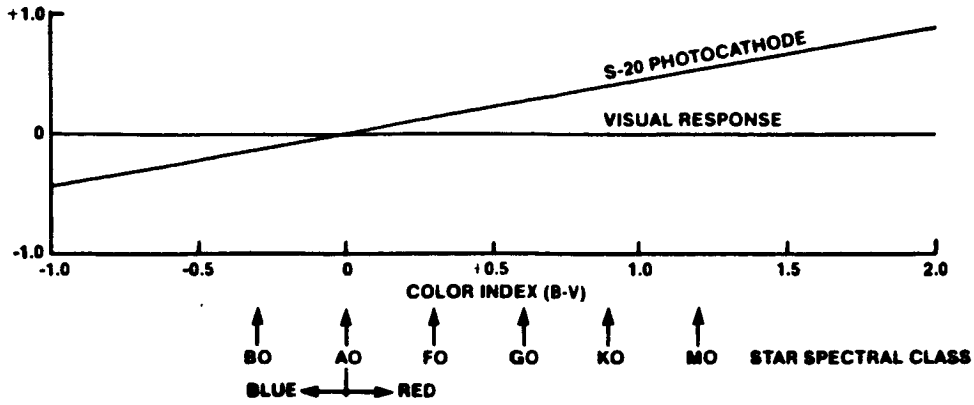
STAR SPECTRAL CLASS MAGNITUDE CORRECTION (m_c)

Figure 2.2-30
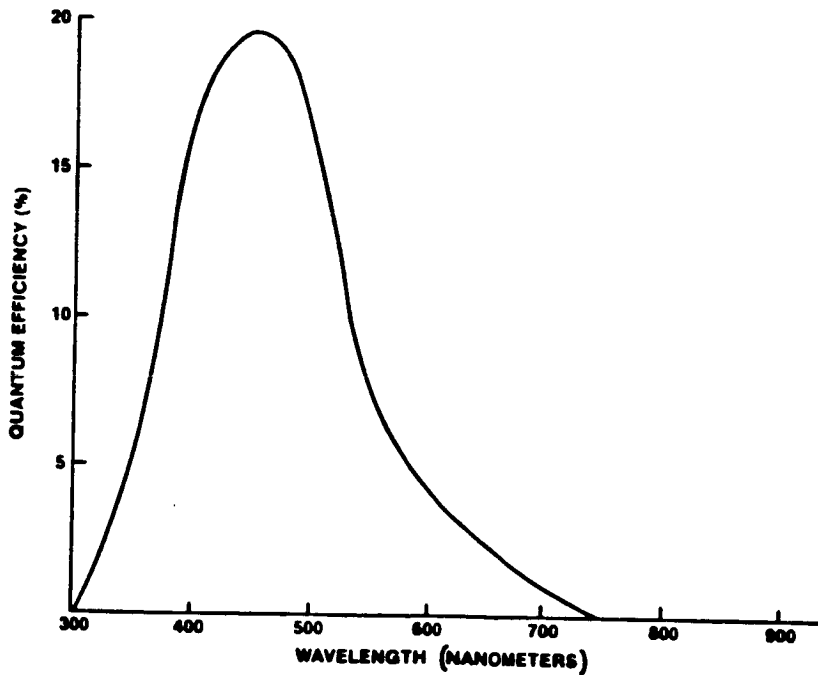
SPECTRAL QUANTUM EFFICIENCY (S-20 PHOTOCATHODE)

Figure 2.2-31

2-59
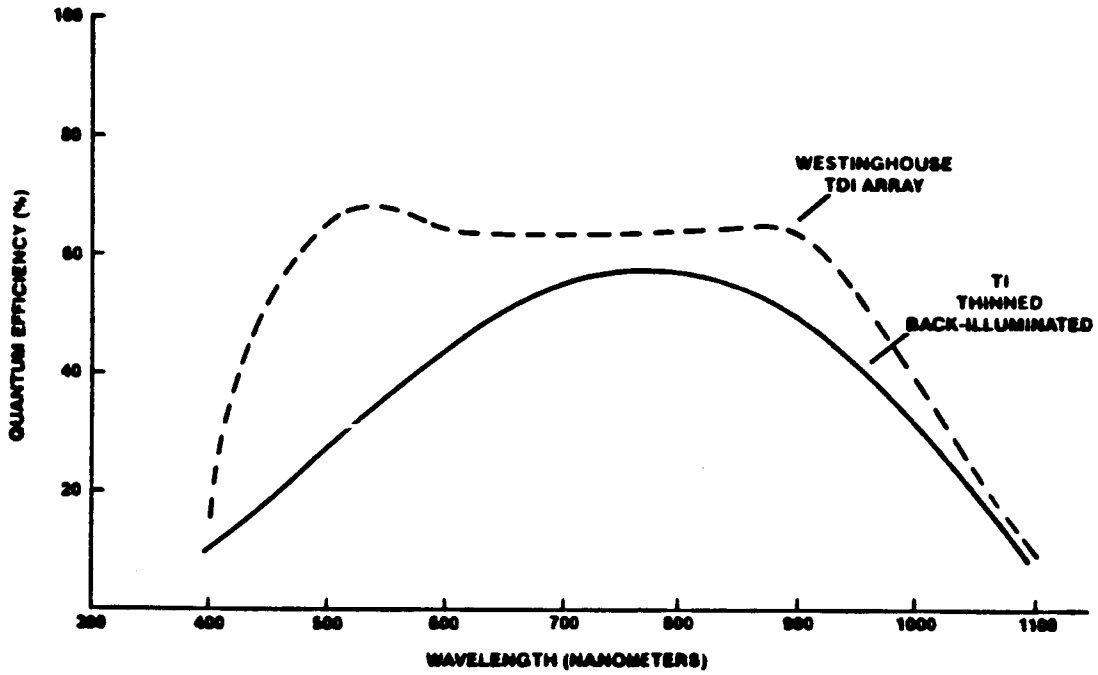
SPECTRAL QUANTUM EFFICIENCY (CCD ARRAY)

Figure 2.2-32

2-60

Shown in Figure 2.2-33 is the distribution of stars in the Henry Draper Catalog. The graph shows a greater number of red stars than blue stars. Shown in Figure 2.2-34 is the distribution of stars near the galactic pole (poorest star density region). There is definite predominance of red stars in this region.
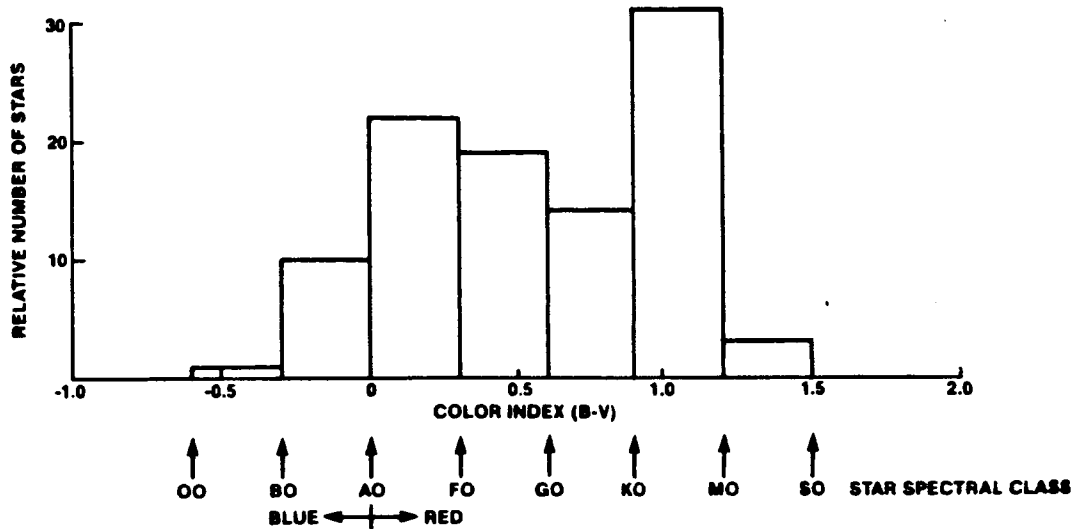
DISTRIBUTION OF STARS (HENRY DRAPER CATALOG)

Figure 2.2-33
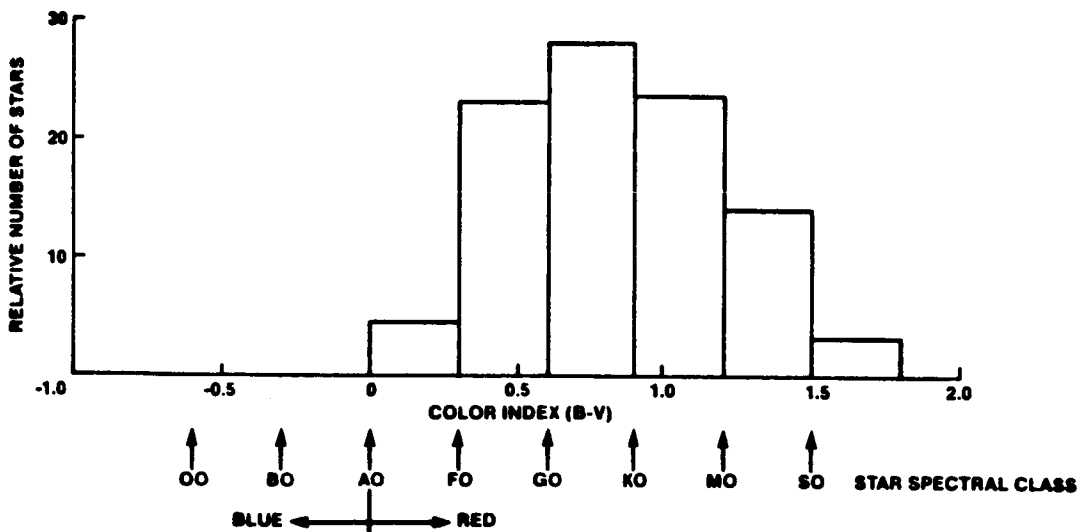
DISTRIBUTION OF STARS NEAR THE GALACTIC POLE

(U. S. NAVAL OBSERVATORY CATALOG)

Figure 2.2-34

2-61

The color corrected irradiance for a 14.5 visual magnitude star is shown in Figures 2.2-35 and 2.2-36 for a S-20 photocathode and a CCD, respectively.
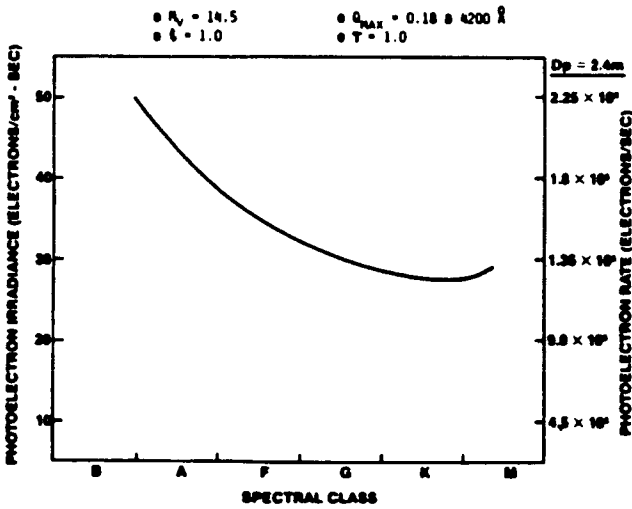
S-20 PHOTOCATHODE RESPONSE

Figure 2.2-35
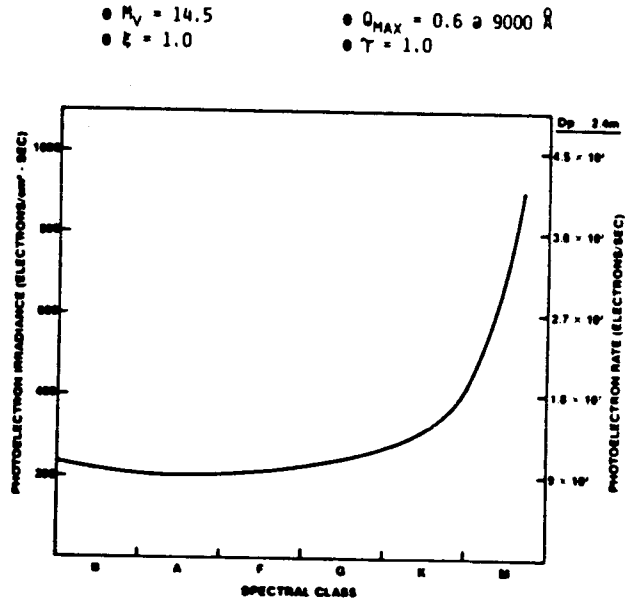
CCD DETECTOR RESPONSE

Figure 2.2-36

2.2.3.2 <u>Noise Level</u> - The fine guidance sensor is subject to two fundamental limits, the diffraction limit of the optical subsystem and the photon limit of the detector subsystem. Any source of uncertainty in the signal is called noise, and the fluctuation in the photon arrival rate is called photon noise. Shown in Figure 2.2-37 is a schematic of noise contributors. The input signal-to-noise ratio is the ratio of the input signal to the rms fluctuations in the input signal. In the limit the ideal detector uses every incident photon assuming the input photon flux follows a Poisson distribution of number of photons, n. The signal S is the mean n and the rms noise is $n^{1/2}$.
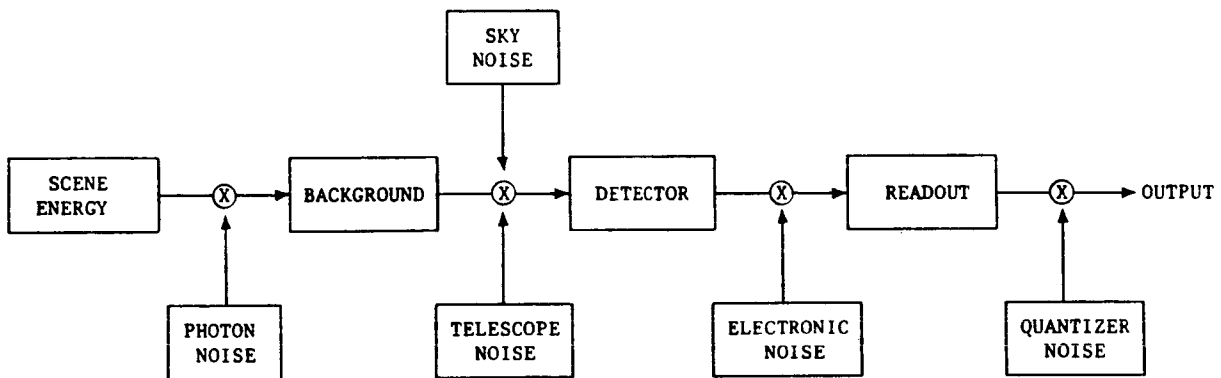
NOISE CONTRIBUTORS

Figure 2.2-37

Therefore for "photon-noise limited" performance:

$$\frac{S}{N} = \sqrt{N}$$

$$\& \; \sigma_T = \sigma_L$$

Each subsequent source of noise will reduce S/N. Apart from the strongest signals, which are photon noise limited, the final accuracy will be limited by one of the following noise contributors. Noise can be introduced by the background or at any stage of the detection process.

Background noise is caused by photons reaching the detector from sources other than the object being observed. The sky background is a major contributor to noise in star detection. The number of photons from the sky background can be as great or more than the number of photons from a faint star. Background noise can also occur in the telescope itself. At infrared wavelengths the telescope structure itself is a source of radiation.

Noise introduced by the detector can be of many kinds. In a photomultiplier, noise manifests itself as random fluctuations in the output current, which could arise at any of the various stages of generation and amplification. The term "dark current" is used to describe the current that is measured in a detector in the absence of an input signal. In a photomultiplier the detector noise can be reduced by cooling.

CCD arrays have a dark current associated with each detector. The total number of electrons collected in the CCD well is equal to the signal electrons plus the dark current. Since the dark current is a steady flow of electrons in time and independent of the signal level the average number of dark current electrons can be subtracted from the total to improve accuracy. The dark current is a statistical quantum process and thus the residual electronic noise is equal to the square root of the number of electrons.

$$\sigma_e = \sqrt{d.c.}$$

The CCD's also have preamplifiers and reset noise terms as well. The total number of electronic noise is a measured quantity for a particular device. The noise is a constant term for all pixels and is essentially signal independent. The total electronic noise standard deviations can thus be lumped into one parameter:

$$\sigma_e = k$$

noise can also be introduced in the readout system.

Each pixel must be quantified by a level, representing the number of signal electrons. Signal levels can range from one hundred to one million electrons. The analog signal from each pixel is converted to a discrete number based on a quantizing scheme. This process introduces some noise characterized by the equation:

$$\sigma_q = \frac{2^{-b} M}{\sqrt{12}}$$

where b is equal to the number of bits used to quantize the levels and m represents the maximum expected signal. If 14 bits are used to quantify the signal, the resultant noise standard deviation would be 17 electrons. Since the number of bits used in the analog to digital conversion is selectable, the quantization noise can be reduced to a negligible level. For instance, if 16 bits were used in the above scheme, the noise standard deviation would be 4.4 electrons.

The total uncertainty in the y_i values is given by taking the root-sum-square of the individual noise sources:

$$\sigma_i = \{ \sigma_r^2 + \sigma_e^2 + \sigma_q^2 \}^{\frac{1}{2}}$$

$$\sigma_i = \{ y_i + k^2 + 2^{-2b} M^2/12 \}^{\frac{1}{2}}$$

The quantizing noise can be made arbitrarily low and thus the expression becomes:

$$\sigma_i = \{ y_i + k^2 \}^{\frac{1}{2}}$$

2.2.4 Guide Field Area

The guide field area must be sized to meet the requirement of acquiring cataloged guide stars throughout an orbit with a high probability. Shown in Figure 2.2-38 is the population of visual stars for several regions of the sky. From this graph it can be seen that there are roughly an order of magnitude fewer stars suitable for tracking near the galactic pole regions in comparison to the galactic equator region. The graph shows that for stars of visual magnitude 14 or brighter, there will be, on the average, one star for every 35 square arcminutes of sky in the region of the galactic poles and one star for every 3.5 square arcminutes of sky in the region of the galactic equator. Therefore, the requirement is to find suitable guide stars in the area of the galactic poles with a high probability.
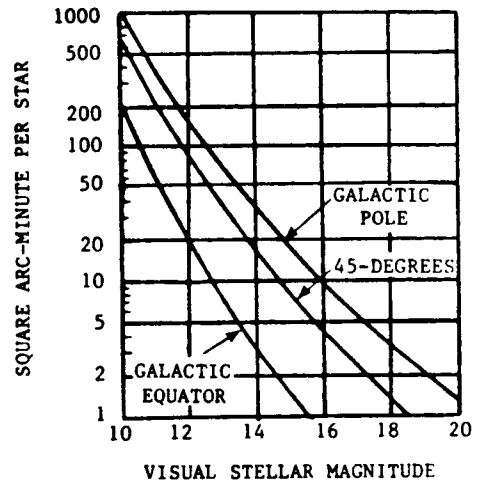
CUMULATIVE STAR DENSITY AS A
FUNCTION OF VISUAL STELLAR MAGNITUDE
Figure 2.2-38

Assume for the following probability analysis:

    N ~ number of available stars

    ΔA ~ guide field area

    Ao ~ total area (Ao >> ΔA)

  P(N,Ao)=1

The probability of not getting any stars in the guide field area is shown in Figure 2.2-39. If there is only one star on the average in the guide field area then the probability is 37% that there will not be any stars in the guide field area.

The probability of getting one and only one star in the guide field area is shown in Figure 2.2-40.
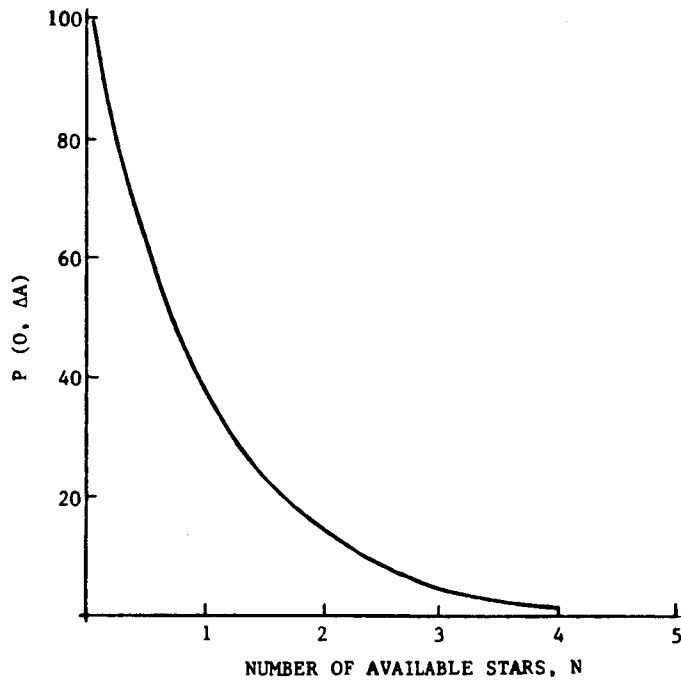
PROBABILITY OF NO STARS IN GUIDE FIELD AREA

Figure 2.2-39
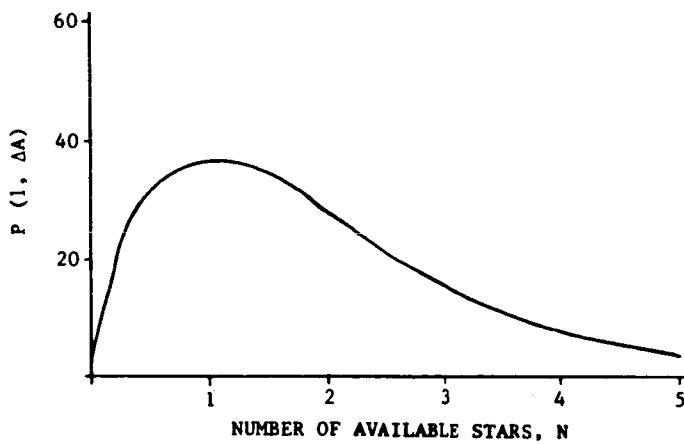
PROBABILITY OF ONE AND ONLY ONE STAR IN GUIDE FIELD AREA

Figure 2.2-40

$$P(1, \Delta A) = N\left(\frac{\Delta A}{Ao}\right)\left(1 - \frac{\Delta A}{Ao}\right)^{N-1}$$

$$\approx Ne^{-N}$$

If there is only one star on the average in the guide field area then the probability is again 37% that is one and only one star in the guide field area.

The probability of getting two and only two stars in the guide field area is shown in Figure 2.2-41.

$$P(2, \Delta A) = \frac{N(N-1)}{2}\left(\frac{\Delta A}{Ao}\right)^{2}\left(1 - \frac{A}{Ao}\right)^{N-2}$$

$$\approx \frac{N^2}{2}e^{-N}$$
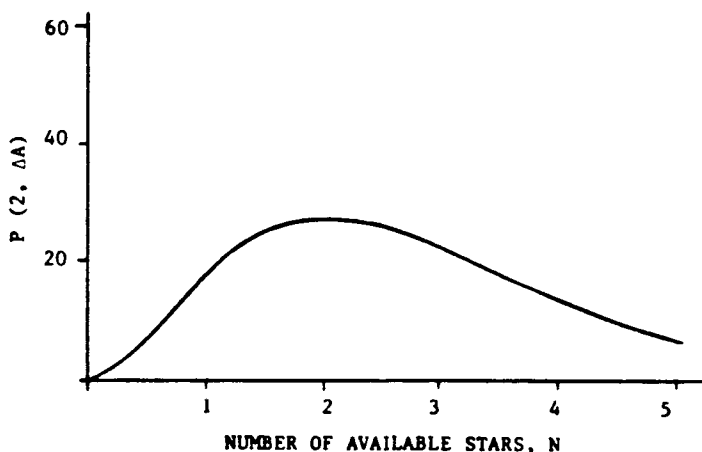
PROBABILITY OF TWO AND ONLY TWO STARS IN GUIDE FIELD AREA

Figure 2.2-41

If there are two stars on the average in the guide field area then the probability is 27% that there is two and only two stars in the guide field area.

The probability of getting one or more stars in the guide field area is shown in Figure 2.2-42. It is equal to the probability of getting all the stars minus the probability of getting no stars.

$$P(\geq 1, \triangle A) = 1 - e^{-N}$$
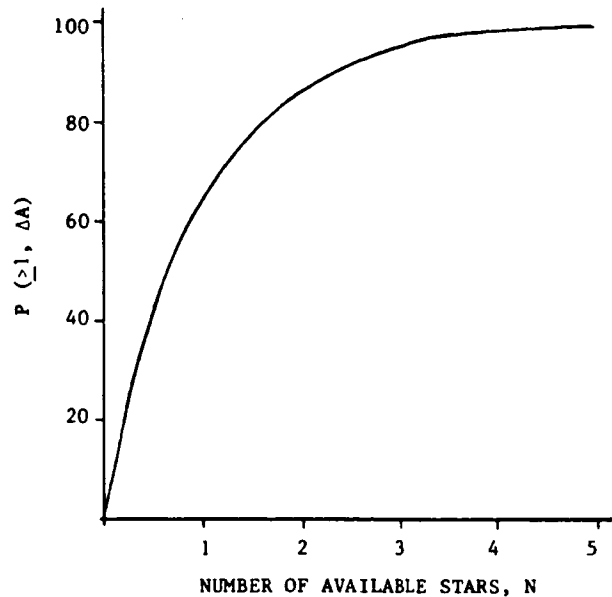
PROBABILITY OF ONE OR MORE STARS IN GUIDE FIELD AREA

Figure 2.2-42

Substituting for a probability of 85% yields N = 1.897. This means that if there are 1.897 stars on the average in the guide field area then the probability is 85% that there will be at least one star in the guide field area.

The probability of getting two or more stars in the guide field area is shown in Figure 2.2-43.

2-69

$$P(\geq 2, \triangle A) = 1 - P(0, \triangle A) - P(1, \triangle A)$$
$$= 1 - e^{-N} - Ne^{-N}$$
$$= 1 - (1+N)e^{-N}$$
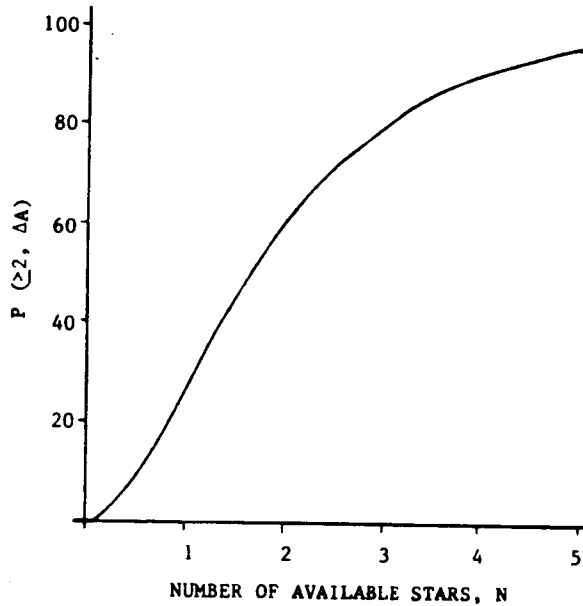
PROBABILITY OF TWO OR MORE STARS IN GUIDE FIELD AREA

Figure 2.2-43

Substituting for a probability of 85% yields N = 3.35. This means that if 3.35 stars are on the average in the guide field area then the probability is 85% that there will be at least two stars in the guide field area. Shown in Figure 2.2-44 is the relationship between the actual guide field area and the guide field area required for each star. For example, assume a guide star area of 130 square arcminutes. In order to get one star in that area with a probability of 85% the average number of stars in 130 square arcminutes will have to be 1.897. Or in other words, (130/1.897) = 68.5 square arcminutes per star.

In order to get two stars in that area with a probability of 85% the average number of stars in 130 square arcminutes will have to be 3.35. Or in other words, (130/3.35) = 38.8 square arcminutes per star.
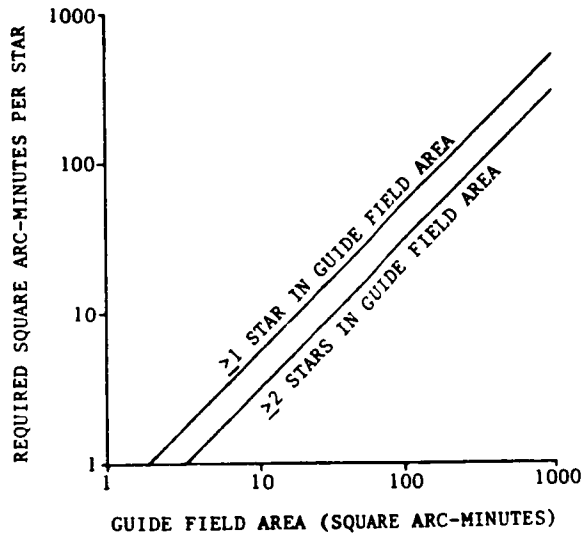
GUIDE FIELD AREA (PROBABILITY = 85%)

Figure 2.2-44

Combining Figure 2.2-44 with Figure 2.2-38 yields Figure 2.2-45. This graph gives the guide field area necessary to have either one or two visual magnitude stars in the field of view with a probability of 85%.

A regression analysis was performed and it was found that a power curve fit was best (correlation coefficient = 0.999). This results in the following expressions for the required guide star area:

$$A_{T,1} = (1.18 \times 10^{13}) \ (m_v)^{-9.7978} \quad \text{(1 star)}$$

$$A_{T,2} = (2.10 \times 10^{13}) \ (m_v)^{-9.7992} \quad \text{(2 stars)}$$

Shown in Figure 2.2-46 is the space telescope guide field area. Each fine guidance sensor currently has a guide field area of 69 square arcminutes. From Figure 2.2-45 stars with visual magnitudes as low as 14.8 would be required to be assured of having at least two stars in a single FGS with a probability of 85%. Stars with visual magnitudes as low as 13.2 would be required to be assured of having at least two stars in the total FGS field area (207 square arcminutes) with a probability of 85%. Stars with visual magnitudes as low as 12.8 would be required to be assured of having at least two stars in the total outer annulus (289 square arcminutes) with a probability of 85%.
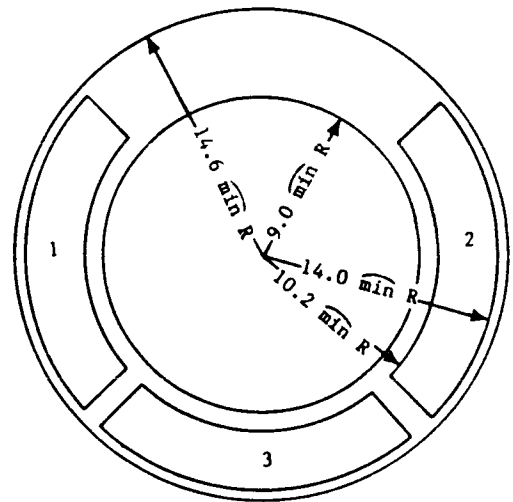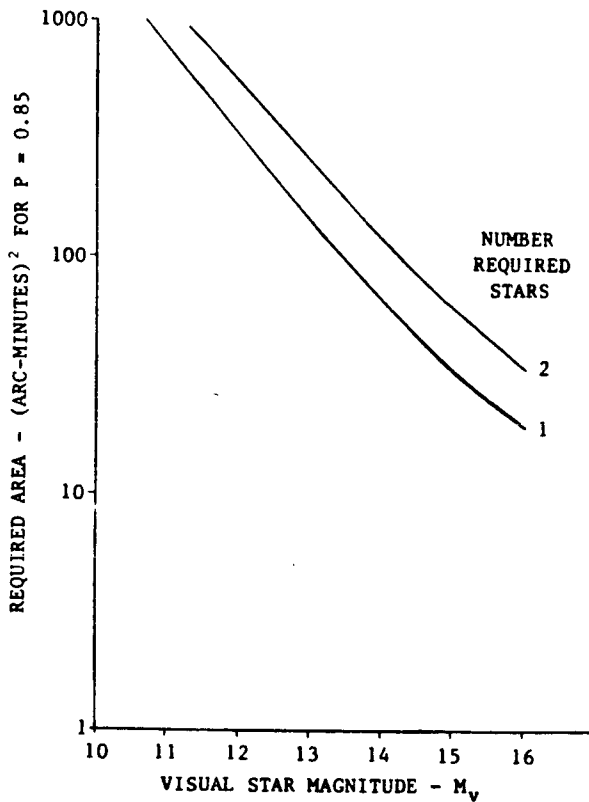
SPACE TELESCOPE GUIDE
FIELD AREA
Figure 2.2-46

GUIDE STAR AREA REQUIRED. A_T
FOR P = 0.85
Figure 2.2-45

The predominance of red stars near the galactic pole when combined with a CCD detector leads to more available stars for a given threshold magnitude than with either the eye or the S-20 photocathode as a detector.

Shown in Figure 2.2-47 is the cumulative star density (near galactic pole) as a function of instrumental magnitude (Note: In this case the instrumental magnitude is equal to the visual magnitude since B-V has been set equal to zero).
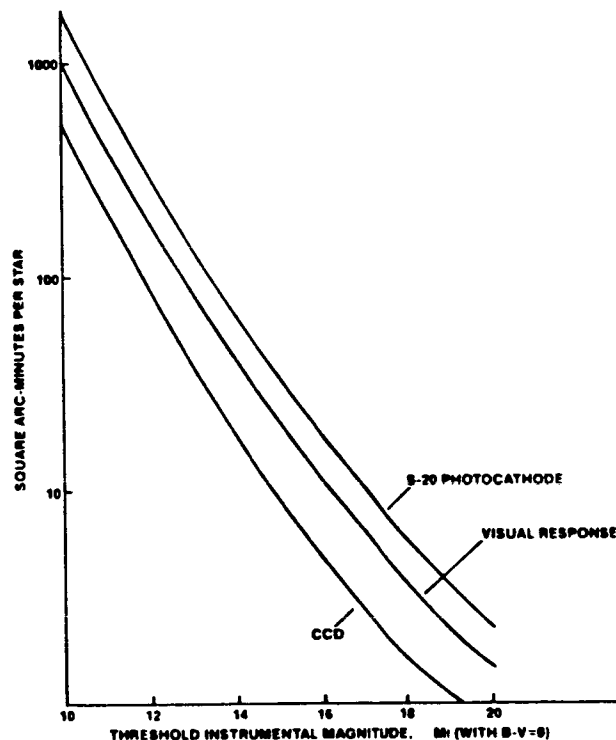
CUMULATIVE STAR DENSITY AS A FUNCTION OF INSTRUMENTAL MAGNITUDE
(NEAR GALACTIC POLE)

Figure 2.2-47

2-73

Shown in Figure 2.2-48 is the guide field area necessary to have two visual magnitude stars in the field of view. The guide star area requirements for a threshold instrumental magnitude of 14.5 are summarized in Table 2.2-6.
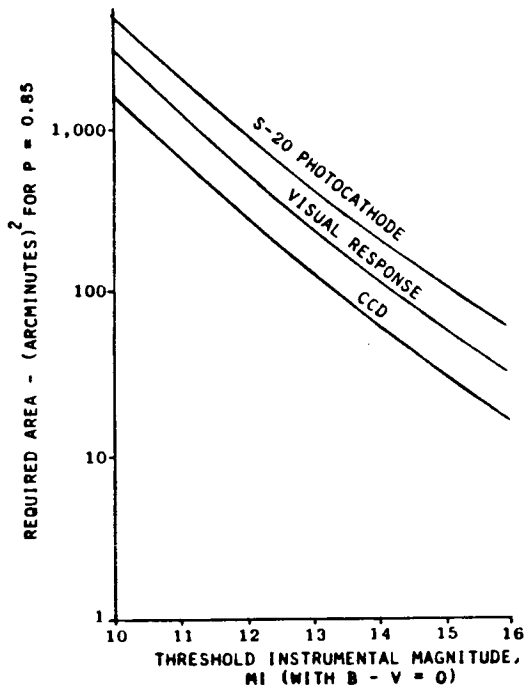
GUIDE STAR AREA REQUIREMENT, A_T

(FOR P = 0.85 OF TWO STARS)

Figure 2.2-48

Table 2.2-6 REQUIRED GUIDE STAR AREA FOR A THRESHOLD INSTRUMENTAL MAGNITUDE OF 14.5	
DESCRIPTION	GUIDE STAR AREA $(MIN)^2$
VISUAL RESPONSE	86
S-20 PHOTOCATHODE	155
CCD	46

Table 2.2-7 THRESHOLD INSTRUMENTAL MAGNITUDE (FOR P = 0.85 OF TWO STARS			
AVAILABLE GUIDE STAR AREA	VISUAL RESPONSE	S-20 PHOTOCATHODE	CCD
SINGLE FGS (69 MIN^2)	14.8	15.8	13.9
THREE FGS (207 MIN^2)	13.2	14.1	12.4
TOTAL OUTER ANNULUS (289 MIN^2)	12.8	13.6	12.1

Conversely if the available guide star area is fixed the threshold instrumental magnitude will vary as summarized in Table 2.2-7. The CCD detector in comparison to the S-20 photocathode allows the use of brighter stars to meet the requirements.

2.3 SCIENCE ASTROMETRY

Astrometry is the study of positions, motions, and distances of stars and
planets. It is therefore, the positional branch of observational astronomy in
comparison to the imaging branch of observational astronomy. Knowledge of
pointing and pointing error is fundamental to satisfying the scientific needs
of astrometry. Therefore, as a by-product in undertaking its primary objec-
tive,--to sense pointing error, data obtained by a fine guidance sensor can be
used in astrometry. There are currently five scientific instruments planned
for the Space Telescope. The fine guidance sensor will also serve as the
sixth scientific instrument. This instrument will monitor the astrometry func-
tion of Space Telescope as chartered by the Astrometry Working Group (AWG).
Each FGS will have the capability to perform astrometry on stars within its
field of view while the two other sensors maintain the pointing error of the
telescope (Figure 2.3-1).
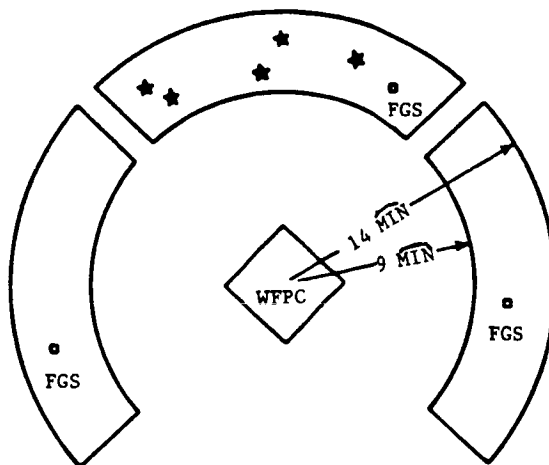
ST IMAGE PLANE, SHOWING LOCATION OF FGS FIELD OF VIEW

Figure 2.3-1

2-75

Table 2.3-1 shows the detailed astrometric requirements for the Space Tele-scope. The basic astrometric requirement is to measure the relative positions of two or more stellar objects within the field of view of a single sensor to an accuracy of ±0.002 arcsecond. This imposes a tighter pointing error accu-racy requirement than on fine guidance sensing (i.e., ±0.01 arcsecond). The minimum visual magnitude has been set at 17 in comparison to 14.5 for fine guidance sensing.

TABLE 2.3-1

ASTROMETRY REQUIREMENTS

- MEASURE THE RELATIVE ANGULAR POSITION OF TWO OR MORE OBJECTS WITHIN ITS FOV TO AN ACCURACY OF ±0.002 ARCSECOND.

- MEASURE OBJECTS WITHIN A WAVELENGTH BAND OF 4,000 TO 6,000 Å AND PROVIDE A MINIMUM OF THREE FILTERS.

- PROVIDE PHOTOMETRIC PRECISION OF ONE PERCENT.

- MEASURE OBJECTS THAT HAVE A BRIGHTNESS RANGE OF 10 TO 17 M_v.

- THE MAXIMUM INTEGRATION TIME OF A SINGLE 17 M_v OBJECT SHALL BE 10 MINUTES.

- MEASURE THE RELATIVE POSITION OF 10 STARS IN 10 MINUTES.

- PROVIDE AT LEAST A 20 SQUARE ARCMINUTE NONVIGNETTED FOV.

Shown in Figure 2.3-2 is a graph of the pointing error equation (with $\Delta f = 0$) for several telescopes. The transit circle is the fundamental telescope used in astrometry. The U. S. Naval Observatory's Six-inch Transit Circle is con-sidered the most accurate telescope in the world from the standpoint of pointing stability and pointing accuracy. It uses a refractive lens with a relatively short focal length. This results in an extremely stable system. However, due to the short focal length the overall pointing accuracy is approx-imately ±0.3 arcsecond. The Navy's astrometric reflector uses a Cassegrain optical configuration. This allows for a relatively long focal length in a compact package. To keep the knowledge of the focal length consistent with the astrometry requirements, secondary mirror to primary mirror alignment and spacing is maintained using cervit metering rods.

2-76
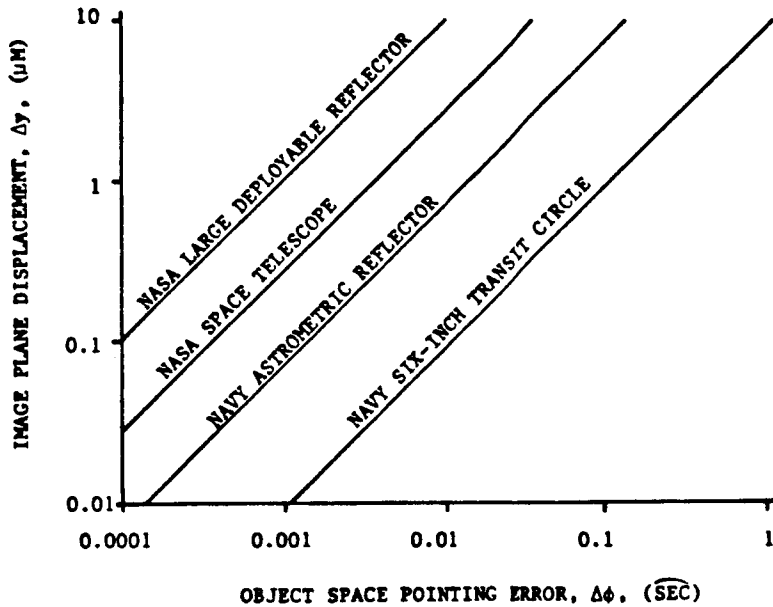
INHERENT ASTROMETRY CAPABILITY OF REPRESENTATIVE TELESCOPES

Figure 2.3-2

Under the assumption that the LOS vector can be established to an accuracy of 0.5 micrometer in the image plane, the Space Telescope with its long focal length (57.6 meters) has the inherent capability. However, the change in the telescope focal length (Δf) must be less than or, known to 137 micrometers.

3.0 LINE OF SIGHT ERROR

A lens transforms object angular information ($\phi \pm \Delta\phi$) into image displacement information ($y \pm \Delta y$) through the scale factor of focal length. The pointing error equation, previously derived is:

$$\Delta\phi = Tan^{-1}\left[\frac{\Delta y}{(f - \Delta f)} - \frac{\Delta f \ Tan \ \phi}{(f - \Delta f)}\right]$$

It can be seen from this equation that the resultant line of sight error ($\Delta\phi$) is dependent on two error sources: (1) image displacement error (Δy) and (2) focal length error (Δf). In order to minimize the line of sight error, these two errors must, therefore be minimized.

3.1 FOCAL LENGTH ERROR

The magnitude of the focal length error due to longitudinal motion of the principal plane can be determined from Figure 3.1-1.
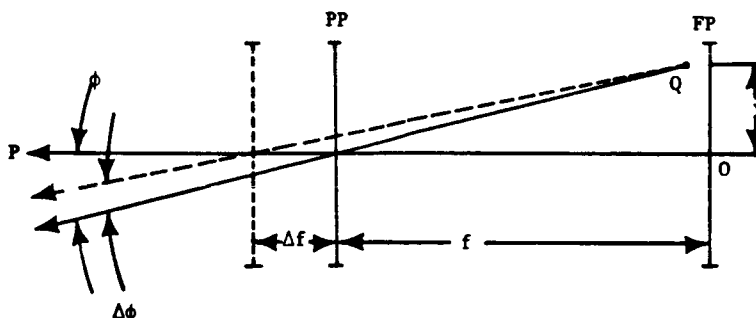
GEOMETRY OF POINTING

Figure 3.1-1

If the principal plane moves longitudinally along the optical axis the telescope focal length changes. The LOS of the telescope would not change but the LOS of any point in the field would change. In a similar manner, if the image

displacement changes, the LOS of the telescope would not change but the LOS of
any point in the field would. To determine the magnitude of the focal length
error due to longitudinal motion of the principal plane the pointing error
equation is used setting Δy =0.

$$\Delta\phi = \phi \frac{\Delta f}{f}$$

The effect of the knowledge of telescope focal length on pointing error is
shown in Figure 3.1-2. To maintain a pointing error of less than 0.010
arcsecond from the telescope LOS (pointing accuracy requirement of Space
Telescope), the change in the telescope focal length must be less than or,
known to 12 parts per million for a field point 14 arcminutes off-axis. Shown
in Figure 3.1-3 is the effect of the knowledge of the Space Telescope OTA
focal length on pointing error. To maintain a pointing error of less than
0.010 arsecond from the telescope LOS, the change in the telescope focal
length must be less than or, known to 690 micrometers for a field point 14
arcminutes off-axis.
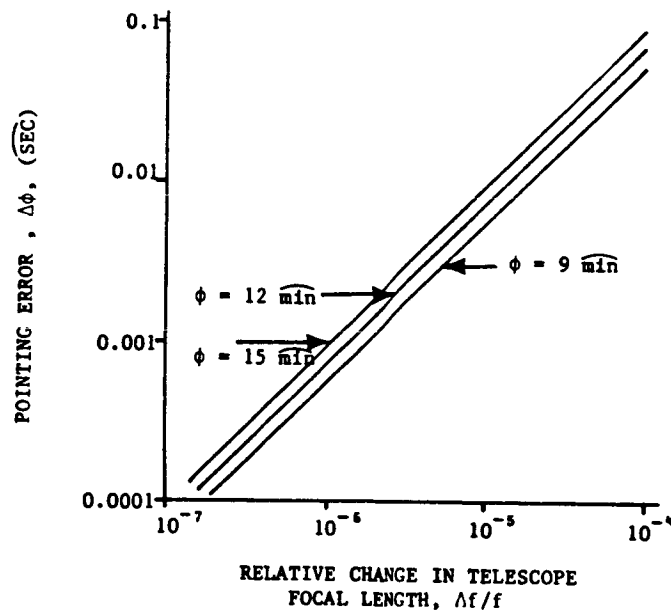
THE EFFECT OF THE KNOWLEDGE OF TELESCOPE FOCAL LENGTH
ON POINTING ERROR

Figure 3.1-2

3-2
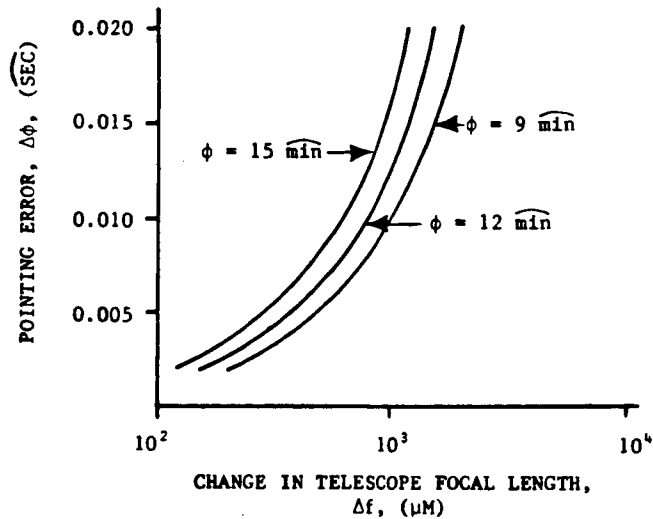
THE EFFECT OF A CHANGE IN SPACE TELESCOPE OTA FOCAL LENGTH
ON POINTING ERROR

Figure 3.1-3

The magnitude of the focal length error due to lateral motion of the principal plane can be determined from Figure 3.1-4. As shown in this figure the line of sight of the field point changes. However, in this case the LOS of the telescope, defined by OP also changes:

$$\Delta\phi = \phi' - \phi$$

$$\frac{\text{Sin } \phi'}{y} = \frac{\text{Sin } \alpha}{\left[(y - \delta)^2 + f^2\right]^{\frac{1}{2}}}$$

where

$$\text{Tan } (90^0 - \alpha) = \frac{\delta}{f}$$

or

$$\text{Sin } \phi' = \frac{y}{\left[(y - \delta)^2 + \delta^2\right]^{\frac{1}{2}}} \text{ Cos } \left(\text{Tan}^{-1} \frac{\delta}{f}\right)$$

By iteration   must be about 4300 micrometers before   reaches 0.010 arsecond. This is about 7 times the effect of longitudinal displacement of the principal plane.

3-3

To produce this amount would require a lateral misalignment of the secondary mirror of about one-tenth of this (430 micrometers). For a Cassegrain telescope this is much larger than the value allocated for secondary mirror misalignment due to wavefront error (see Figure 2.1-8). Therefore, even though both longitudinal and lateral motion of the principal plane produce focal length changes, the former is of more concern.

Also of concern is the sensitivity of lens design parameters (radius, thickness, glass) on focal length error.

The baseline optical subsystem is a Ritchey-Chretien telescope. The Cassegrain configuration consists of two hyperbolic mirrors. The focal length is a function of the primary mirror and secondary mirror focal lengths, and the secondary mirror to primary mirror spacing.

GEOMETRY OF POINTING

Figure 3.1-4

The change in focal length can be given by the following first order expression:

$$\Delta f = \pm \left(\frac{f + f_p}{f_p - S} \right) \Delta S \pm \left(\frac{f - S - B}{f_p - S} \right) \Delta f_p \pm \left(\frac{f_p}{f_p - S} \right) \Delta f_S$$

where: $f \sim$ system focal length

$f_p \sim$ primary mirror focal length

$f_s \sim$ secondary mirror focal length

$S \sim$ secondary mirror to primary mirror spacing

$B \sim$ back focal length (relative to primary mirror)

substituting for OTA parameters:

$$\Delta f = \pm 110 \ \Delta S \pm 83 \ \Delta f_p \ \pm 9 \Delta f_S$$

Assuming $\Delta S \approx \Delta f_p$ and $\Delta f_S \approx 0$

$$\Delta S = \Delta f_p \leq \frac{690}{\sqrt{2}} = 488 \text{ micrometers}$$

$$\frac{\Delta S}{S} = \frac{488}{4.9 \times 10^6} = 0.996 \times 10^{-6}$$

$$\frac{\Delta f_p}{f_p} = \frac{488}{5.52 \times 10^6} = 0.884 \times 10^{-6}$$

Thus, to point with an accuracy of 0.010 arcsecond from a field point 14 arc-minutes off-axis requires the change in the primary mirror to secondary mirror spacing, and the change in the radius of curvature of the primary mirror to be less than or known to about one part in a million.

3.2 IMAGE DISPLACEMENT ERROR

The ability to satisfy the pointing requirements can be ultimately reduced to the ability to sense a displacement of the guide stars in the focal surface corresponding to the angular pointing requirement. Changes in the calculated star image center provide a measure of the change in the line of sight of the telescope. For 0.005 arcsecond, this amounts to 1.4 micrometers at the OTA focal plane.

While the star image in the field of the OTA is highly astigmatic, the image midway between the sagittal and tangential focal surfaces is symmetrical and varies in diameter from 94 to 233 micrometers (96% encircled energy) corresponding to field positions from 9 to 15 arcminutes. Thus to sense 0.005 arcsecond requires the ability to sense a displacement of the image from 1/67 to 1/166 of its spot diameter. This also means that the energy distribution within the image spread function must remain sufficiently stable such that its centroid is determinable to at least the same fraction of diameter as the displacement requirement so that true image motion can be separated from an apparent shift in its centroid from noise sources.

3-5

3.2.1 Mathematical Definition of a Distribution Centroid

The mathematical center of a distribution can be defined for a continuous function by the following relation:

$$\xi_0 = \frac{\int_{-\infty}^{\infty} \xi f(\xi) d\xi}{\int_{-\infty}^{\infty} f(\xi) d\xi}$$

The ξ_0 value that satisfies the equation is the mathematical center. An ensemble of discrete elements also has a mathematical center. The center of mass of a three dimensional object characterized by a discrete collection of mass units can be calculated by summing the multiple of each unit and its distance from the center. Mathematically this can be represented by:

$$0 = \Sigma (\bar{r}_i - \bar{r}_c) \, m_i$$

where r_i represents the position vector of the i th unit of mass m_i. r_c is the position vector of the center of mass. Solving for r_c the equation becomes:

$$\bar{r}_c = \frac{\Sigma \bar{r}_i m_i}{\Sigma m_i}$$

The equation presented is in vector notation and thus represents three independent equations. A similar equation for each orthogonal coordinate can be written:

$$x_c = \frac{\Sigma_i x_i m_i}{\Sigma_i m_i}$$

$$y_c = \frac{\Sigma_i y_i m_i}{\Sigma_i m_i}$$

$$z_c = \frac{\Sigma_i z_i m_i}{\Sigma_i m_i}$$

The center position of a spot of light can be calculated in much the same way. Light is quantized in indivisable units called photons. If the position of each photon is known, the center of the distribution is given by:

$$x_c = \frac{\Sigma x_i p_i}{N}$$

$$y_c = \frac{\Sigma y_i p_i}{N}$$

where $N = \sum_i p_i$; the number of total photons, and p_i is the number of photons in the i th pixel.

As a matter of practicality, the position of an incident photon cannot be known. Instead the number of photons incident on a region of space (detector) is the experimental observable. Detectors by their nature are discrete.

Therefore, the signal output from a detector is given by the integration of the number of photons over its entire area. Thus the positional information of each photon is lost.

Consider the case of linear array CCD. Let x_i represent a sequence of numbers corresponding to the center positions of the pixels. Let y_i represent a sequence of numbers corresponding to the number of photons incident on the i th pixel. If the theoretical spot profile is characterized by the continuous function $g(x)$, then the discrete values y_i are given by:

$$y_i = \int g \, da$$

where the integration is taken over the i th pixel's area.

The y_i values can equivalently be represented by discrete values of the continuous function $h(x)$.

The function h(x) is related to the spot profile function g(x) by the convolution process. Mathematically this is given by:

$$h(x) = r(x) \bullet g(x)$$

$$h(x) = F\{R(w) \star G(w)\}$$

where $R(w) = F\{r(x)\}$

and $G(w) = F\{g(x)\}$

$F\{ \ \}$ represents the Fourier transform operations and $F^{-1}\{ \ \}$ represents the inverse transform such that:

$$g(x) = \overset{-1}{F}\{F\{g(x)\}\}$$

The function h(x) is useful because the number of incident photons falling on the i th pixel, y_i is given by the relation:

$$y_i = h(x_i)$$

3.2.2 Centroid Error

A mean algorithm will be used to calculate the centroid from the energy incident on each pixel of an array on which the spot was incident. The error between the calculated centroid and the true centroid (the position of the mean of the Gaussian) has been expressed as a fraction of the spot diameter. Theoretical and hardware error sources limit the accuracy of the centroid calculation. Among the error sources considered were discrete distribution sampling, photon arrival statistics, electronic noise, and level quantization noise.

3.2.2.1 Discrete Distribution Sampling – An ensemble of discrete samples is an approximation to a continuous function. The calculated center for the discrete samples does not in general yield the same value as that for its continuous analog. The magnitude of the error depends on the placement of the center of a pixel relative to the center of the continuous distribution.

3-8

The exact center is given by:

$$x_o = \frac{\int x g(x) dx}{\int g(x) dx}$$

The discrete sampled center is given by:

$$x_c = \frac{\Sigma_i x_i h(x_i)}{\Sigma_i h(x_i)}$$

The discrete sampling error is then given by:

$$\varepsilon_{ds}(x_o) = x_c - x_o$$

The error is a function of the mathematical center x_o and the number of discrete samples. As the number of pixels used to characterize the light distribution increases, the error diminishes. The symmetry of the situation also dictates that for the case of the distribution centered exactly over a pixel center or pixel edge, the error is zero.

The previous analysis assumed that the y_i values corresponding to the light collected by the i th pixel were continuous and exact.

The y_i values in reality can be characterized as a Gaussian random variable with an average value plus a random value. The uncertainty in the Yi values σ_i leads to an uncertainty in the calculated center of the light distribution.

Consider a sequence of values V_k such that:

$$V_k = V(x_k, y_k)$$

where x_k and y_k represent independent variables associated with the k_{th} value of V. The average and most probable value of V is given by:

$$V = V(x, y)$$

3-9

C-2

where:

$$x = \lim_{N \to \infty} \frac{1}{N} \Sigma x_j$$

and

$$= \lim_{N \to \infty} \frac{1}{N} \Sigma y_i$$

The deviation from the average value $\bar{V}$ is given by:

$$\delta V_n = V_n - V(\bar{x}, \bar{y})$$

Using a first order approximation:

$$\delta V_n = \frac{\partial V}{\partial x} \delta x_n + \frac{\partial V}{\partial y} \delta y_n$$

where:

$$\delta x_n = x_n - \bar{x}$$

and

$$\delta y_n = y_n - \bar{y}$$

The standard deviation in the variable V is thus given by taking the limit as k approaches infinity of δV^2.

$$\sigma_v = \lim_{k \to \infty} \frac{\Sigma (\delta V_n)^2}{k}$$

3-10

The result in terms of the independent variables X and Y is given as:

$$\sigma_v = \left\{ \left(\frac{\delta V}{\delta x}\right)^2 \sigma_x^2 + \left(\frac{\delta V}{\delta y}\right)^2 \sigma_y^2 + 2P_{xy}\left(\frac{\delta V}{\delta x}\right)\left(\frac{\delta V}{\delta y}\right)\sigma_x \sigma_y \right\}^{1/2}$$

If the variables X and Y are independent of each other P_{xy} is equal to zero. The general equation for the standard deviation of a sequence V, a function of an independent variable $x_1, x_2, \ldots, x_n$ is given below.

$$\sigma_y = \left\{ \Sigma_i \left(\frac{\partial V}{\partial x_i}\right)^2 \sigma_{x_i}^2 \right\}^{1/2}$$

This equation relates the propagated system error of an observable to the error of individual elements. For the case of centroid error calculation due to uncertainties in the Y_i values, the characteristic error equation becomes:

$$\sigma_y = \left\{ \Sigma_i \left(\frac{\partial x_c}{\partial y_i}\right)^2 \sigma_{y_i}^2 \right\}^{1/2}$$

where:

$$x_c = \frac{\Sigma_i x_i y_i}{\Sigma_i y_i}$$

and

$$y_i = h(x_i)$$

Differentiating x_c with respect to y_i yields:

$$\frac{\partial x_c}{\partial y_i} = \frac{x_i}{\Sigma y_i} - \frac{\Sigma x_i y_i}{(\Sigma y_i)^2}$$

This can be simplified:

$$\frac{\partial x_c}{\partial y_i} = \frac{1}{\Sigma y_i}(x_i - x_c)$$

Combining expressions produces the following results:

$$\sigma_y = \frac{1}{\Sigma y_i} \{ \Sigma_i (x_i - x_c)^2 \sigma_{y_i}^2 \}^{1/2}$$

The form of this equation is remarkably similar to the expression for the centroid calculation:

$$x_c = \frac{1}{\Sigma y_i} \{ \Sigma_i x_i y_i \}$$

The standard deviation in the centroid calculation is equal to the centroid of the uncertainties in the individual pixel values.

The term σy represents the uncertainty of the centroid calculation due to the individual pixel signal electrons. The term σ_x is correspondingly the uncertainty due to the x_i values. The expression for σ_x therefore simplifies to:

$$\sigma_x = \{ \Sigma \sigma_{x_i}^2 \}^{1/2}$$

The centroid calculation error due to uncertainties in the x_i and y_i values is given by:

$$\sigma_{xy} = \{ \sigma_y^2 + \sigma_x^2 \}^{1/2}$$

$$\sigma_{xy} = \{ \frac{1}{(\Sigma y_i)^2} \Sigma_i (x_i - x_c)^2 \sigma_{y_i}^2 + \Sigma_i \sigma_{x_i}^2 \}^{1/2}$$

The total error incorporating the error due to the discrete sampling process is thus:

$$\sigma_t = \{ \epsilon_{ds}^2 + \sigma_x^2 + \sigma_y^2 \}^{1/2}$$

The terms σ_x and σ_y represent the standard of the centroid calculation x_c. The term ϵ_{ds} represents the deviation of the centroid calculation from the theoretical distribution center. This equation describes the expected error in the centroid calculation as a function of the uncertainties in the pixel values and pixel locations as well as the placement of the light distribution relative to a pixel center. The error term due to discrete sampling ϵ_{ds}, is a systematic error. It does not affect the precision of the centroid calculation, just the accuracy. As such the error can be mapped as a function distance across a pixel and subtracted from the calculated value yielding a more accurate result. The error function ϵ depends on the shape and size of the light distribution. As long as these two parameters are not changed, the error function is uniquely defined.

Let the following terms be defined as:

$\epsilon(X)$: error function

X_s: a particular centroid calculation

X_c': the centroid calculation without error correction

X_c the error corrected centroid calculation

xs: standard deviation of X_s

xc: standard deviation of X_c

The standard deviation of each centroid value X_s is σ_{xs} and the systematic error associated with it is $\epsilon(X_s)$. The total uncertainty in the centroid calculation is thus:

$$\sigma_{xc} = \{ \sigma_{xs}^2 + \epsilon(x) \}^{1/2}$$

The error corrected sampled centroid value is given by:

$$x_c = x_s + \epsilon(x_s)$$

The standard deviation of X_c is defined as σ_{x_c}. It can be mathematically determined by using the error sensitivity equation.

$$\sigma_v = \left\{ \ \Sigma_i (\frac{\partial V}{\partial x_i})^2 \ \sigma_{x_i}^2 \ \right\}^{1/2}$$

The expression for x_c becomes

$$\sigma_{xc} = \left\{ \ (\ 1 + \frac{\partial \epsilon}{\partial x_s})^2 \sigma_{xs}^2 \ \right\}^{1/2}$$

This can be simplified as:

$$\sigma_{xc} \simeq \sigma_{xs} \ (\ 1 + \frac{\partial \epsilon}{\partial x_s} \ )$$

The error function due to the symmetry of the geometry is periodic and anti-symmetric. Thus the error function ϵ can be approximated as a sinusoid with a unity frequency and amplitude,

Let $\quad \epsilon(x) = \epsilon_0 SIN(x)$

then $\quad \dfrac{\partial \epsilon}{\partial x} = \epsilon_0 COS(x)$

and $\quad < \dfrac{\partial \epsilon}{\partial x} > = \epsilon_0 /\sqrt{2}$

The error corrected centroid standard deviation is thus:

$$\sigma_{xc} = \sigma_{xs} \; (\; 1 \; + \; \epsilon_o / \sqrt{2} \;)$$

The expression for the standard deviation needs some interpretation. The amplitude of the error function ϵ_o is calibrated in units of pixels.

If $\qquad \epsilon_o \ll 1$ pixel

then $\qquad \sigma_{xc} \simeq \sigma_{xs}$

The error corrected centroid standard deviation is approximated by the standard deviation of sampled values regardless of the relative magnitude of the error function amplitude. A numerical example is provided below:

let $\qquad \epsilon_o = .05$
$\qquad \sigma_{xs} = .05$

then
$\qquad \sigma_{xc} = .0518$
$\qquad \sigma_{xc} = .0707$

The error corrected standard deviation is essentially equal to the standard deviation of the sampled centroid values. In other words, the systematic error can be essentially neglected.

If the systematic error in centroiding is corrected, the remaining calculation errors are due to the uncertainity in the Yi and Xi values.

The $\ddot{x}_i$ and y_i variables contain both systematic and random errors. The systematic error sources are time invariant and can, in general, be corrected by mapping the array's characteristics.

3-15

Photo response nonuniformity is the most notable systematic error in the y_i's. The response to a uniform light source varies from pixel to pixel. The measured response of each pixel can be used to adjust the image data. The response characteristics of array tends to be a weak function of temperature and irradiance level. Therefore, most of the systematic error due to photo response characteristics can be neglected.

The systematic error in the x_i values arises from inaccuracies in the integrated circuit masking process. The pixels are not equally spaced. usually The inaccuracies of the center-to-center pixel distances are exceedingly small. The array does not change its intrapixel spacings with time and therefore any errors incurred of this type can be compensated.

The random error sources in the centroiding calculation limit the accuracy of the process. Randomness of the x_i variables relates to the uncertainties in the center location of the entire array. The uncertainty in the y_i variables impacts accuracy of the centroid calculation relative to the array coordinate system.

A Fast Fourier Transform algorithm was used to calculate the h(x) function. The sequence of $h(x_i)$ numbers were stored in an array with i th element representing the number of photons collected by the i th pixel for a normalized Gaussian beam. The centroid X_c, the error function ε, and the standard deviation σxc were calculated directly. The definition for the width of a Gaussian beam was taken as the $\pm 2\sigma$ points. The "spot" size for all numerical cases is a distance equal to 4σ for a Gaussian distribution characterized by a σ standard deviation.

The general shape of the linearity bias error (ε) is shown in Figure 3.2-1. It is independent of the number of incident photons, and results from the discrete sampling of the Gaussian spot by pixels of finite width. It is a function of the
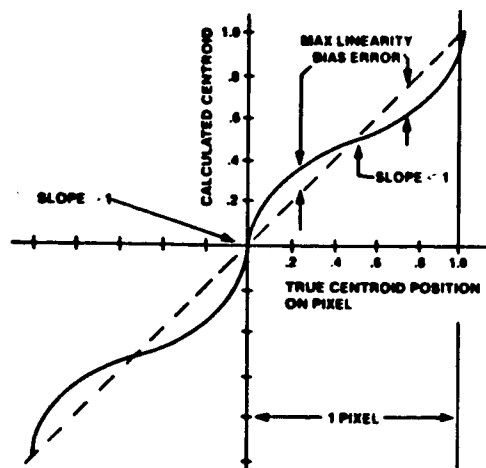
LINEARITY BIAS ERROR
Figure 3.2.1

3-16

position of the true spot centroid within a pixel and the number of pixels per spot.

Figure 3.2-2 shows the ε function value dependence on the location of the center of a continuous Gaussian X_0, relative to the pixel center. The X distance 0, 0.5, and 1.0 represent the edge; center and edge of pixel, respectively. The function was calculated for different X_0 values for a spot size equal to 2.0 pixels.

CENTROID NON LINEARITY
(ε ERROR FUNCTION)
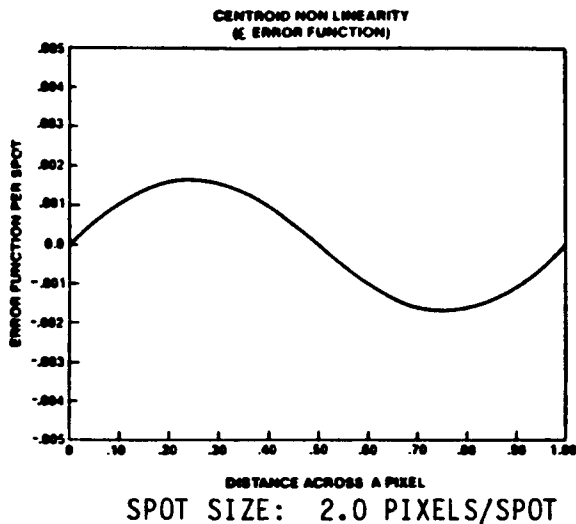
SPOT SIZE: 2.0 PIXELS/SPOT
Figure 3.2-2

The error function represents an inherent inaccuracy in the centroid calculation unless otherwise compensated.

The function appears to be sinusoidal and antisymmetric about the center of the pixel. The amplitude is low; less than 1/500 of a spot.

The ε error function maximum amplitude is shown as a function of the spot size in Figure 3.2-3. Its maximum value occurs when the true centroid is located either at 1/4 or at 3/4 the width of a pixel. The maximum value is less than 0.01 spot for 1.7 or more pixels per spot.

For small spot sizes this term can represent a problem. It should be noted that a spot size equal to one pixel represents the situation of nearly all of the energy on one pixel. Enhanced centroid accuracy can be obtained by increasing the spot size

CENTROID ALGORITHM ERROR FUNCTION
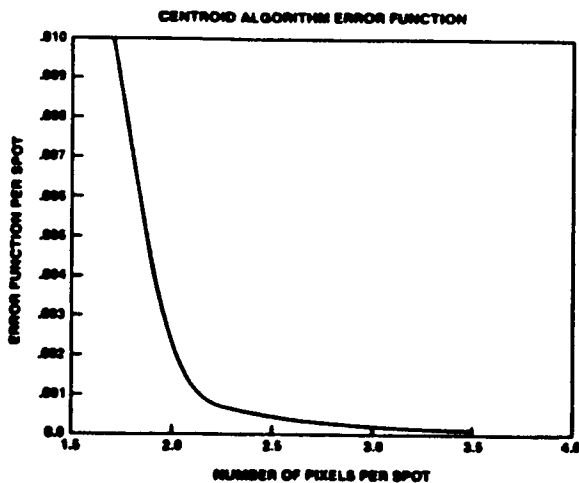
MAXIMUM LINEARITY BIAS ERROR
Figure 3.2-3

3-17

relative to the pixel width. The curve significantly flattens out at about 2.0 pixels per spot.

3.2.2.2 <u>Photon Arrival Statistics</u> - The number of signal electrons for each pixel is described by the Yi values. The result and statistical photon shot noise is thus given as:

$$\sigma_i = \sqrt{y_i}$$

This term is signal dependent and vanishes for pixels not receiving light. It is inherent in every light source.

The error from photon shot noise results from the statistical behavior of a finite number of incident photons on each pixel of the array covered by the Gaussian spot as calculated by the mean algorithm.

The standard deviation σ_{xc} due to photon shot noise alone is shown as a function of spot size in Figure 3.2-4 and expanded in Figure 3.2-5.

The error represents a variation about the linearity bias error (standard deviation about an average $\bar{X}s$). It is a function of the position of the true centroid (X_o) as shown by curves numbered 0 to 0.5 representing the position of the true spot within the pixel.

The ordinate is in subspot resolution units and normalized to $\sqrt{N}$ where N is equal to the average number of photoelectrons contained in the spot. Even though the ε error function is small it has an effect on the photon shot noise process. An X_o value of 0 represents the situation of the spot directly centered on the pixel.

The spread in σ_{xc} values as a function of the true spot location changes with spot size. The figures indicate that the centroid inaccuracy becomes independent of the relative location of the spot center to the pixel center as the spot size is increased.
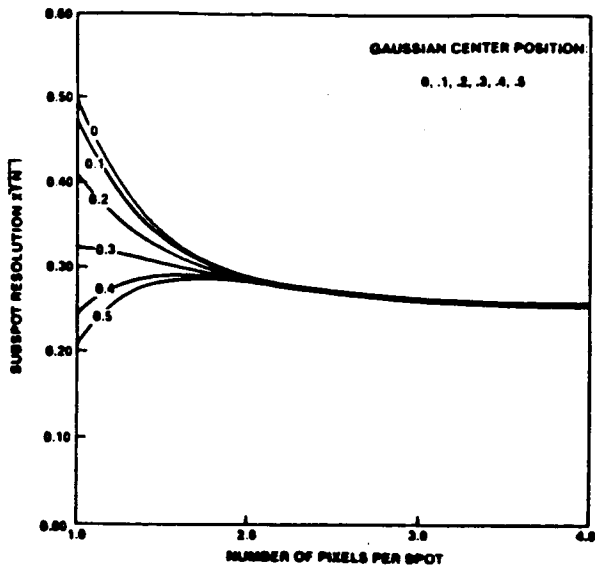
SPOT RESOLUTION (PHOTON SHOT NOISE)

Figure 3.2-4
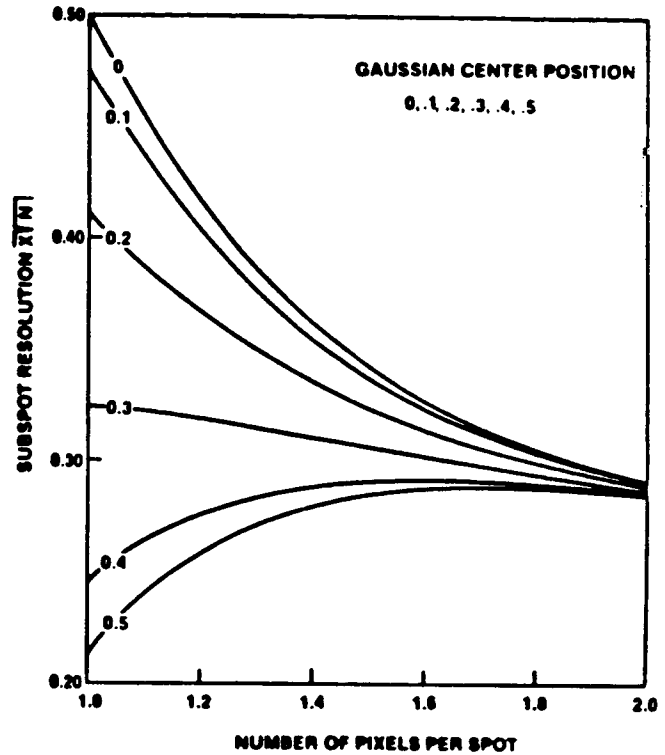
SUBSPOT RESOLUTION (PHOTON SHOT NOISE)

Figure 3.2-5

Subspot resolution as displayed in Figures 3.2-4 and 3.2-5 must, however, be modified to indicate the real ability to sense displacement within the limit of shot noise. From Figures 3.2-4 and 3.2-5 the subspot resolution is smallest at the midpoint. The slope of linearity bias error curve is a measure of sensitivity to detect displacement. At the pixel midpoint, the sensitivity to motion is less than at the edge. Figures 3.2-6 and 3.2-7 reflect an adjustment to the subspot resolution. The pixel midpoint has the highest error. It should be noted how rapidly the variation within a pixel becomes negligible. At two pixels per spot it is barely perceptible. The standard deviation of the shot noise error taking the sensitivity to displacement into account is less than 0.01 of a spot at 2 pixels per spot and for 1000 total photons within the spot.

EASTMAN KODAK COMPANY · 901 ELMGROVE ROAD · ROCHESTER, NEW YORK 14650 ·
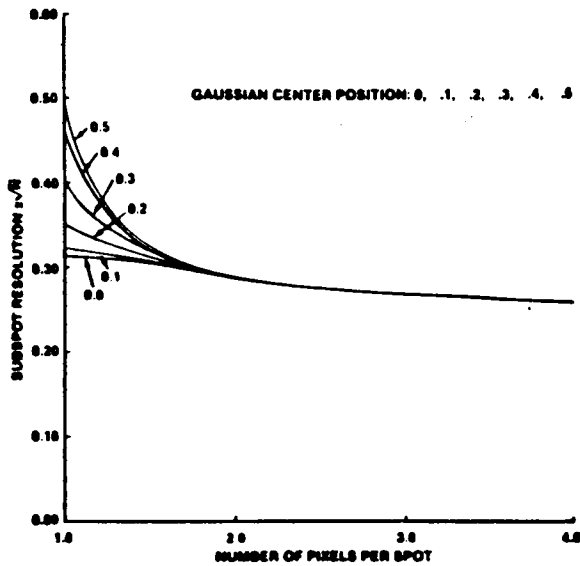
ADJUSTED SUBSPOT RESOLUTION
(PHOTON SHOT NOISE)
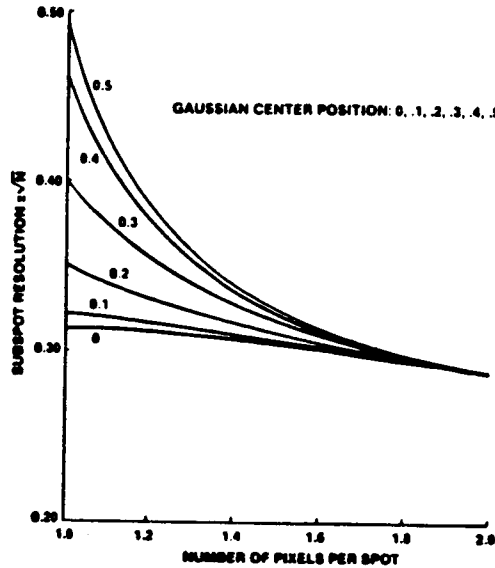
Figure 3.2-6

ADJUSTED SUBSPOT RESOLUTION
(PHOTON SHOT NOISE)

Figure 3.2-7

Figure 3.2-8 shows the advantage of using more pixels (samples) to calculate the centroid. No appreciable advantage is obtained by using more than about 3.0 pixels per spot. The family of curves demonstrates the photon shot noise limit of centroiding. The photon shot noise is proportional to the square root of the number of photons and thus the accuracy of centroiding is inversely proportional to the square root of the number of photo electrons.
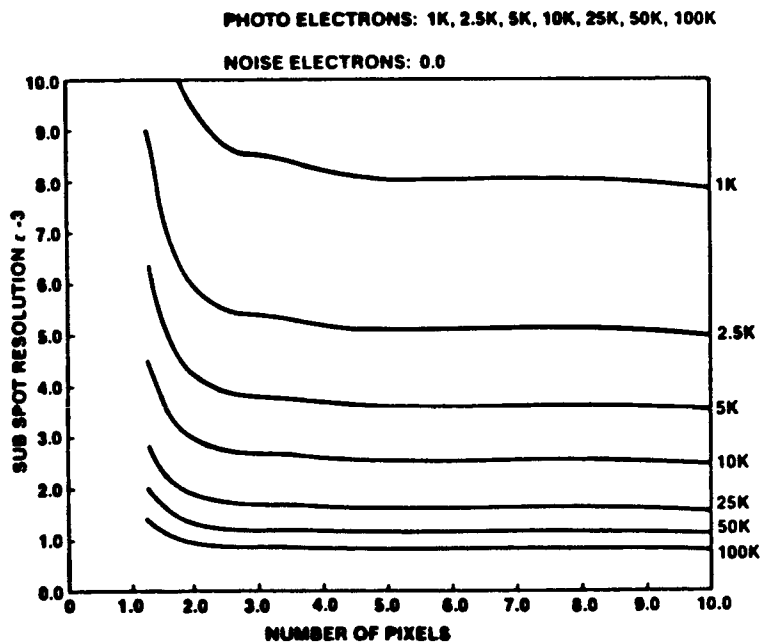
SUBSPOT RESOLUTION (PHOTON SHOT NOISE)

Figure 3.2-8

3.2.2.3 <u>Electronic Noise</u> - Included in this category are detector noise sources, such as pixel dark current, quantization noise, and reset amplifier noise. For this analysis electronic noise sources were lumped together as dark current and assumed to be bandwidth dependent.

The calculated centroid is given by:

$$x_c = \frac{1}{\Sigma y_i} \, \Sigma x_i y_i$$

and the standard deviation is given by:

$$\sigma_{xc} = \frac{1}{\Sigma y_i} \left\{ \, \Sigma_j (x_j - x_c)^2 \sigma_j^2 \, \right\}^{1/2}$$

$$\sigma_j^2 = y_i + k^2$$

In Figures 3.2-9 through 3.2-13 the effect of electrical noise is added to the sensitivity adjusted photon shot noise to display the minimum meaningful ability to sense image displacement for a range of the number of incident photons in the presence of possible values of detector electrical noise. The effect of the linearity bias error is not included. It can be reduced to a negligibly small value by a backout technique. For the Space Telescope it is already sufficiently small (0.002 of a spot under the conditions of an image centroiding requirement of 0.023 and 2 pixels per spot) to neglect the effect. It can be seen that to achieve less than 1/50 of a spot, about 5000 photoelectrons are needed with 100 noise electrons. It is also apparent that there is no advantage in many pixels per spot. Two pixels per spot is just about right. It should be noted that the cases with zero noise electrons indicate the centroid uncertainty for the photon shot noise limit. These curves initially drop as the spot size is increased but then asymotitically flatten out at a spot size of about 3.0 pixels.

NOISE ELECTRONS/PIXEL
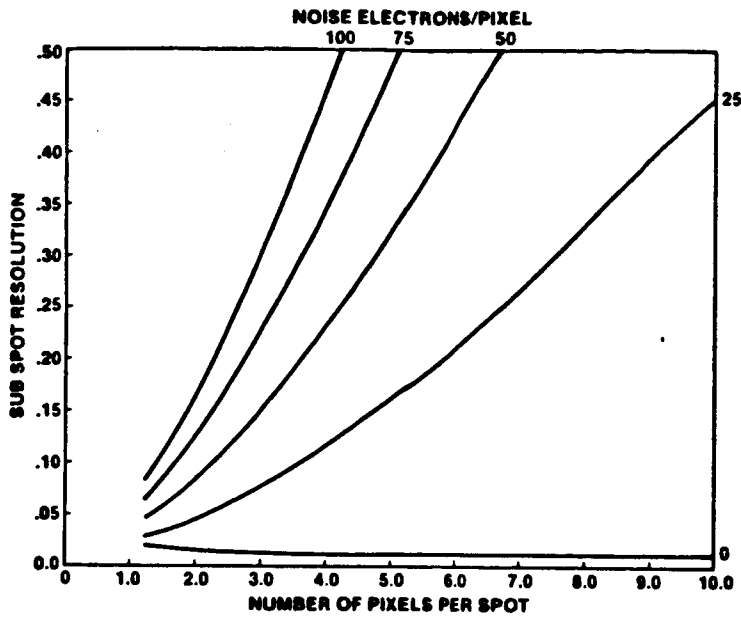
IMAGE CENTROIDING (0.5K PHOTOELECTRONS)

Figure 3.2-9
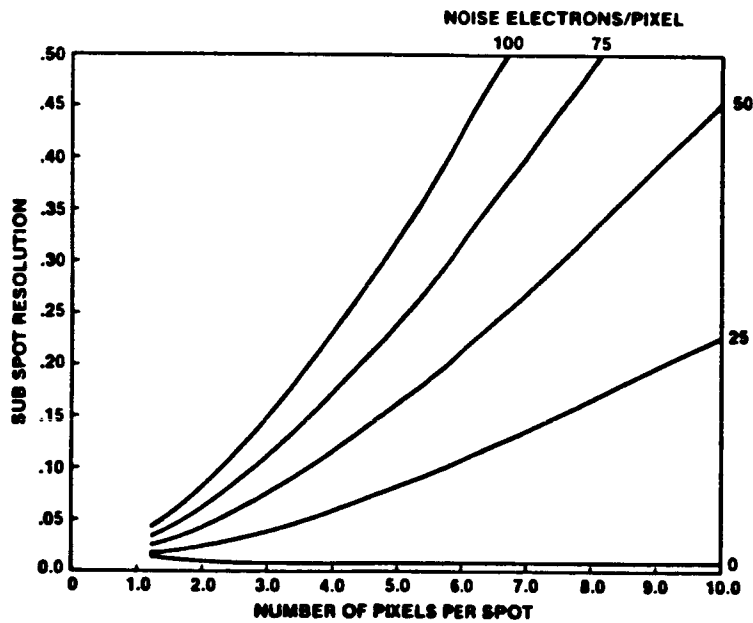
IMAGE CENTROIDING (1K PHOTOELECTRONS)

Figure 3.2-10
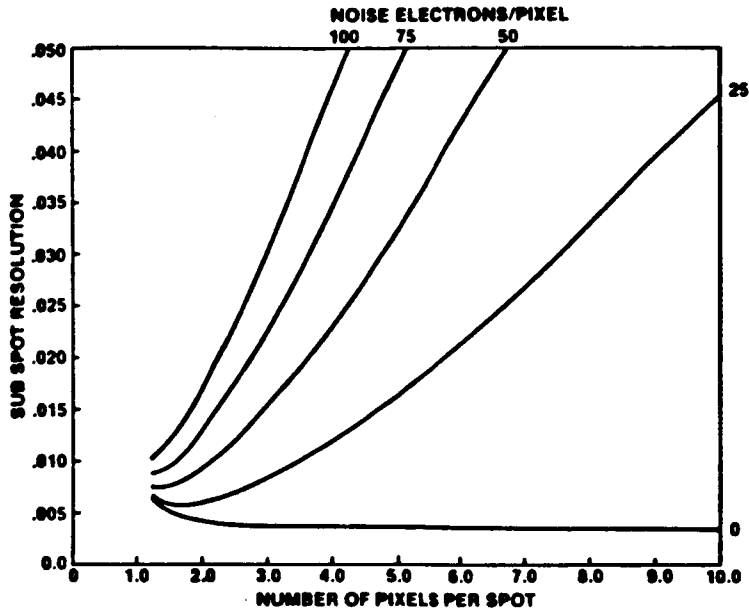
IMAGE CENTROIDING (5K PHOTOELECTRONS)

Figure 3.2-11
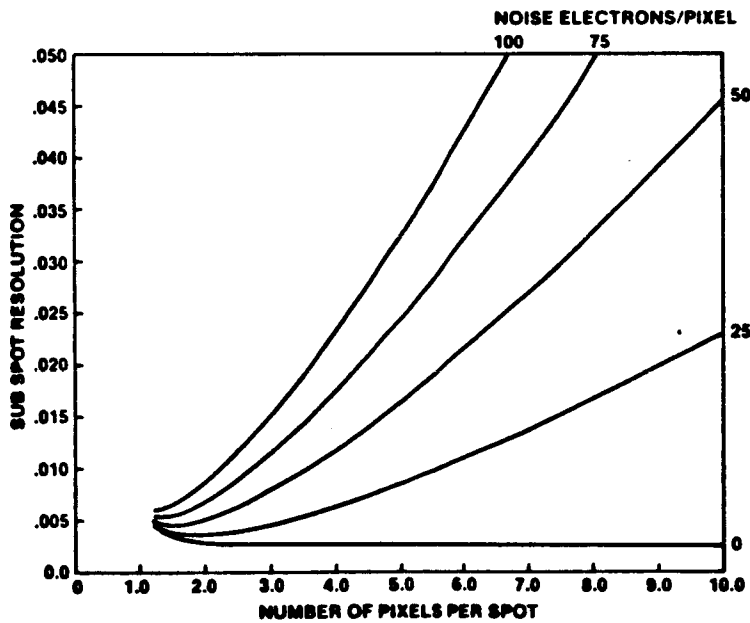
IMAGE CENTROIDING (10K PHOTOELECTRONS)

Figure 3.2-12

NOISE ELECTRONS/PIXEL
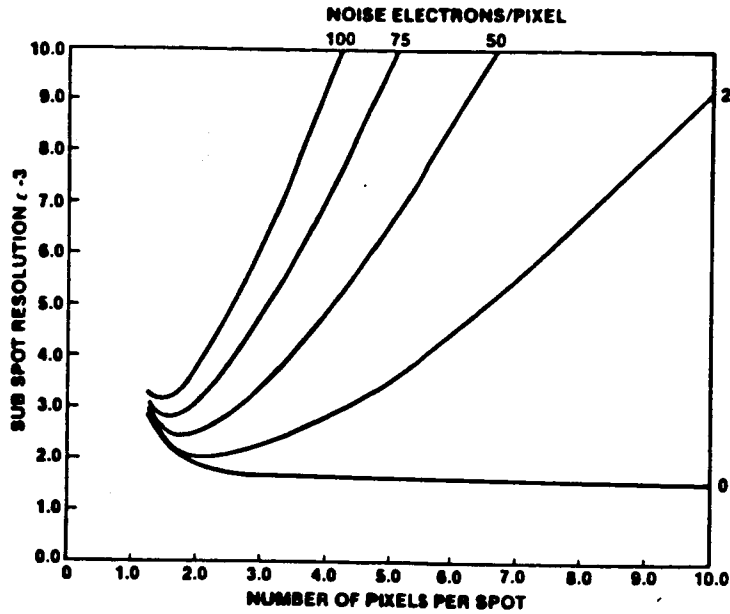
IMAGE CENTROIDING (25K PHOTOELECTRONS)
Figure 3.2-13

Figure 3.2.14 shows a family of
curves for a constant elec-
tronic noise term of 75 elec-
trons per pixel for different
cases of photo electrons. The
curves suggest that the greatest
accuracy in centroiding is ob-
tained with relatively small
spot sizes. Even the curves for
fifty and one hundred thousand
photo electrons give optimum
results for spot sizes of under
3.0 pixels.

PHOTO ELECTRONS: .5k, 1k, 2.5k, 5k, 10k, 25k, 50k, 100k
NOISE ELECTRONS : 75 PER PIXEL
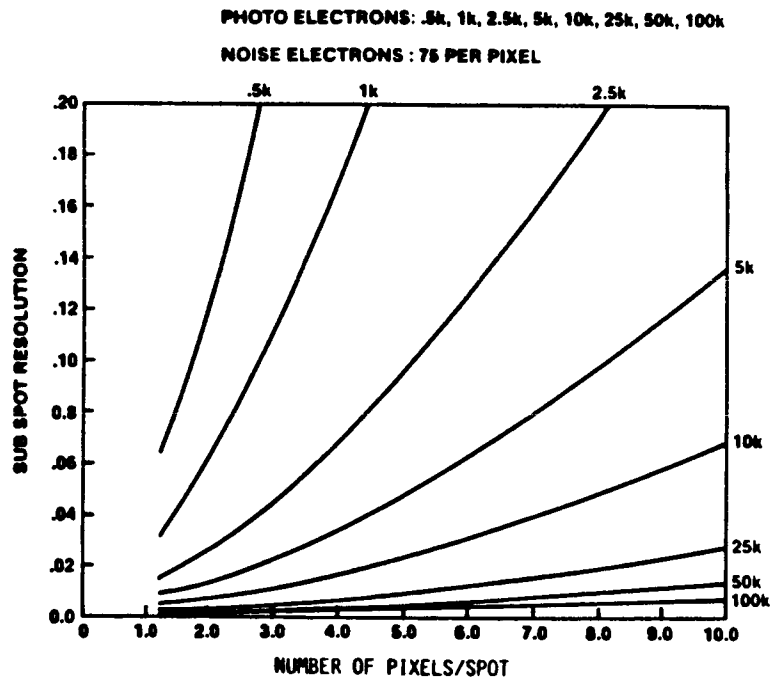
SUBSPOT RESOLUTION (WITH NOISE ELECTRONS)
Figure 3.2-14

The center of a distribution of
light can be determined by imaging
the light onto a detector. The
two most important factors limiting
the accuracy are the number of incident photons (thus the number of photo-

electrons) and the number of noise electrons. The magnitudes for the various noise terms is shown in Table 3.2-1 for the case of ten thousand photo electrons with spot size of 2.0 pixels and a CCD noise factor of 75 electrons per pixel.

Subspot resolutions on the order of 1/100 of a spot are theoretically possible. The noise sources considered do not preclude accuracies of 1/1000 of a spot. However, the analysis presented does not include other effects present in practical systems that may limit the ability to centroid (i.e., calibration of pixel variations).

Table 3.2-1
IMAGE CENTROIDING

CASE:	
PHOTON ELECTRONS	10,000/SPOT
CCD NOISE ELECTRONS	75/PIXEL
SPOT SIZE	2.0 PIXELS/SPOT
GAUSSIAN σ	0.5 PIXELS
QUANTIZING SCHEME	16 BITS
CENTROID ERROR:	
ELECTRONIC NOISE	$\simeq 6 \times 10^{-3}$
PHOTON SHOT NOISE	$\simeq 3 \times 10^{-3}$
ERROR FUNCTION VALUE	$\simeq 1.5 \times 10^{-3}$
QUANTIZING NOISE	$\simeq 0.3 \times 10^{-3}$
TOTAL ERROR	$\simeq 7 \times 10^{-3}$

This analysis has assumed the electronic noise exists only under the $\pm 2\sigma$ points of the Gaussian. In reality the electronic noise exists for each pixel and thus a choice in the processing algorithm must be made to include or exclude a pixel. The error introduced is known as "truncation error" and is strongly dependent on the incident number of photons, the spot size, and electronic noise and the truncation scheme. Threshold level and/or proximity to the maximum level pixel are two possibilites. The truncation scheme should be integral with the centroiding algorithm. The mean algorithm gives good results in the absence of truncation. However, it is blind to the possibility that one edge pixel may be just above the threshold and the other edge pixel just below. Best fit curve algorithms should produce superior results.

A Gaussian light distribution was assumed for the image of a distant star. In reality the point spread function of an optical system will not be Gaussian. If the spot distribution has a convoluted profile the centroiding accuracy will be degraded. Changes in the spot profile will yield an error function that may not be systematically compensated. The amplitude may also be larger.

Shifts in the focal length of the system will produce lateral movements in the imaged spot. A subspot resolution of 1/100 for a spot located 1000 pixels away from the optical axis translates into a 0.002 percent change in the focal length. In many applications, knowledge of the absolute directions of a star is not as important as in changes in the direction for pointing stability. Thermal gradients and mechanical vibrations on the order of a sampling interval could produce sizable centroiding errors and, in general, cannot be compensated. Complete characterization of optical system requires the measurement of these additional noise sources and integrating the results with the above equations.

4.0 CANDIDATE IDENTIFICATION

4.1 DETECTOR CANDIDATES

Historically, photomultiplier tubes have been used for low light level astro-nomical applications. Photons incident on the photocathode cause photoelec-trons to be released and to be directed by focusing electrodes onto the dynode of an electron multiplier. The first dynode is maintained at a potential of a few hundred volts positive with respect to the photocathode so that the photoelectrons strike the dynode with sufficient energy to release several secondary electrons per primary photoelectron. This process is repeated at successive dynodes so that the charge pulse leaving the last dynode will contain at least a million electrons for each primary photoelectron. The principal reason for using photomultiplier tubes in astronomy is to achieve virtually noiseless photoelectron amplification so that the accuracy is determined by the randomness of the light being measured (photon noise) rather than the external circuitry connected to the tube. The main source of noise in an uncooled photomultiplier tube is thermal emission from the photocathode and first dynode. Since thermal electrons from the photocathode are indistin-guishable from true photoelectrons and are produced even in the absence of any photocathode illumination, they are usually collectively called the dark current and can be reduced by cooling the tube to below $-20^\circ C$. The photo-cathodes used in astronomy are summarized in Table 4.1-1. The reference detector for photometric astronomy is the 1P21 tube using U, B, and V filters. The 1P21 is cesium antimonide of the S20 photocathode type. In this study the blue sensitive S20 photocathode has been used in the analyses for comparison.

Table 4.1-1 PHOTOCATHODES USED IN ASTRONOMY			
	λ_{MAX} (NM)	QE_{MAX} (%)	THERMIONIC EMISSION AT $20^\circ C$ (ELECTRONS/CM^2-SEC)
● S20	380	22	300
● S20-ER	400	20	400
● S11	390	21	70

A solid state image sensor is a photosensitive device for converting an irradiance image into a corresponding video signal. The photon flux at each image point is absorbed in a corresponding elemental area of the material of the sensor, which then generates free electrons and holes. Either the electrons or the holes are collected at localized sites in the sensor that correspond to a one or two dimensional lattice of discrete image points. After the conversion and collection process has proceeded for a designated integration time, the lattice of collection sites is interrogated in a scanning pattern so that a signal corresponding to the charge at each collection site in turn is developed and delivered to the output terminal of the device. In silicon solid state image sensors, photons in the image are absorbed by exciting electrons in the silicon from the filled valence band across the gap into the conduction band. These devices respond only to light with a photon energy greater than about 1.1 eV and a wavelength shorter than about 1.1 micrometers. It should be noted that the spectral response is higher toward the red end of the spectrum.

Shown in Tables 4.1-2 and 4.1-3 are "first cut" lists of solid state sensors (photodiode arrays; CCD's and CID's) which have potential for star tracking applications. The earliest form of solid state sensor used a matrix of photodiodes to sense the radiation. Individual photodiode sensor elements are combined into line or area arrays.

Charge Coupled Devices (CCD's) have become increasingly attractive for astronomical imaging. This is due to low readout noise, high quantum efficiency, high dynamic range, linearity, and stability. For faint stars the low noise of a CCD detector is important since the system noise level determines the amount of light which must be detected before signal shot noise dominates the signal to noise ratio.

Table 4.1-2
CANDIDATE SOLID STATE SENSORS (AREA ARRAYS)

MANUFACTURER	TYPE	FORMAT	PIXEL SIZE (µM)	PREVIOUS USE
TEXAS INSTRUMENT	CCD	800 x 800	15 x 15	WF/PC
TEXAS INSTRUMENT	CCD	1024 x 1024	18.2 x 18.2	GALILEO
RCA	CCD	512 x 320	30 x 30	SCIENTIFIC INSTRUMENTS
HUGHES	ICCD	324 x 324	25 x 25	MADAN
FAIRCHILD	CCD 211	244 x 190	18 x 12	
FAIRCHILD	CCD 221	488 x 380	18 x 12	
FAIRCHILD	CCD	488 x 430	18 x 12	INTERLINE IMAGE SENSOR

MANUFACTURER	TYPE	FORMAT	PIXEL SIZE (µM)	PREVIOUS USE
RETICON	RA-100 (CCD)	128 x 128	60 x 60	
RETICON	RL-256 (CCD)	256 x 256	25 x 25	
SONY	CCD	570 x 480	16 x 14	
TOSHIBA	PHOTODIODE	492 x 398		
KODAK	CCD	740 x (242 x 2)	12 x 12	COLOR IMAGE SENSOR
KODAK	CCD	248 x 192	32 x 32	MOTION ANALYZER
WESTINGHOUSE	CCD	100 x 100	20 x 20	

MANUFACTURER	TYPE	FORMAT	PIXEL SIZE (µM)	PREVIOUS USE
HUGHES	ICCD	648 x 648		
GENERAL ELECTRIC	CID	256 x 256	20 x 20	
GENERAL ELECTRIC	CID	388 x 244	27 x 22.7	
FORD AEROSPACE	CCD	1024 x 1024	11 x 11	
THOMPSON	CCD	576 x 462		

Table 4.1-3 CANDIDATE SOLID STATE SENSORS (LINEAR ARRAYS)					
● MANUFACTURER	TEXAS INSTRUMENT	TEXAS INSTRUMENT	TEXAS INSTRUMENT	FAIRCHILD	FAIRCHILD
● TYPE	TC 101	TC 103	TC 104	CCD 143	CCD 151
● FORMAT	1728 x 1	2048 x 1	3456 x 1	2048 x 1	3456 x 1
● PIXEL SIZE (µM)	12.7 x 12.7	12.7 x 12.7	10.7 x 10.7	13 x 13	7 x 7
● PREVIOUS USE					
● MANUFACTURER	TOSHIBA	TOSHIBA	RETICON	RETICON	XEROX
● TYPE	TC 106	TC 105	PHOTODIODE	PHOTODIODE	
● FORMAT	5066 x 1	3456 x 1	4096 x 1	25 µ x 2 NM	5732 x 1
● PIXEL SIZE (µM)	7 x 7	8 x 8	15 x 15		
● PREVIOUS USE			ALIGNMENT IN LASER FUSION	SPECTROMETERS	

Also included in the list is the Charge Injection Device (CID) developed by General Electric. It is more closely related to a diode array image sensor than to a CCD but offers advantages over both. The charge signal at each sensing site is transferred only between potential wells under adjacent gate electrodes. This implies that operation is not compromised by moderate transfer inefficiency. The signal can be stored, read, and erased at each site by properly pulsing one row and one column gate bus. A full rectangular sensing array can be constructed with no extra address switch components within the light sensitive area.

4.2 FINE GUIDANCE SENSING CONCEPTS

From a physical optics standpoint a lens transforms a plane wave front emanating from a point object into a converging spherical wave front resulting in the image point spread function. Fine Guidance Sensing Concepts can be separated into two categories--those that operate on the wave front emanating from the point object and those that operate on the point spread function (intensity distribution of the image of a point object).

4.2.1 Fine Guidance Sensing Using The Point Spread Function

Figure 4.2-1 represents the "ideal" case
for a fine guidance sensor. The detector
surface is attached directly to the image
surface. Positional information deter-
mined at the detector is transformed into
angular information in object space.
There are no additional optics. In this
concept hardware simplicity minimizes the
number of error sources and therefore
optimizes the potential for precision
pointing. Concept I, as the "ideal"
case, serves as the reference for comparison with other concepts.
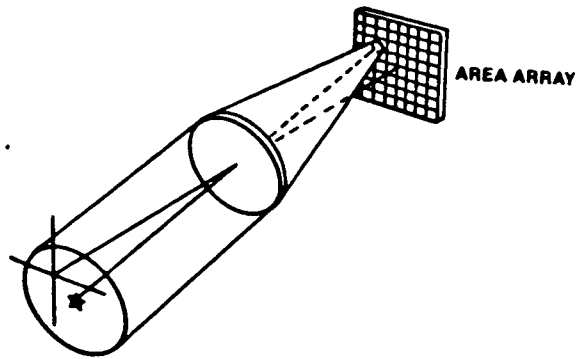
CONCEPT I (AREA ARRAY WITH NO
OPTICAL CORRECTORS)

Figure 4.2-1

There are several reasons for additional optics in the fine guidance sensor.
The first reason is to correct the astigmatism in the optical subsystem field.
The fine guidance sensor (optical subsystem and detector subsystem) can then
be considered field curvature limited (one well defined image surface. The
field curvature can be "accommodated" by a similarly curved detector surface.
The size of the image will be smaller than in Concept I. Concept II, shown in
Figure 4.2-2 represents the case with an astigmatic field corrector.
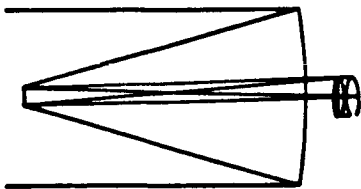
CONCEPT II
(AREA ARRAY WITH
OPTICAL CORRECTORS)

Figure 4.2-2

The second reason for additional optics is
to change the optical subsystem focal
length. This will affect the plate scale
factor, image size, and field of view. Con-
cept III, shown in Figure 4.2-3, represents
the case with a different system focal
length.

The third reason for additional optics is to
increase the flux concentration in the image. Concept IV, shown in Figure
4.2-4, represents this case utilizing a field lens.
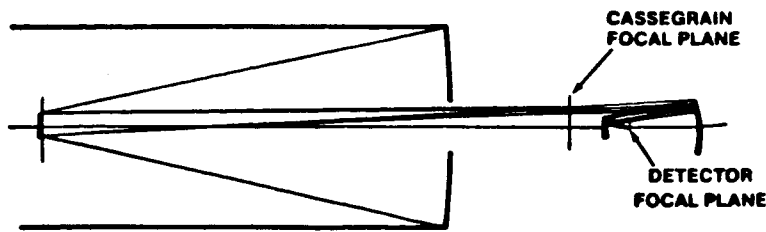
CONCEPT III (AREA ARRAY WITH FOCAL LENGTH REDUCER)

Figure 4.2-3

4.2.2 FINE GUIDANCE SENSING USING THE WAVE FRONT

The basic concept of pointing involves the transformation of the line of sight vector in object space (in angular units) through a lens to image space. The previous concepts transformed the angular information into a linear displacement at the image surface. Knowledge of the angle

CONCEPT III (LINEAR ARRAY WITH OPTICAL CORRECTOR)

Figure 4.2-4

in object space could be interpreted from the knowledge of the position of the image on an image surface. The alternate concepts involve relating the tilt of the incoming wave front to knowledge of the angle in object space.

A collimator can be attached to the optical subsystem as shown in Figure 4.2-5.
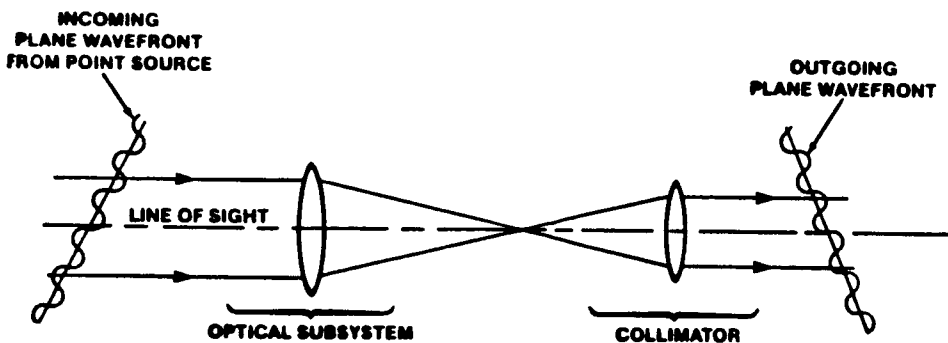
RELATION OF OUTGOING WAVE FRONT TO INCOMING WAVE FRONT

Figure 4.2-5

By the selection of the focal length of the collimator, an afocal magnification is provided. Tilt of the outgoing plane wave front is directly related to the tilt of the incoming plane wave front. By monitoring the larger angular changes in the collimated space, the smaller values can be predicted in object space. Concept V in Figure 4.2-6 shows the first version of Fine Guidance Sensing using the wave front angle encoding. The second image is monitored for null rather than for position. Two orthogonal flats are inserted in the collimated space. After null, the orientation of these orthogonal flats are established with shaft encoders. These angles in collimated space can then be related to object space angular information.
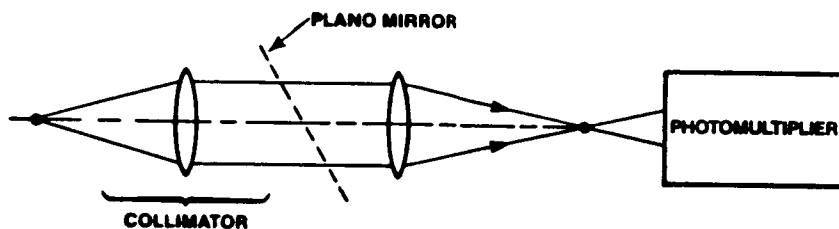
CONCEPT V (NULL WITH ANGLE ENCODING)
Figure 4.2.6

Concept VI, Figure 4.2-7, shows the second version of star tracking using the wave front interferometry. The current FGS represents Concept VI. The collimated beam is fed to Koester's prisms which provide a set of interferometric fringes to the pairs of detecting photomultipliers. These detectors do not scan the fringes but interrogate the total intensity of the signal which varies as the star moves.
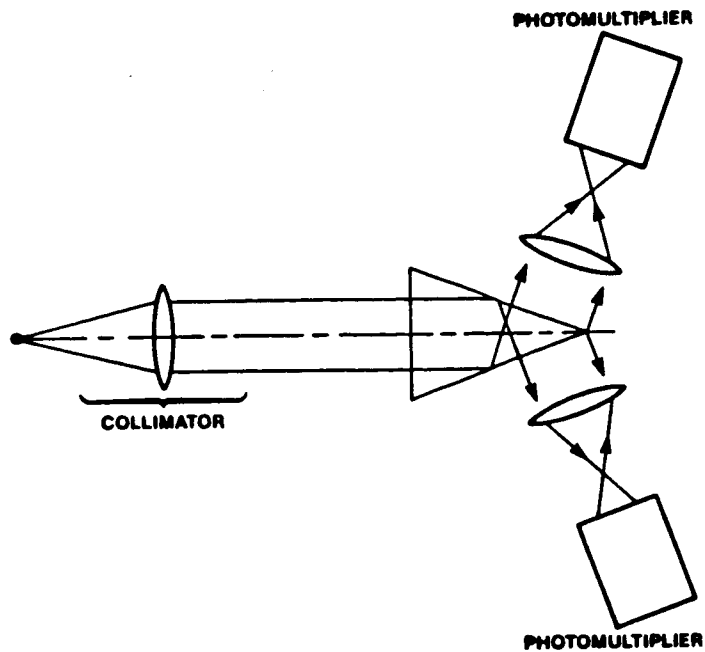
CONCEPT VI (NULL WITH INTERFEROMETER)
Figure 4.2-7

5.0 COMPARISON WITH REQUIREMENTS

5.1 COMPARISON OF DETECTOR PERFORMANCE

Four detectors were analyzed in this study. Three are versions of CCD's: a CCD array area, a CCD linear array, and a CCD spectroscopic linear array. The spectroscopic array is a linear array with long rectangular pixels (2 millimeters by 25 micrometers). The first three detectors were assumed to have the same spectral response curve and the same quantum efficiency but different noise electrons per pixel. The fourth detector for comparison was a photomultiplier with an S-20 photocathode. The photoelectrons generated from stars of three different color temperatures (10,000, 6,000, and 4,000°K) but with the same visual magnitude were calculated as collected from a 2.4 meter diameter collector with a transmittance of 0.83. The solar constant 0.1388 watts/cm^2, coupled with the solar visual magnitude of -26.78 was used as the reference irradiance. Table 5.1-1 gives the quantum efficiency, noise electrons per pixel at 60 hertz bandwidth, and the calculated photoelectrons for each detector corresponding to the three stars at 14.5 visual magnitude. The number of photoelectrons generated includes a factor ξ which represents an efficiency in the utilization of the flux within a spot by the linear or area array. The spectroscopic array utilizes all the flux incident but requires a beam splitter to separate the two orthogonal displacements. The linear array assumes a spot in the form of a line straddling the array as well as a beam splitter and is the least efficient in utilizing the spot energy. The area array assumes a circular spot on 4 pixels. The photomultiplier configuration must employ a beam splitter and nulling optics. Figures 5.1-1 to 5.1-10 shows subspot resolution as a function of star magnitude for the four detectors for the three stars of different spectral class. Figure 5.1-11 compares the performance of the detectors on the basis of threshold visual magnitude to achieve a 1/43 subspot resolution. The CCD area array with its high efficiency factor is substantially better than the other detectors.

Table 5.1-1

DETECTOR COMPARISON

AREA ARRAY	Q_{max}	NUMBER OF NOISE ELECTRONS PER PIXEL	ξ	NUMBER OF PHOTOELECTRONS		
				AO 10000°K	GO 6000°K	MO 4000°K
AREA ARRAY	0.60	70	0.785	104,798	124,815	188,165
LINEAR ARRAY	0.60	50	0.10	13,350	15,900	23,970
SPECTROSCOPIC ARRAY	0.60	500	0.50	66,750	79,500	119,850
PHOTOMULTIPLIER	0.18	10	0.30	9,060	6,270	4,800

- 2 PIXELS/SPOT
- QE = 70%
- σ_e = 70 ELECTRONS AT 60 HZ
- ξ = 0.785
- BANDWIDTH = 40 HZ
- CCD AREA ARRAY
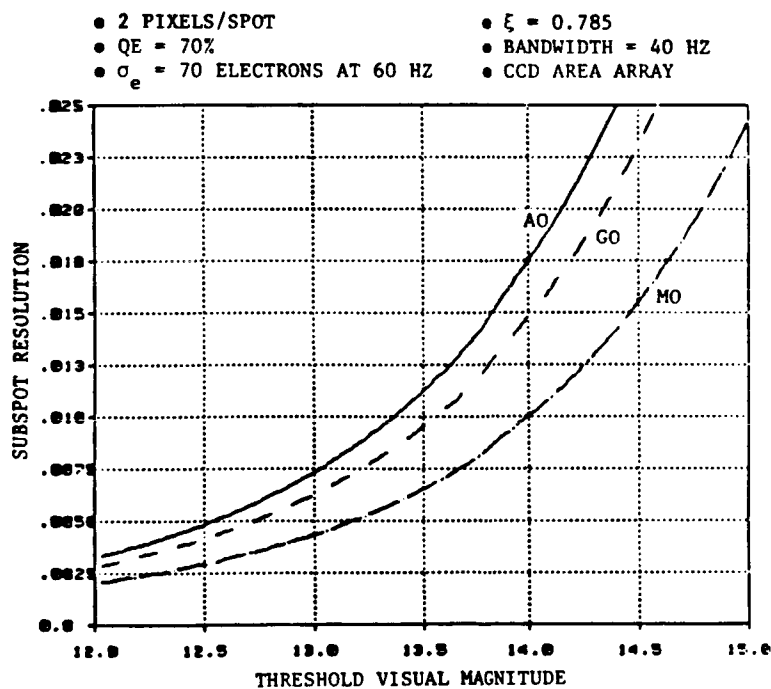
SUBSPOT RESOLUTION

Figure 5.1-1

- 2 PIXELS/SPOT
- QE = 70%
- σ_e = 70 ELECTRONS AT 60 HZ
- ξ = 0.785
- BANDWIDTH = 10 HZ
- CCD AREA ARRAY
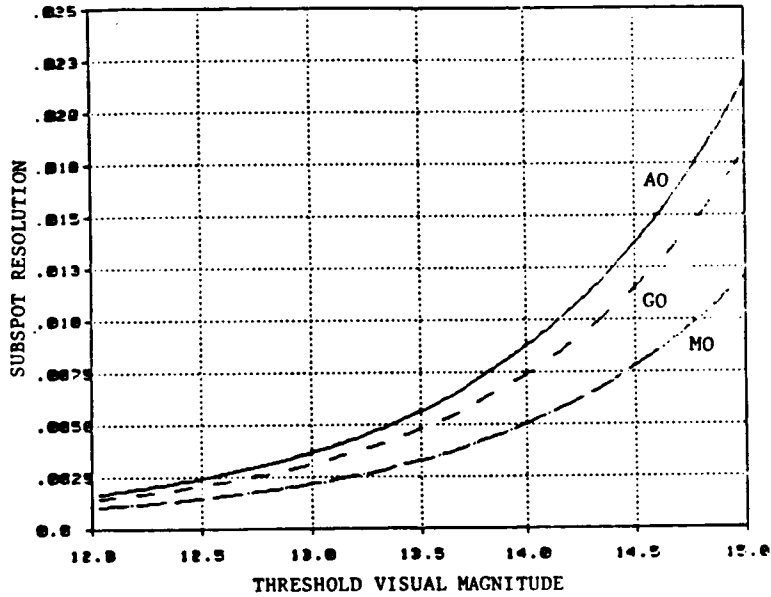
SUBSPOT RESOLUTION

Figure 5.1-2

- 2 = PIXELS/SPOT
- QE = 70%
- σ_e = 70 ELECTRONS AT 60 HZ
- ξ = 0.785
- BANDWIDTH = 2.5 HZ
- CCD AREA ARRAY
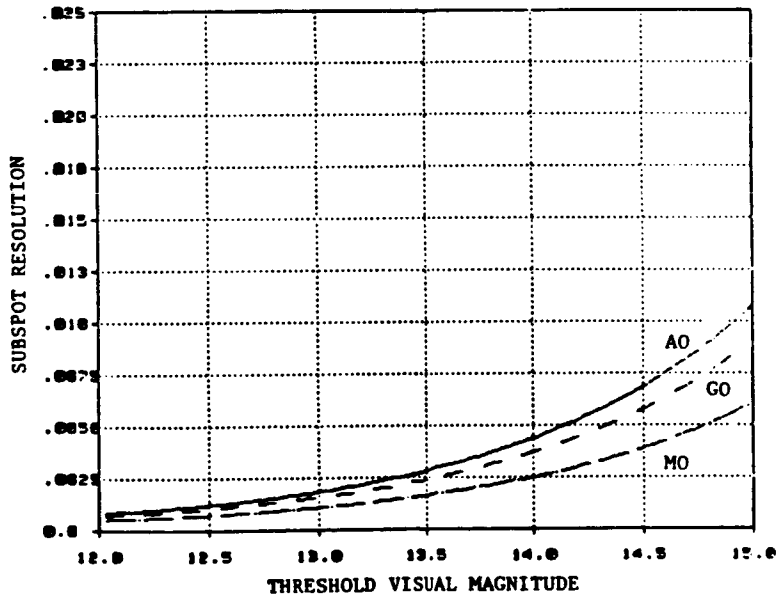
SUBSPOT RESOLUTION

Figure 5.1-3

5-3

- 2 PIXELS/SPOT
- QE = 70%
- σ_e = 50 ELECTRONS AT 60 HZ

- ξ = 0.10
- BANDWIDTH = 40 HZ
- CCD LINEAR ARRAY

SUBSPOT RESOLUTION

Figure 5.1-4

- 2 PIXELS/SPOT
- QE = 70%
- σ_e = 50 ELECTRONS AT 60 HZ

- ξ = 0.10
- BANDWIDTH = 10 HZ
- CCD LINEAR ARRAY
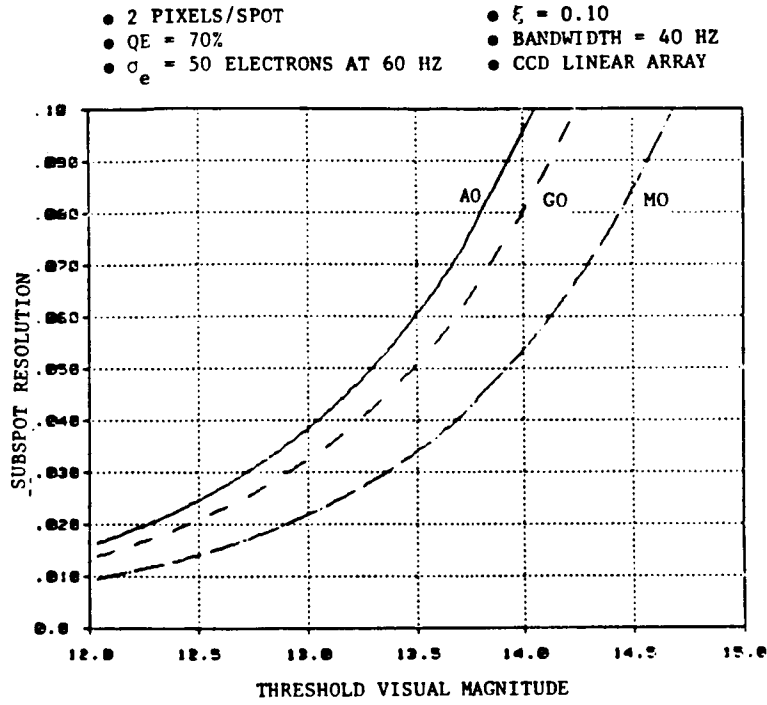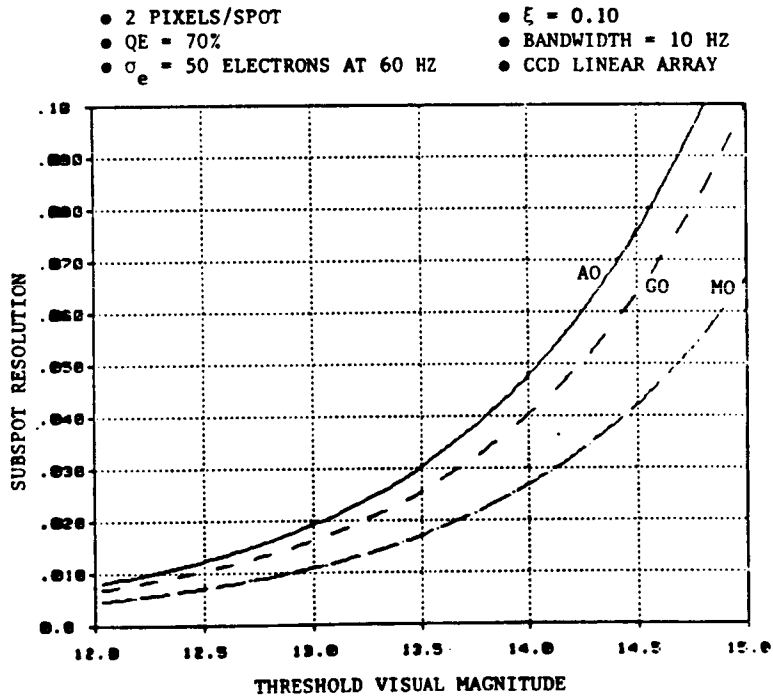
SUBSPOT RESOLUTION

Figure 5.1-5

- 2 PIXELS/SPOT
- QE = 70%
- σ_e = 500 ELECTRONS AT 60 HZ
- ξ = 0.50
- BANDWIDTH = 40 HZ
- LINEAR ARRAY (SPECTROSCOPIC)
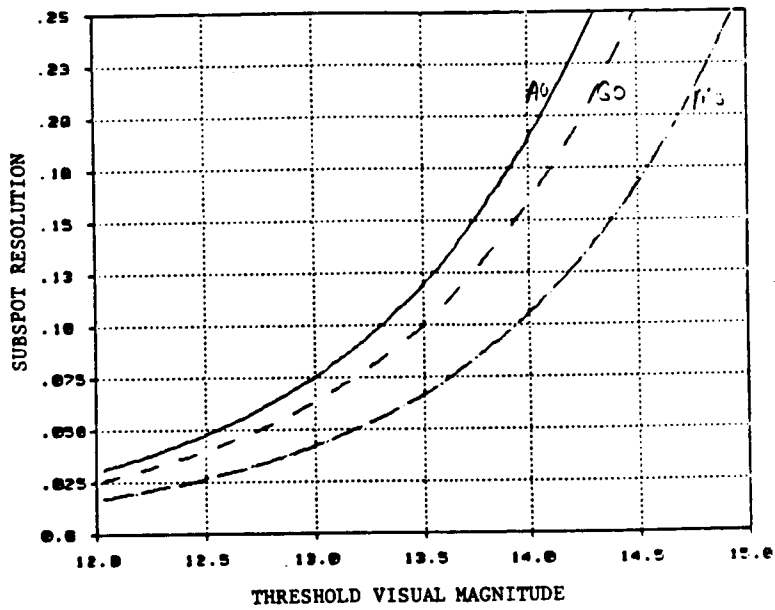
SUBSPOT RESOLUTION

Figure 5.1-6

- 2 PIXELS/SPOT
- QE = 70%
- σ_e = 500 ELECTRONS AT 60 HZ
- ξ = 0.50
- BANDWIDTH = 10 HZ
- LINEAR ARRAY (SPECTROSCOPIC)
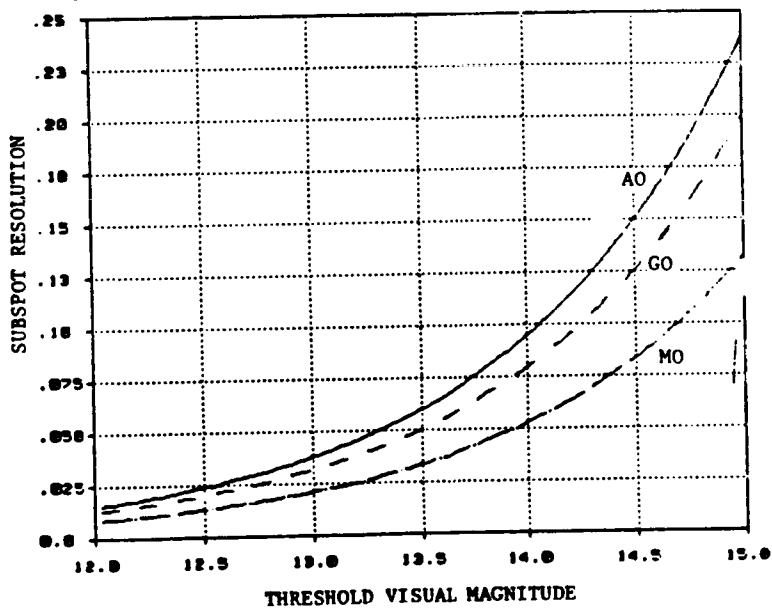
SUBSPOT RESOLUTION

Figure 5.1-7

- 2 PIXELS/SPOT
- QE ∿ 18%
- σ_e = 10 ELECTRONS AT 60 HZ
- ξ = 0.30
- BANDWIDTH = 40 HZ
- S-20 PHOTOCATHODE
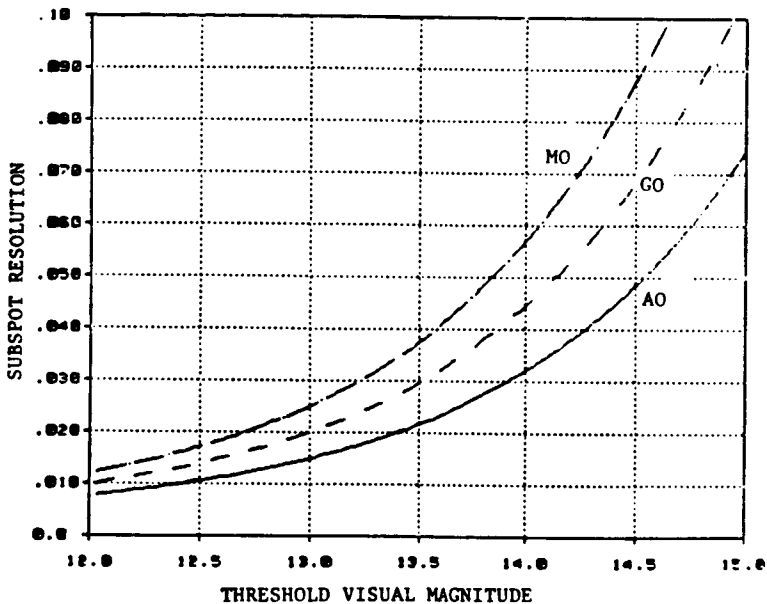
SUBSPOT RESOLUTION

Figure 5.1-8

- 2 PIXELS/SPOT
- QE ∿ 18%
- σ_e = 10 ELECTRONS AT 60 HZ
- ξ = 0.30
- BANDWIDTH = 10 HZ
- S-20 PHOTOCATHODE
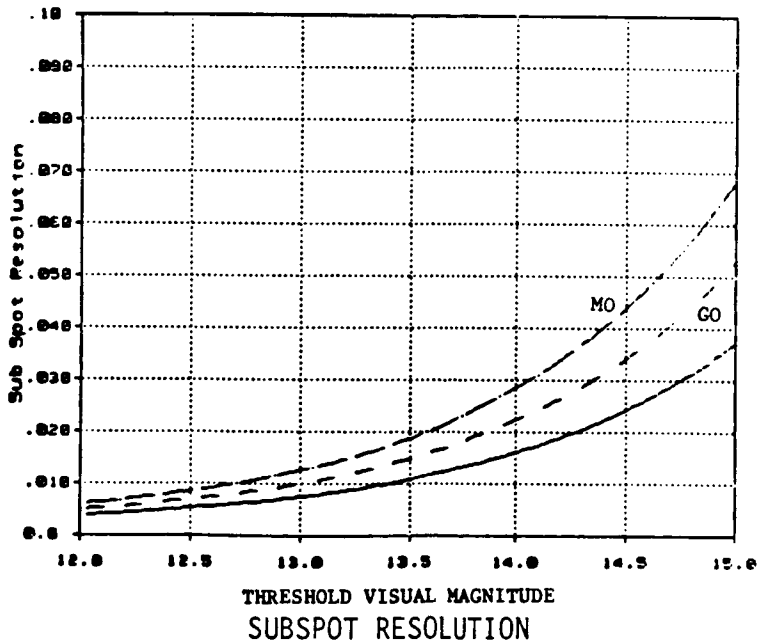
SUBSPOT RESOLUTION

Figure 5.1-9

5-6

- 2 PIXELS/SPOT
- QE ~ 18%
- σ_e = 10 ELECTRONS AT 60 HZ
- ξ = 0.30
- BANDWIDTH = 2.5 HZ
- S-20 PHOTOCATHODE
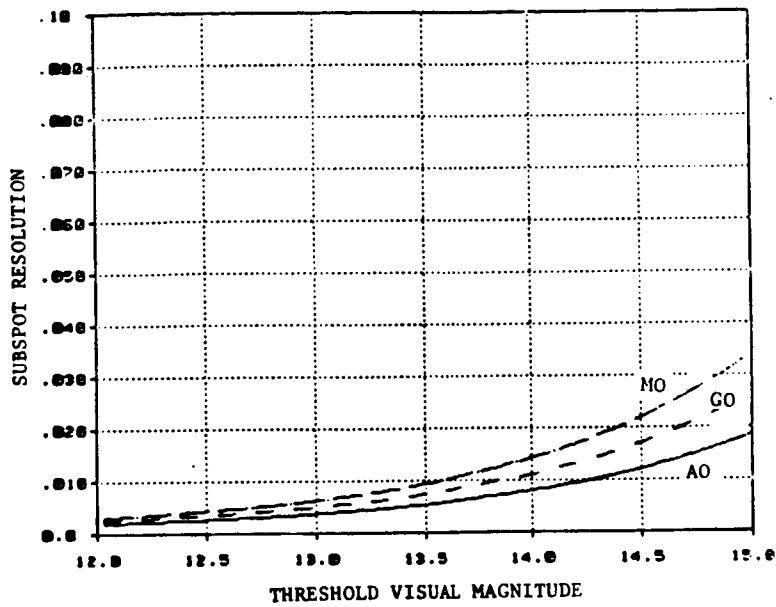
SUBSPOT RESOLUTION

Figure 5.1-10
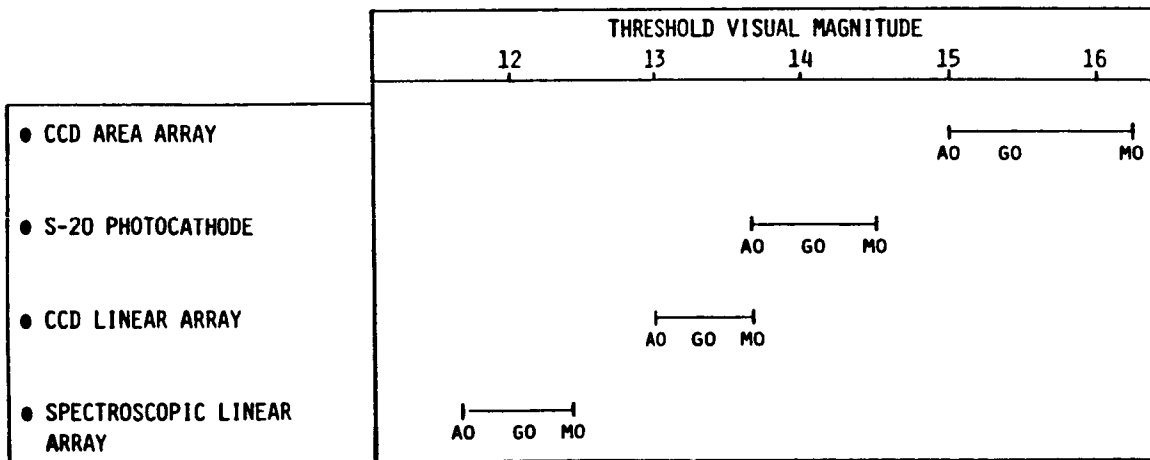
DETECTOR COMPARISON

(IMAGE CENTROIDING = 1/43)

Figure 5.1-11

The RCA SID501D CCD area array and the RETICON "S" series linear photodiode array have been selected for further analysis in this study. The spectral response curves for these detectors are shown in Figures 5.1-12 and 5.1-13. The expected total noise is 50 electrons per pixel at 60 hertz for the area array and 120 electrons per pixel at 60 hertz for the linear array when cooled to -40°C. Shown in Figure 5.1-14 is the integrated intensity of blackbodies normalized to a visual wavelength (i.e., all stars therefore have the same visual magnitude). Shown in Figure 5.1-15 is the integral of the product of the visually normalized blackbodies (Figure 5.1-14) and the CCD spectral responsivity (Figure 5.1-12). The ratio of the areas represents the relative responsivity of the CCD arrays to blackbodies of different color temperatures but having the same visual magnitude.
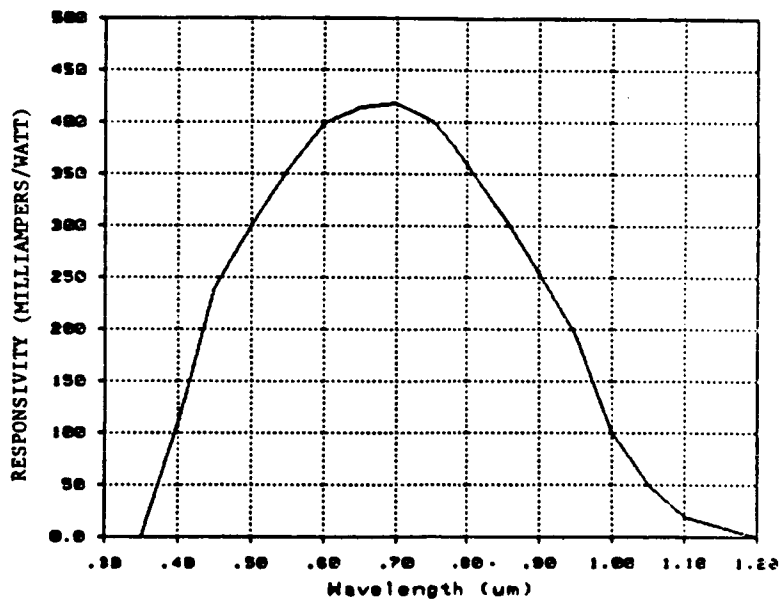
RESPONSIVITY: RCA SID 501D CCD AREA ARRAY

Figure 5.1-12
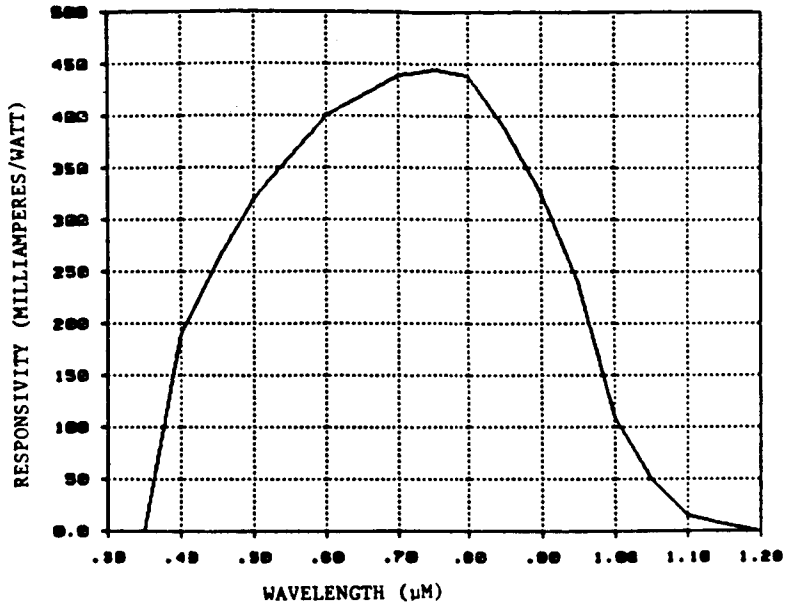
RESPONSIVITY, RETICON S-SERIES LINE SCANNER LINEAR ARRAY RESPONSE

Figure 5.1-13
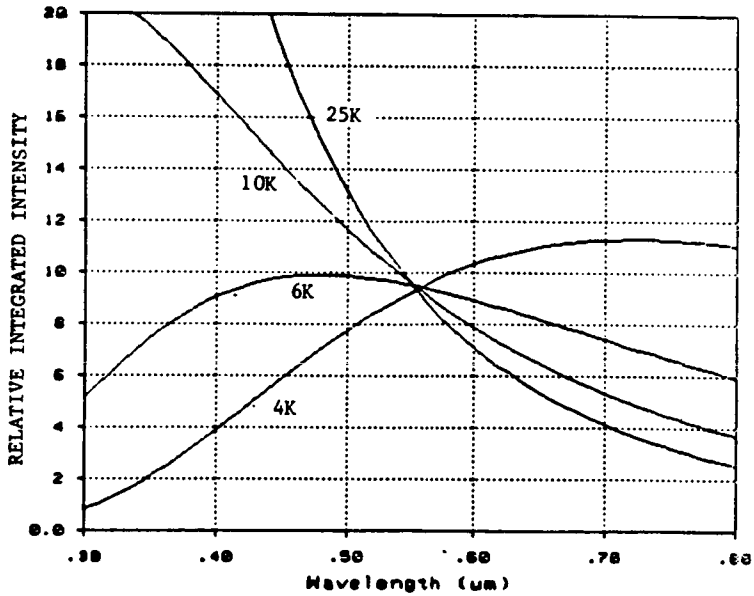
RELATIVE INTEGRATED INTENSITY OF BLACKBODIES
NORMALIZED TO A VISUAL WAVELENGTH

Figure 5.1-14
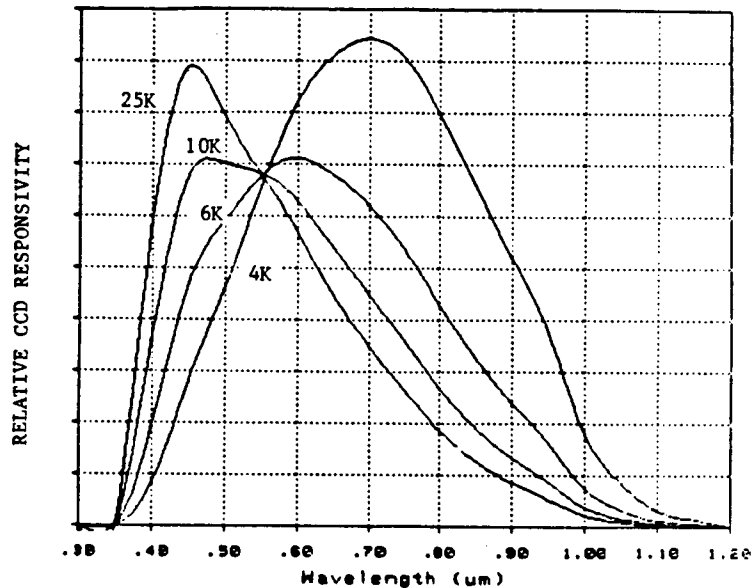
RELATIVE SPECTRAL RESPONSIVITY
(RCA SID 501D CCD)
Figure 5.1-15

The resultant number of the photoelectrons is shown in Figure 5.1-16 and Table 5.1-2. The figure illustrates the spectral irradiance from a zero visual magnitude star of differing spectral classes collected by a 1 square centimeter aperture and focused onto the RCA CCD array over an integration time of 1 second. The solar constant 0.1388 watts/cm^2, coupled with the solar visual magnitude of -26.78 was used as the reference irradiance. The table illustrates the spectral irradiance from a 14.5 visual magnitude star for conditions of the OTA (2.4 meter aperture and optical transmittance of approximately 83%).
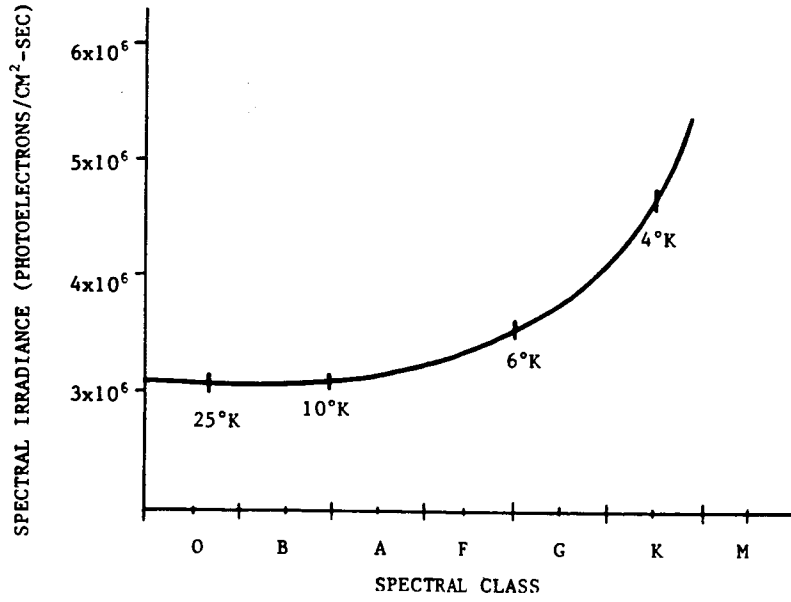
SPECTRAL IRRADIANCE

Figure 5.1-16

Table 5.1-2			
NUMBER OF PHOTOELECTRONS D = 2.4 M; τ = 0.83; t = 1 SEC; M_v = 14.5; RCA SID 50ID			
BO	AO	GO	MO
(25,000°K)	(10,000°K)	(6,000°K)	(4000°K)
184,000	189,000	211,000	283,000

5.2 COMPARISON OF FINE GUIDANCE SENSING CONCEPTS

Six concepts were identified as having potential for fine guidance sensing. A comparison of these concepts is shown in Table 5.2-1. Concept I was eliminated from further analysis in this study. The requirement for image centroiding (1/166) is considered beyond the state-of-the-art. Concept II was selected for conceptual design. Concept III meets the requirements. However, the major advantage is on yield of detectors and therefore indirectly cost. Improvements in yield have been made in the past decade and is expected to continue. This concept was eliminated for this reason. Concept IV was selected for conceptual design. Concepts V and VI require some moving parts. In addition these two concepts require additional optics (relay optics and/or beam splitters). Therefore, the throughput will be reduced. For these reasons Concepts V and VI were eliminated from further analysis in this study.

Table 5.2-1

CONCEPT COMPARISON

	CONCEPT I AREA ARRAY WITH NO OPTICAL CORRECTORS	CONCEPT II AREA ARRAY WITH OPTICAL CORRECTORS	CONCEPT III AREA ARRAY W/ FOCAL LENGTH REDUCER	CONCEPT IV LINEAR ARRAY (1)	(2)	CONCEPT V NULL WITH ANGLE ENCODING	CONCEPT VI NULL WITH INTERFEROMETRY
MISSION REQUIREMENT							
● NOISE EQUIVALENT ANGLE ≤0.005 SEC	0.005	0.005	0.005	0.005		0.005	0.005
SYSTEM REQUIREMENTS							
● THRESHOLD VISUAL MAGNITUDE ≤14.5	13.4	14.8	14.8	13.2	12.5	14.5	14.5
● GUIDE FIELD AREA* ≥60 (ARCMINUTES)^2	100	37**	37**	120	200	160	160
● BANDWIDTH = 40 Hz	40	40	40		40	2.5	2.5
● INTEGRATION TIME =25 MILLISECONDS	25	25	25		25	400	400
● IMAGE CENTROIDING	1/166	1/43	1/43	1/40		1/43	1/43
GOALS							
● NO MOVING PARTS	NO	NO	NO	NO		YES	YES
● HIGH THROUGHPUT EFFICIENCY	YES	ZERO POWER OPTICAL CORRECTOR	RELAY OPTICS	BEAM SPLITTER		RELAY OPTICS	BEAM SPLITTERS

*FOR PROBABILITY = 85% OF TWO STARS

**RED SENSITIVE CCD REQUIRES SMALLER GUIDE FIELD AREA TO MEET THRESHOLD VISUAL MAGNITUDE

5.2.1 Concept I: Area Array With No Optical Correctors

This concept is shown in Figure 5.2.1. While the star image in the field of the OTA is highly astigmatic, the image midway between the sagittal and tangential focal surfaces is symmetrical and varies in diameter from 94 to 233 micrometers (96% encircled energy) corresponding to field positions from 9 to 15 arcminutes. Shown in Figure 5.2-2 are the subspot resolution requirements to implement optical pointing using the off-axis image at the circle of least confusion. To sense 0.005 arcsecond requires the ability to sense a displacement of the image from 1/67 to 1/166 of its spot diameter.
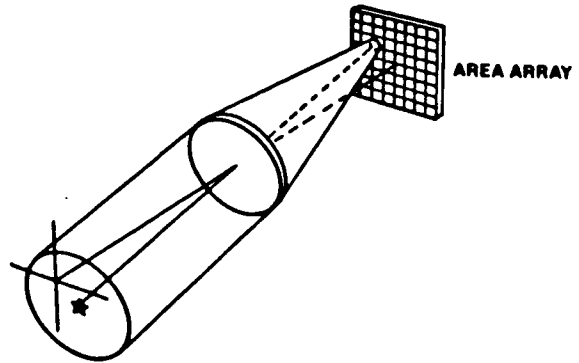
CONCEPT I

AREA ARRAY WITH NO OPTICAL CORRECTORS

Figure 5.2-1

This also means that the energy distribution within the image spread function must remain sufficiently stable such that its centroid is determinable to at least the same fraction of diameter as the displacement requirement so that the true image motion can be separated from an apparent shift in its centroid from noise sources.
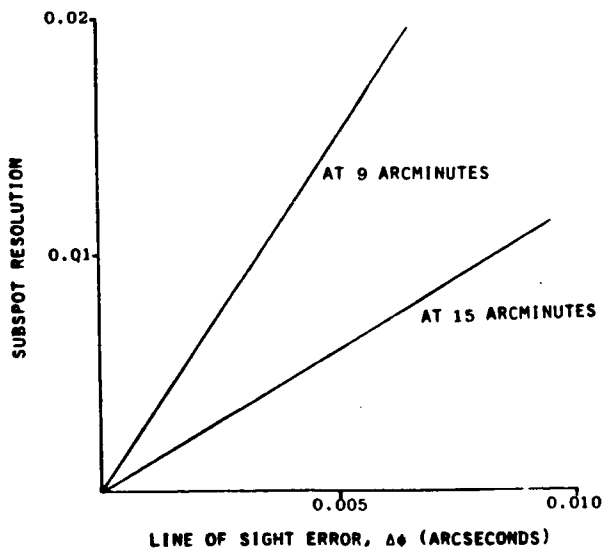
SUBSPOT RESOLUTION REQUIREMENTS
(AT CIRCLE OF LEAST CONFUSION)

Figure 5.2-2

The threshold visual magnitude requirements for the field angle extremes (9 and 15 arcminutes) are shown in Figures 5.2-3 and 5.2-4. The line of sight requirement can be met with 14.5 visual magnitude M0 stars at 9 arcminutes. However, at the edge of the field (15 arcminutes) brighter stars will be required due to the increased astigmatism.

- 2 PIXELS/SPOT
- QE = 70%
- σ_E = 70 ELECTRONS AT 60 HZ
- ξ = 0.785
- BANDWIDTH = 40 HZ
- T = 0.83
- CCD AREA ARRAY
- SFA = 9 ARCMINUTES
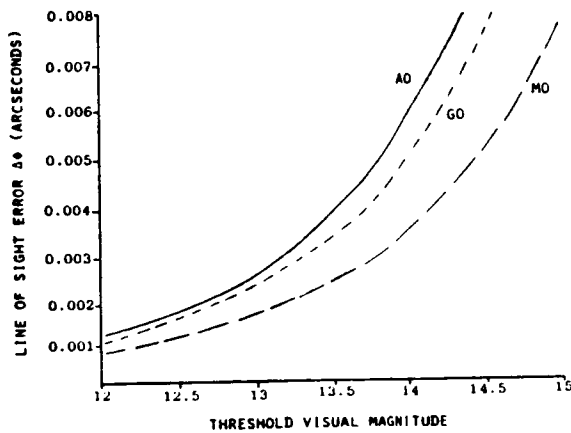
THRESHOLD VISUAL MAGNITUDE REQUIREMENT

Figure 5.2-3

- 2 PIXELS/SPOT
- QE = 70%
- σ_E = 70 ELECTRONS AT 60 HZ
- ξ = 0.785
- BANDWIDTH = 40 HZ
- T = 0.83
- CCD AREA ARRAY
- SFA = 15 ARCMINUTES
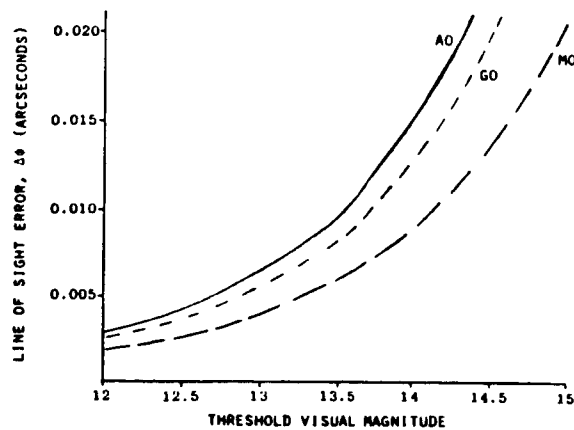
THRESHOLD VISUAL MAGNITUDE REQUIREMENT

Figure 5.2-4

5-15

Shown in Figure 5.2-5 is the interrelationship between guide field area and integration time. The threshold visual magnitude requirement can be met by increasing the field area with the same integration time. Shown in Figure 5.2-6 is the interrelationship between integration time and the threshold visual magnitude. The threshold visual magnitude requirement can be met by increasing the integration time with the same field area. Concept I implementation is summarized in Table 5.2-2.
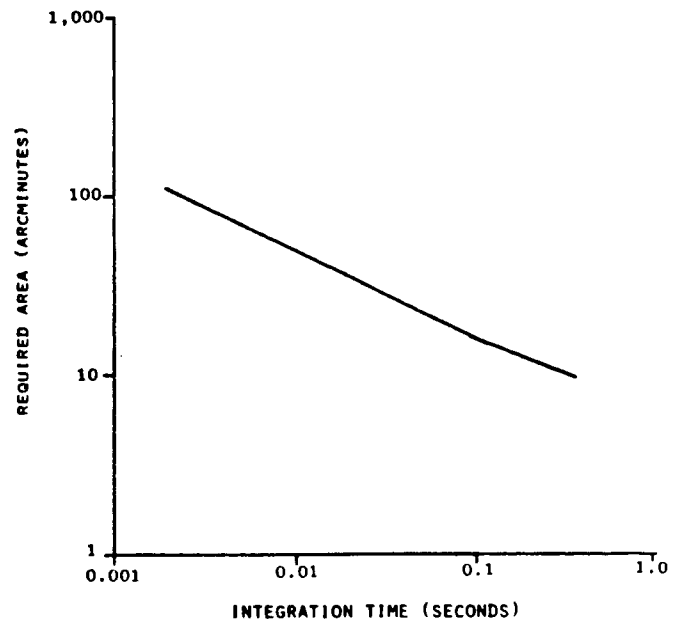
GUIDE FIELD AREA REQUIREMENT
(P = 85% FOR TWO STARS)

Figure 5.2-5

- Δφ = 0.005 ARCSECONDS
- CCD AREA ARRAY
- IMAGE CENTROIDING = 1/166
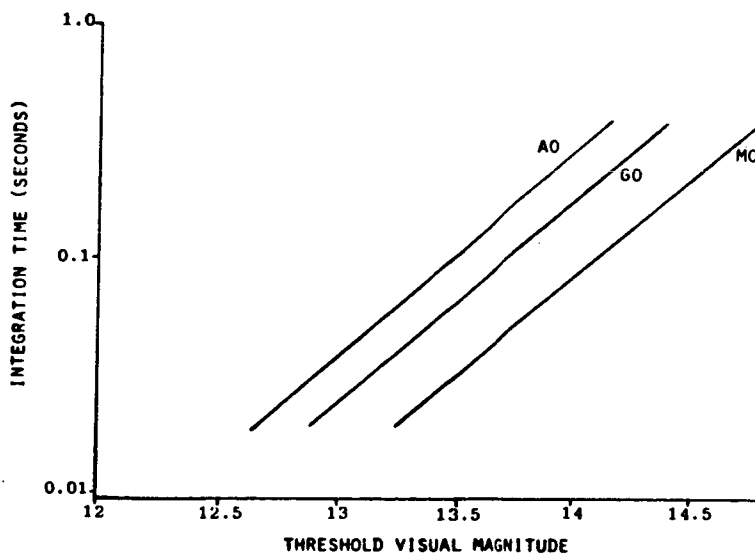
INTEGRATION TIME VS. THRESHOLD VISUAL MAGNITUDE

Figure 5.2-6

Table 5.2-2

CONCEPT IV IMPLEMENTATION

OPTION NO. 1 (INCREASE GUIDE FIELD AREA)

- THRESHOLD VISUAL MAGNITUDE $\qquad$ 13.4 M_v
- GUIDE FIELD AREA $\qquad$ 46 $\widehat{MIN}^2 \longrightarrow$ 100 $\widehat{MIN}^2$
- INTEGRATION TIME $\qquad$ 25 MSEC (40 HZ)
- IMAGE CENTROIDING $\qquad$ 1/166

OPTION NO. 2 (INCREASE INTEGRATION TIME)

- THRESHOLD VISUAL MAGNITUDE $\qquad$ 13.4 $M_v \longrightarrow$ 14.5 M_v
- INTEGRATION TIME $\qquad$ 0.025 SEC (40 HZ) $\longrightarrow$ 0.25 SEC (4 HZ)
- GUIDE FIELD AREA $\qquad$ 46 $\widehat{MIN}^2$
- IMAGE CENTROIDING $\qquad$ 1/166

5.2.2 Concept II: Area Array With Optical Corrector

This concept is shown in Figure 5.2-7. The OTA configuration is an all-reflect-
ing (catoptric) design. The Ritchey-Chretien system was chosen over other two
mirror designs because third-order spherical aberration and coma are complete-
ly corrected. The main disadvantage is the remaining astigmatism which cannot
also be corrected with the two mirrors. Recently several well corrected three
and four mirror catoptric telescopes have been proposed which have the advant-
age of eliminating astigmatism as well as flattening the field. However, the
configurations require modifying the lens parameters (radii and conical
shapes) of the existing primary and secondary mirrors. An alternate approach
is to use refractive field correctors with the same two mirror telescope.
This in essence changes the telescope configuration from the catoptric Ritchey-
Chretien version to a catadioptric Ritchey-Chretien version. This was pre-
viously suggested by Solomon ("An Image Stabilization System for the Large
Space Telescope", Space Optics, SPIE Seminar Proceedings (1976), Volume 19).
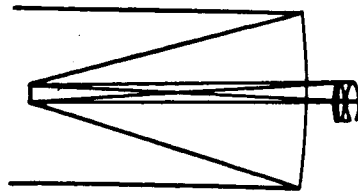
CONCEPT II: AREA ARRAY WITH OPTICAL CORRECTORS

Figure 5.2-7

In this concept the field correctors are made into an annulus lens. The central portion without refractive elements is used with the scientific instruments. The outer annulus is used in the fine guidance sensing guide area. Chromatic aberrations are minimized by having a zero power corrector group and by using the same type of glass (fused silica) for each corrector element. The uncorrected aberrations are field curvature and distortion. It should be noted that in this concept a Petzval lens which should produce a flat field is not required. By matching the detector surface to the image field the astigmatisim will be corrected and the image diameter will be reduced to about 60 microns over the full 9 to 15 arcminute field. By using a zero power corrector the system focal length will remain unchanged and therefore the plate scale factor (displacement sensitivity) will remain the same. Shown in Figure 5.2-8 are the subspot, resolution requirements to implement optical pointing using the corrected image. To sense 0.005 arcsecond requires the ability to sense a displacement of the image 1/43 of its spot diameter. The threshold visual magnitude requirements are shown in Figure 5.2-9. The line of sight requirement can be met with 14.8 visual magnitude M0 stars. Shown in Figure 5.2-10 is the interrelationship between integration time and threshold visual magnitude. The threshold visual magnitude requirement can be met with the integration time requirement. Concept II implementation is summarized in Table 5.2-3.

- 2 PIXELS/SPOT
- QE = 70%
- σ_E = 70 ELECTRONS AT 60 Hz
- ξ = 0.785

- BANDWIDTH 40 Hz
- γ = 0.83
- CCD AREA ARRAY
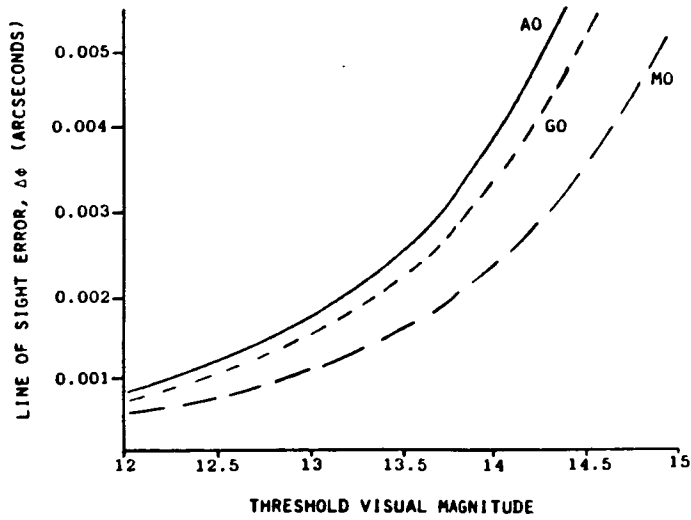
THRESHOLD VISUAL MAGNITUDE REQUIREMENT

Figure 5.2-8

$\Delta\phi$ = 0.005 $\widehat{SEC}$ → IMAGE CENTROIDING = 1/43
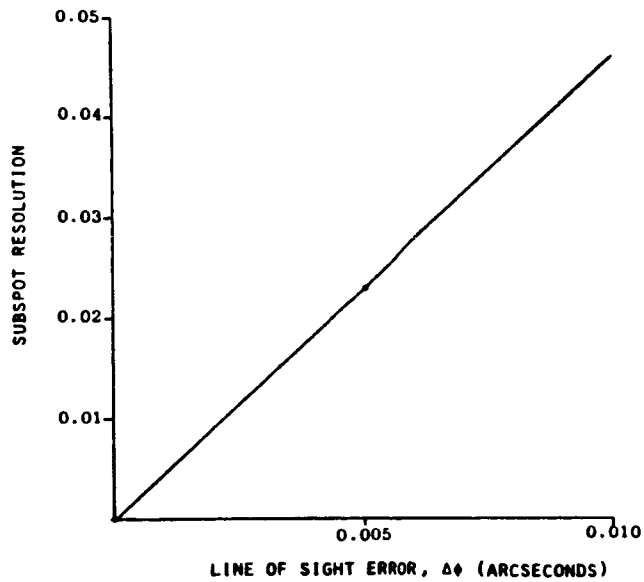
SUBSPOT RESOLUTION REQUIREMENTS
(AT CIRCLE OF LEAST CONFUSION)

Figure 5.2-9

- Δφ = 0.005 ARCSECOND
- CCD AREA ARRAY
- IMAGE CENTROIDING = 1/43
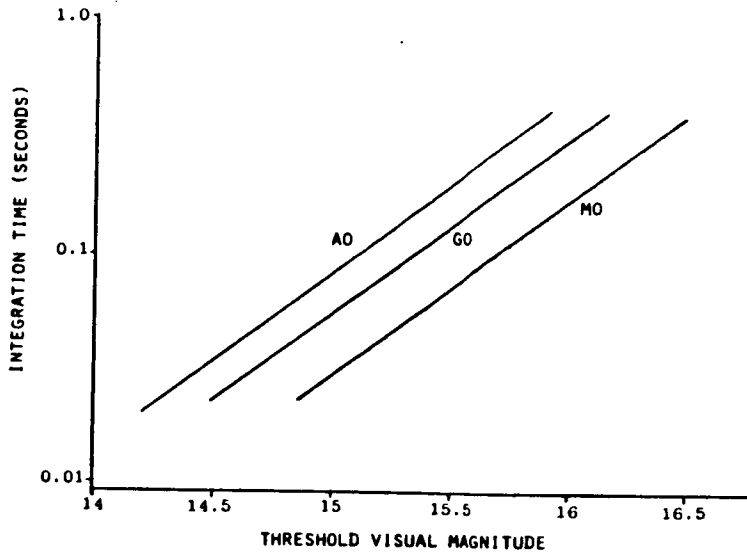

INTEGRATION TIME VS. THRESHOLD VISUAL MAGNITUDE

Figure 5.2-10

Table 5.2.3

CONCEPT II IMPLEMENTATION

● THRESHOLD VISUAL MAGNITUDE	14.8
● GUIDE FIELD AREA	37 $\widehat{MIN}^2$
● INTEGRATION TIME	25 MSEC
● IMAGE CENTROIDING	1/43

5.2.3 Concept III: Focal Length Reducer

This concept is shown in Figure 5.2-11. It was previously suggested by
Stanton ("CCD Star Sensor for Fine Pointing Control of Spaceborne Telescopes",
J. Guidance and Control, Volume 3, No. 2, March-April 1980).
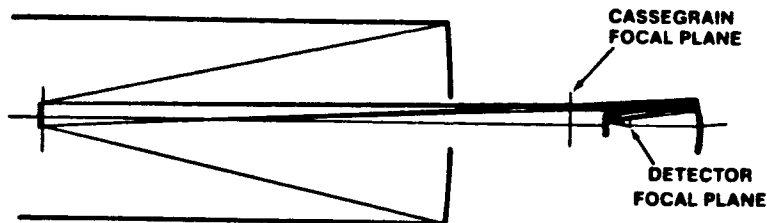
CONCEPT III: AREA ARRAY WITH FOCAL LENGTH REDUCER
Figure 5.2-11

In this concept the additional optics are used to change the optical subsystem
focal length. This will affect the plate scale factor, image size, and field
of view. Shown in Table 5.2-4 is a comparison of field areas to meet the
visual threshold magnitude and integration time requirements. Decreasing the
focal length by 5 decreases the field area by 25, thereby reducing the de-
tector area by 25. This concept will theoretically meet the technical require-
ments and has merit from a detector cost standpoint.

Table 5.2-4 GUIDE STAR AREA (M^2)			
	5xf	1xf	1/5xf
● SINGLE FGS (60 MIN^2)	0.69	0.028	0.0011
● THREE FGS (207 MIN^2)	2.07	0.084	0.0032
● TOTAL OUTER ANNULUS (289 MIN^2)	2.89	0.117	0.0045

5.2.4 Concept IV: Linear Arrays With Optical Corrector

In this concept linear arrays are located at the image surface. Two arrays
are employed; one perpendicular to the sagittal field curve and one perpen-
dicular to the tangential field curve of the astigmatic image. Positional
information is obtained along the length of each array, and this displacement
divided by the optical subsystem focal length yields the line of sight error
of the star. A beam splitter before the two arrays compensates for the
physical separation between the sagittal and tangential focal surfaces. The
length of the astigmatic image permits motion orthogonal to the length of the
array up to 2 arcseconds. Motion in the other direction can be about one
inch, or 90 arcseconds.

Theoretically this is a low throughput approach. The beam splitter will
reduce the transmittance by 50%. The length to width of the PSF at the astig-
matic focal surface could be as large as 10 to 1 at the edge of the field.
The overall result is that only about 1/20 of the flux in the astigmatic image
strikes the array. Figure 5.2-12
shows a scheme for getting all the
flux from the astigmatic image focused
on the array. Linear arrays used in
spectrometers have pixel dimensions of
25 micrometers by 2 millimeters. A

CONCEPT IV: LINEAR ARRAY WITH
OPTICAL CORRECTOR
Figure 5.2-12

cylindrical f/2.3 lens would image the
optical subsystem exit pupil onto the
array, but only in the Y direction. A collimated beam entering the optical
subsystem and within the field of view of the cylindrical lens forms a line-
like image onto the linear array. The width of the line is the diffraction
width. The length of the line is equal to the image of the aperture, which is
equal to the array width (2 millimeters). The system is insensitive to
rotation of the input beam about the X-axis. For beam rotations about the
Y-axis, the image moves along the array. The cylindrical lens will be about
1-inch by 1-inch corresponding to a capture range of 100 by 100 arcseconds.

The star image in the field of the OTA is highly astigmatic. The image midway between the sagittal and tangential focal surfaces is symmetrical and varies in diameter. The geometrical image at either the sagittal or tangential focal surface is asymmetrical. At the sagittal focal surface the line width retains its on-axis diffraction limited performance at the expense of an increase in line width. At the tangential focal surface the line width and line length would be revised. Shown in Figure 5.2-13 are the subspot resolution requirements to implement optical pointing using the off-axis image at either the sagittal or tangential focus (80% encircled energy). To sense 0.005 arc-seconds requires the ability to sense a displacement of the image to 1/40 of its spot width.

The threshold visual magnitude requirements for an integration time of 25 milliseconds are shown in Figures 5.2-14 and 5.2-15. A CCD linear array with pixel dimensions of 25-micrometers by 25-micrometers was used in the former, and a CCD linear array with pixel dimensions of 25-micrometers by 2-millimeters was used in the latter. This yields a threshold visual magnitude of 13.2 for the former and 12.5 for the latter. Shown in Figure 5.2-16 is the integration time requirements to reach threshold visual magnitude.
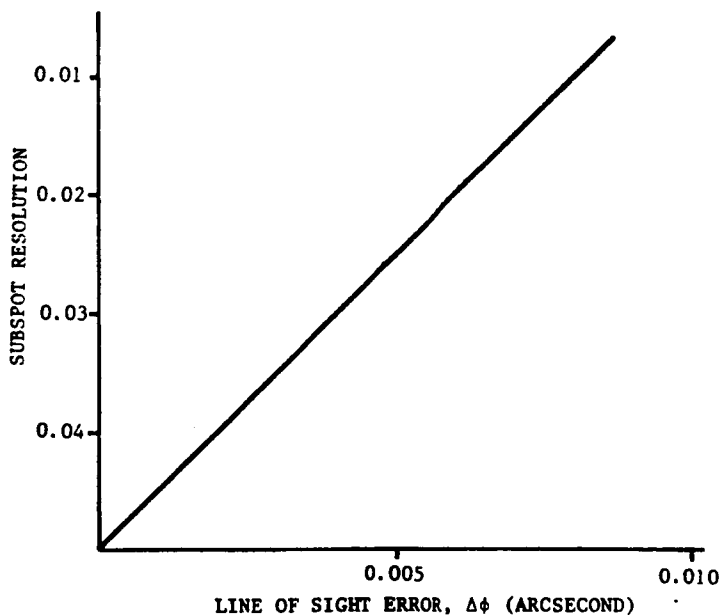
SUBSPOT RESOLUTION REQUIREMENTS

Figure 5.2-13

- 2 PIXELS/SPOT
- QE = 70%
- σ_E = 50 ELECTRONS AT 60 Hz

- ξ = 0.10
- BANDWIDTH = 40 Hz
- CCD LINEAR ARRAY

- 2 PIXELS/SPOT
- QE = 70 PERCENT
- σ_E = 500 ELECTRONS AT 60 Hz

- ξ = 0.50
- BANDWIDTH = 40 Hz
- CCD LINEAR SPECTRO-SCOPIC ARRAY
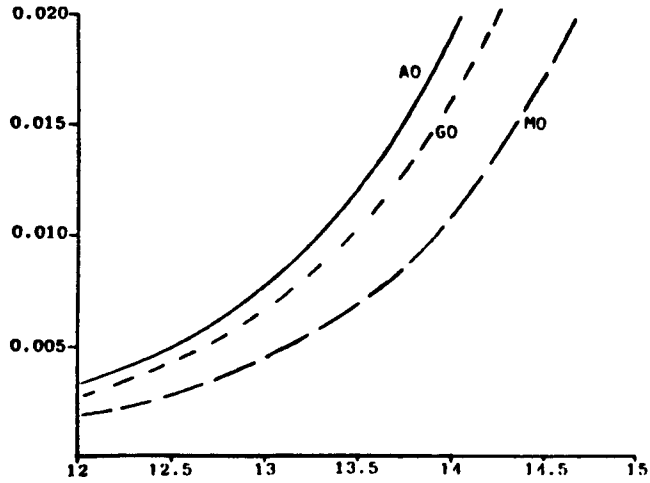
THRESHOLD VISUAL
MAGNITUDE REQUIREMENT

Figure 5.2-14
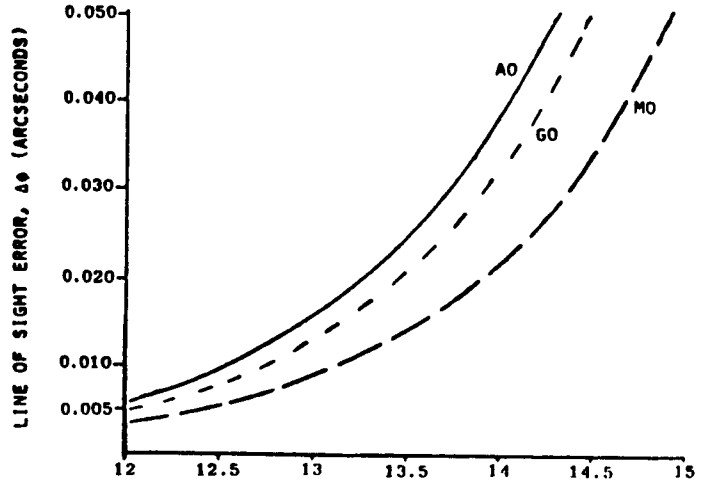
THRESHOLD VISUAL
MAGNITUDE REQUIREMENT

Figure 5.2-15

- $\Delta\phi$ = 0.005 ARCSECOND
- CCD LINEAR ARRAY
- IMAGE CENTROIDING = 1/40
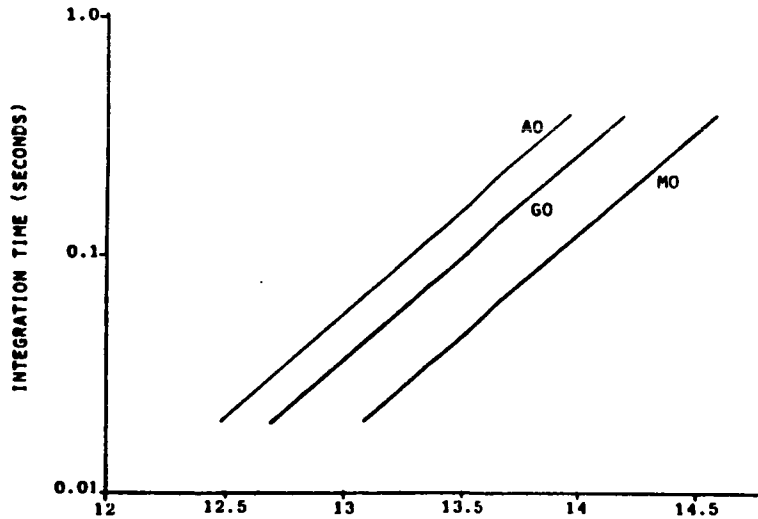
INTEGRATION TIME VS. THRESHOLD VISUAL MAGNITUDE

Figure 5.2-16

To meet the 14.5 visual magnitude requirement requires an integration time of 400 milliseconds. An alternate approach would be to leave the integration time at 25 milliseconds and allow the threshold visual magnitude to be 12.5. This can be accomplished by increasing the guide field area from 46-square arcminutes to 200-square arcminutes. Implementation of Concept IV is summarized in Table 5.2-5.

Table 5.2.5
CONCEPT IV IMPLEMENTATION

OPTION NO. 1 (INCREASE GUIDE FIELD AREA)	
● THRESHOLD VISUAL MAGNITUDE	12.5 M_v
● GUIDE FIELD AREA	46 $MIN^2 \longrightarrow 200\ MIN^2$
● INTEGRATION TIME	0.025 SEC (40 HZ)
● IMAGE CENTROIDING	1/40
OPTION NO. 2 (INCREASE INTEGRATION TIME)	
● THRESHOLD VISUAL MAGNITUDE	12.5 $M_v \longrightarrow 14.5\ M_v$
● INTEGRATION TIME	0.025 SEC (40 HZ) $\longrightarrow$ 0.40 SEC (2.5 HZ)
● GUIDE FIELD AREA	46 MIN^2
● IMAGE CENTROIDING	1/40

5.2.5 Concept V: Null With Angle Encoding

In this concept, knowledge of the angle in object space is related to knowledge of the tilt of the incoming plane wavefront. By the selection of the focal length of a collimator, an afocal magnification is provided. Tilt of the outgoing plane wavefront will be directly related to the tilt of the incoming plane wavefront. By monitoring the larger angular changes in the collimated space, the smaller values can be predicted in object space. Figure 5.2-17 shows this concept. The second image is monitored for null rather than for position. Two orthogonal flats are inserted in the collimated space. After null, the orientation of these orthogonal flats are established with shaft encoders. These angles can then be related to object space angular information. This concept was selected for the Automatic Transit Circle (ATC) of the U. S. Naval Observatory. The threshold visual magnitude requirements for an integration time of 25 milliseconds is shown in Figure 5.2-18. In this concept a photomultiplier with an S-20 photocathode was selected. The curves for the AO and MO stars are therefore reversed from those previously shown for the solid state sensors.
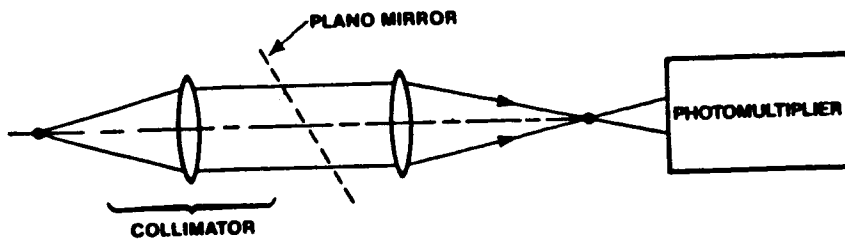
CONCEPT V: NULL WITH ANGLE ENCODING

Figure 5.2-17

- 2 PIXELS/SPOT
- QE = 18%
- σ_E = 10 ELECTRONS AT 60 Hz

- ξ = 0.30
- BANDWIDTH = 40 Hz
- S-20 PHOTOMULTIPLIER
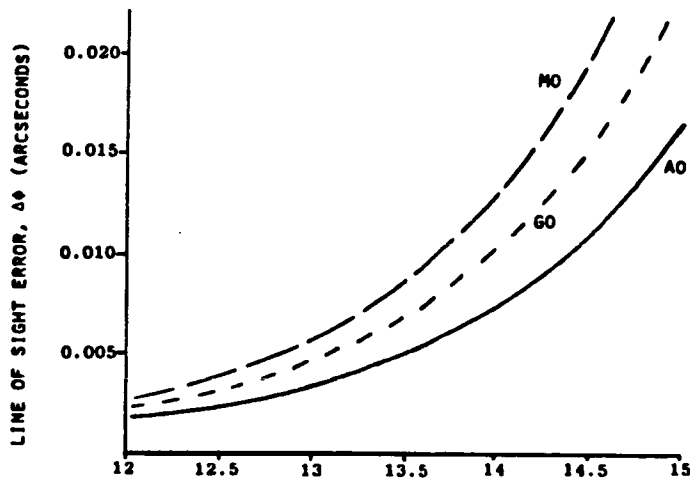
THRESHOLD VISUAL MAGNITUDE REQUIREMENT

Figure 5.2-18

Shown in Figure 5.2-19 is the integration time requirement to reach threshold visual magnitude. It should be noted from this figure that with an integration time of 25 milliseconds the 14.5 threshold visual magnitude requirement is not met. However, in practice the data can be sampled over a time of 25 milliseconds and averaged over many samples. The number of samples chosen here was 16. This allows for a longer integration time of 400 milliseconds. From Figure 5.2-20 it can be seen that threshold visual magnitude requirement can then be met.

- $\Delta\phi$ = 0.005 ARCSECOND
- S-20 PHOTOCATHODE
- IMAGE CENTROIDING = 1/43
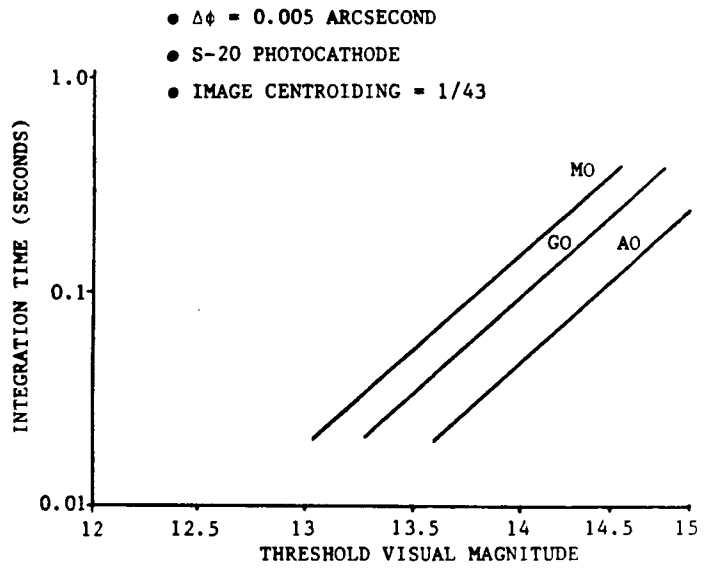
INTEGRATION TIME VERSUS THRESHOLD VISUAL MAGNITUDE

Figure 5.2-19

- 2 PIXELS/SPOT
- QE 18%
- σ_E = 10 ELECTRONS AT 60 HZ
- ξ = 0.30
- BANDWIDTH = 2.5 HZ
- S-20 PHOTOMULTIPLIER
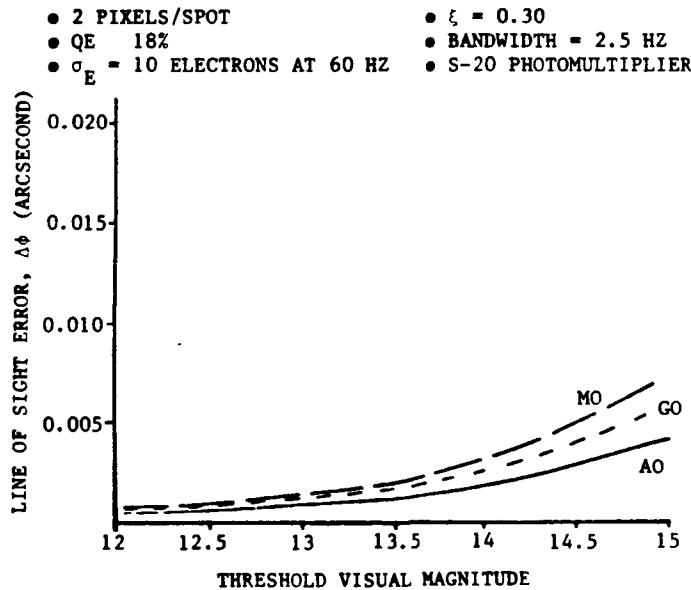
THRESHOLD VISUAL MAGNITUDE REQUIREMENT

Figure 5.2-20

5.2.6 Concept VI: Null With Interferometer

Figure 5.2-21 shows the second version using the wavefront. The detectors interogate the total intensity of the signal which varies as the star moves. The collimated beam is split into two orthogonal channels. Each channel illuminates a refractive prism ("Koester's prism"). When the collimated beam is exactly perpendicular to the prism base, the interference patterns seen by the photomultipliers are the same and the signal is balanced. As the angle of the collimated beam changes, the fringe patterns and the subsequent intensities change.
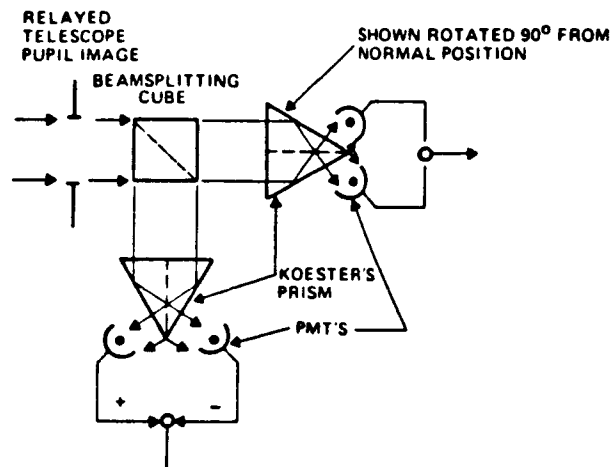
KOESTER'S PRISM INTERFEROMETER

Figure 5.2-21

The threshold visual magnitude requirement for a bandwidth of 40 Hertz is shown in Figure 5.2-22. A photomultiplier with an S-20 photocathode was selected. It shold be noted that a 14.5 threshold visual magnitude requirement is not met with an integration time of 25 milliseconds.

- 2 PIXELS/SPOT
- QE ≈ 18%
- σ_E = 10 ELECTRONS AT 60 HZ
- ζ = 0.30
- BANDWIDTH = 2.5 HZ
- S-20 PHOTOMULTIPLIER
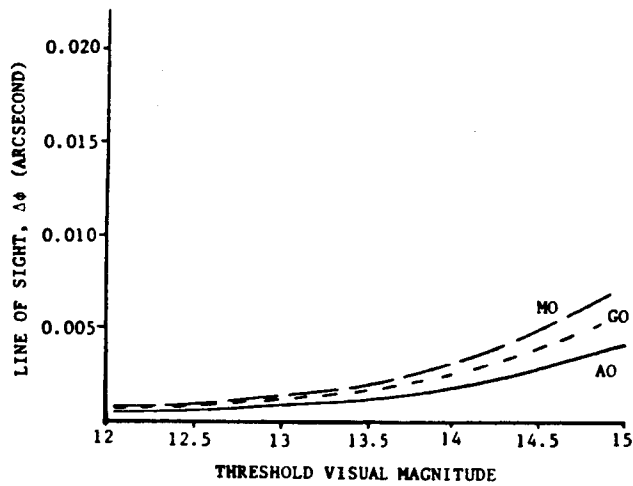
THRESHOLD VISUAL MAGNITUDE REQUIREMENT

Figure 5.2-22

It is assumed that a longer integration time can be used by averaging over many samples. From Figure 5.2-23 it can be seen the line of sight error requirements and the threshold visual magnitude requirement can be met for all spectral classes from AO to MO with an integration time of 400 milliseconds.

- Δφ = 0.005 ARCSECOND
- S-20 PHOTOCATHODE
- IMAGE CENTROIDING = 1/43
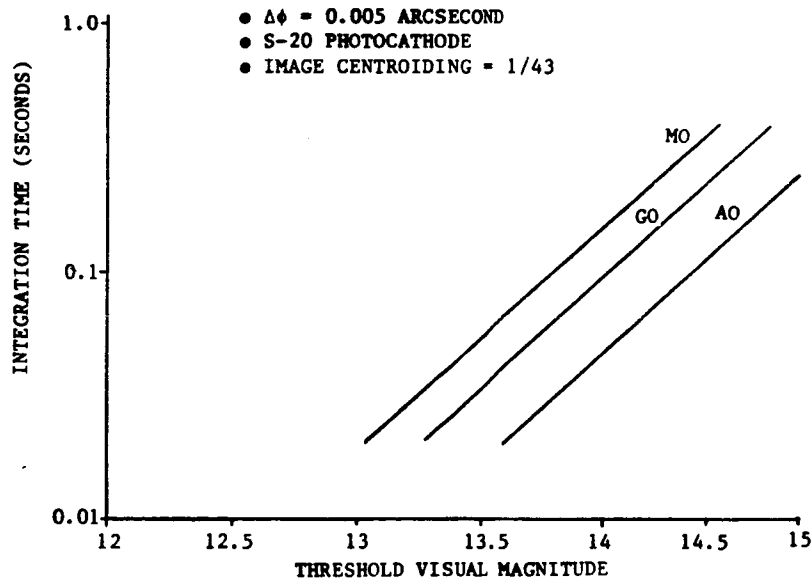
INTEGRATION TIME VS. THRESHOLD VISUAL MAGNITUDE

Figure 5.2-23

5-29

6.0 <u>CONCEPTUAL DESIGN</u>

Major elements of the Uprated Fine Guidance Sensor include the optics, support structure for the optics/detector and the detector itself (Figure 6.0-1).
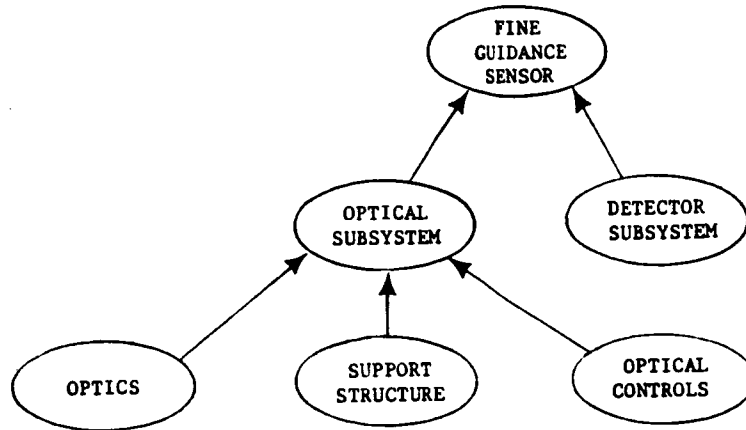
MAJOR ELEMENTS IN FINE GUIDANCE SENSOR

Figure 6.0-1

Two concepts have been selected for conceptual design layout and analysis: (1) area arrays with optical correctors, and (2) linear arrays with optical corrector.

6.1 AREA ARRAY WITH OPTICAL CORRECTORS

6.1.1 <u>Optical Subsystem</u>

The optical subsystem chosen is a catadioptric Ritchey-Chrétien telescope (catoptric Ritchey-Chrétien OTA with refracting correctors). The intent is to correct the astigmatism in the optical subsystem field. The size of the image will be smaller. This will allow the image centroiding parameter, which would be as large as 1/166, without the correctors to be reduced to a value less than 1/50.

Shown in Table 6.1.1 is a "preliminary" lens formula. The reflective portion represents the OTA. The optical corrector consists of two refractive elements made from fused silica. With this "zero-power" correction the overall system focal length (57.6 meters) will be retained from the OTA design. It should be

noted that in this preliminary design the two refractive elements have some negative power which could be eliminated in an optimized design.

Table 6.1-1
RITCHEY-CHRETIEN WITH TWO-SEPARATED REFRACTING CORRECTORS
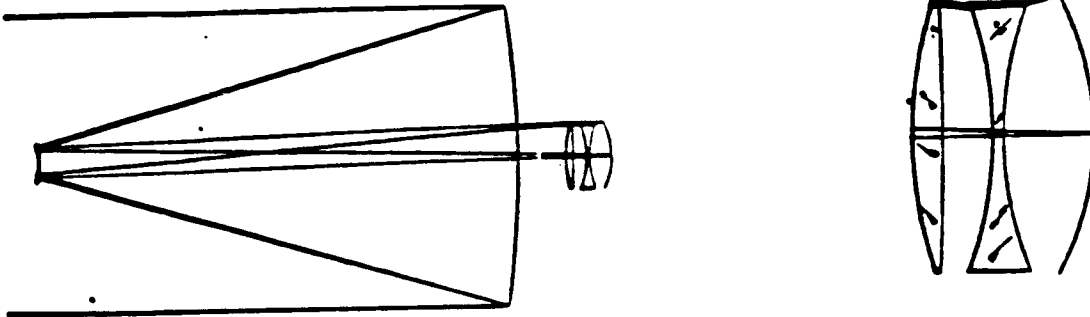
BASIC LENS DATA

SURF	CV	TH	MEDIUM	RN	BF
0	0.0	0.399998D+10	AIR		
1	0.0	0.0	AIR		
2	-0.060521	-7.313381	REFL		
3	-0.612617	8.273657	REFL		
4	0.584388	0.117125		1.457710	21.052
5	-0.078848	0.197704	AIR		
6	-0.651733	0.041553		1.457710	21.052
7	0.679709	0.0	AIR		
8	0.0	0.349678	AIR		
9	-0.849648	0.0	AIR		

REFRACTIVE INDICES

SURF	N1	N2	N3	N4	N5
4	1.457710	1.464143	1.450234	1.000000	1.000000
6	1.457710	1.464143	1.450234	1.000000	1.000000

CC AND ASPHERIC DATA

SURF	CC	AD	AE	AF	AG
2	-1.00221D+00				
3	-1.42817D+00				

CLEAR APERTURES AND OBSTRUCTIONS

SURF	TYPE	CAY	CAX
2	CIRCLE	2.3600	

REF OBJ HT	REF AP HT	OBJ SURF	REF SURF	IMG SURF
0.275999D+08 (-0.40 DG)	2.35999	0	1	9

EFL	BF	F/NBR	LENGTH	SIH
100.0000	0.3497	21.19	8.6300	-0.6900

WAVL NBR	1	2	3	4	5
WAVELENGTH	0.61000	0.47000	1.01400	0.0	0.0
SPECTRAL WT	1.0000	1.0000	1.0000	0.0	0.0

APERTURE STOP AT SURF 2

The corrector lens sizes and locations are shown in Figure 6.1-1. It should be noted that the central section has been removed for use with the scientific instruments.
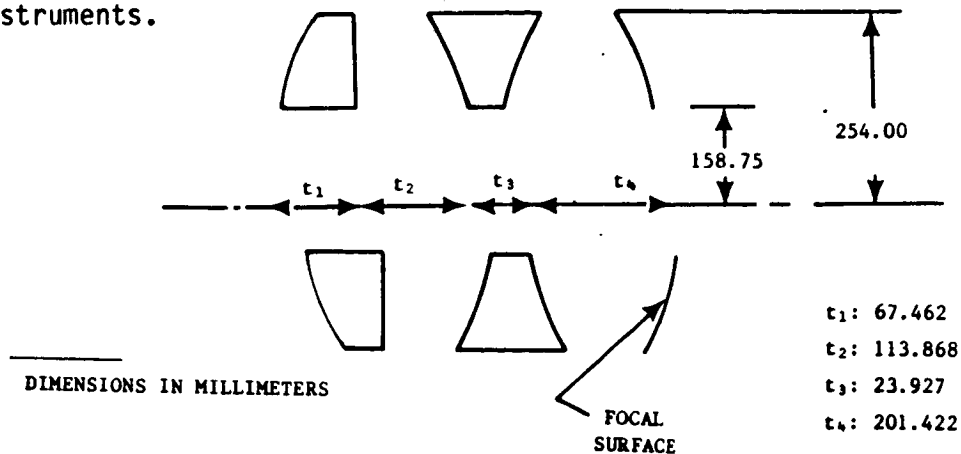
LOCATION AND SIZE OF CORRECTOR ELEMENTS

Figure 6.1-1

Shown in Figure 6.1-2 is the anticipated image diameter at the circle of least confusion. At the edge of the field (15 arcminutes) the spot size for the catoptric subsystem could be as large as 215 micrometers. To obtain a line of sight error in object space of 0.005 arcsecond requires a subimage resolution of 1 part in 166. This is currently beyond the state-of-the-art. With the corrector lens this spot size could be reduced to 60 micrometers. Therefore, to obtain a line of sight error

OTA IMAGE DIAMETER (AT CIRCLE OF LEAST CONFUSION)

Figure 6.1-2

in object space of 0.005 arcsecond would require a subimage resolution of 1 part in 43. This is within the current capability.
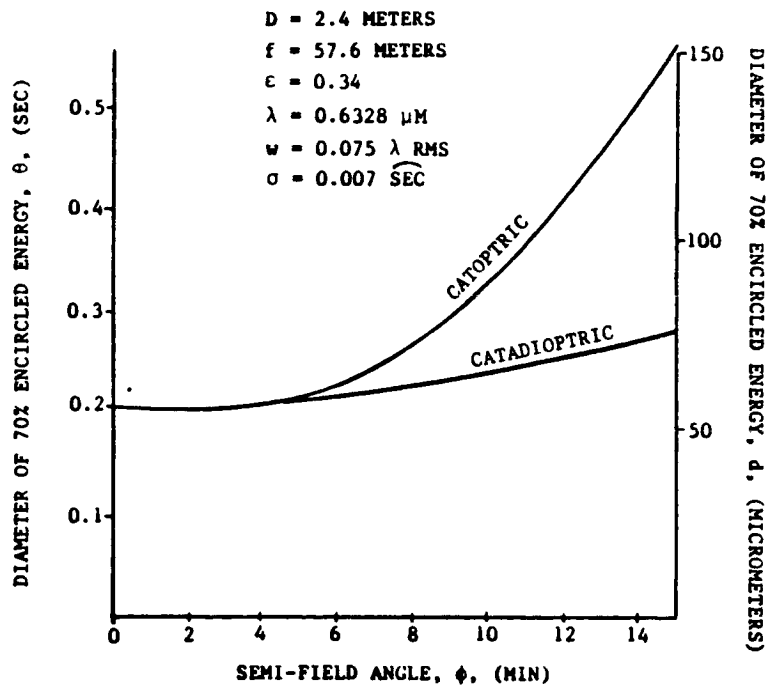
If a catoptric optical subsystem is used the image surface presented to the detector surface will consist of two well defined surfaces (tangential and sagittal). These surfaces must be matched to the array surfaces. In this case the intermediate surface (I) between the tangential and sagittal surfaces would probably be optimum for matching. If the catadioptric optical subsystem is used, the astigmatism will be reduced and the two focal surfaces will coalesce onto a single surface (Petzval surface). The area arrays would be installed onto this surface (Figure 6.1-3). It should be emphasized that in this case the catadioptric subsystem is field curvature limited. No attempt has been made to design a flat field. The field curvature presented by the optical subsystem is accommodated by an overall curved detector subsystem curvature. Over a localized area of the surface (i.e., the area of the active area of a single array) the array is tangent to the Petzval surface.
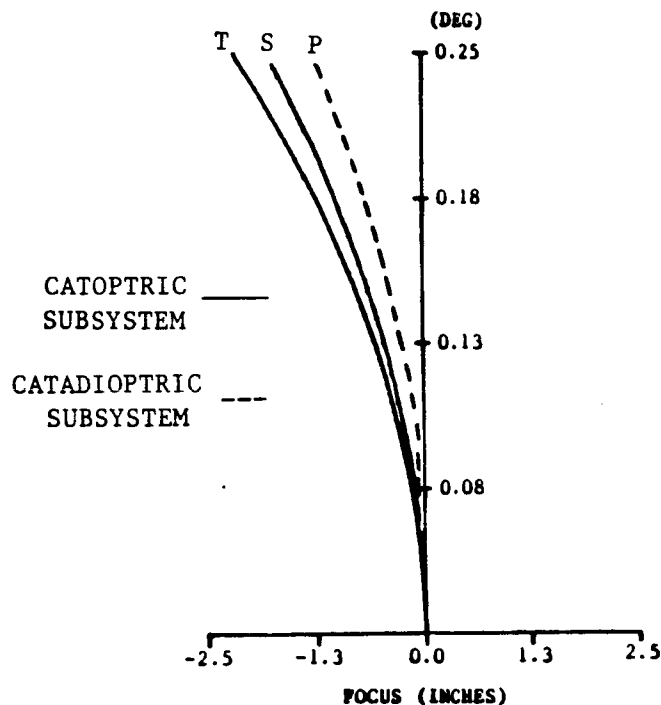
FOCAL PLANE TOPOGRAPHY

Figure 6.1-3

6.1.2 Detector Subsystem

Potential area arrays for star tracking applications were tabulated in Table 4.1-2. The RCA SID501D area array was selected for this analysis. This is a

large format, square pixel CCD having the following features: 1) frame transfer or full array imaging, 2) 512 x 320 pixels, each 30 by 30 micrometers in full array, 3) 12.2 millimeter image diagonal for frame transfer operation, 4) low noise (typically 50 electrons when slow scanned and cooled). The optical subsystem image spot will be approximately 60 micrometers. This results in approximately 2 pixels per spot--the preferred value.

The dimensional outline of the RCA SID501D area array is shown in Figure 6.1-4. The active area will cover a field of view of 0.26 square arcminute.
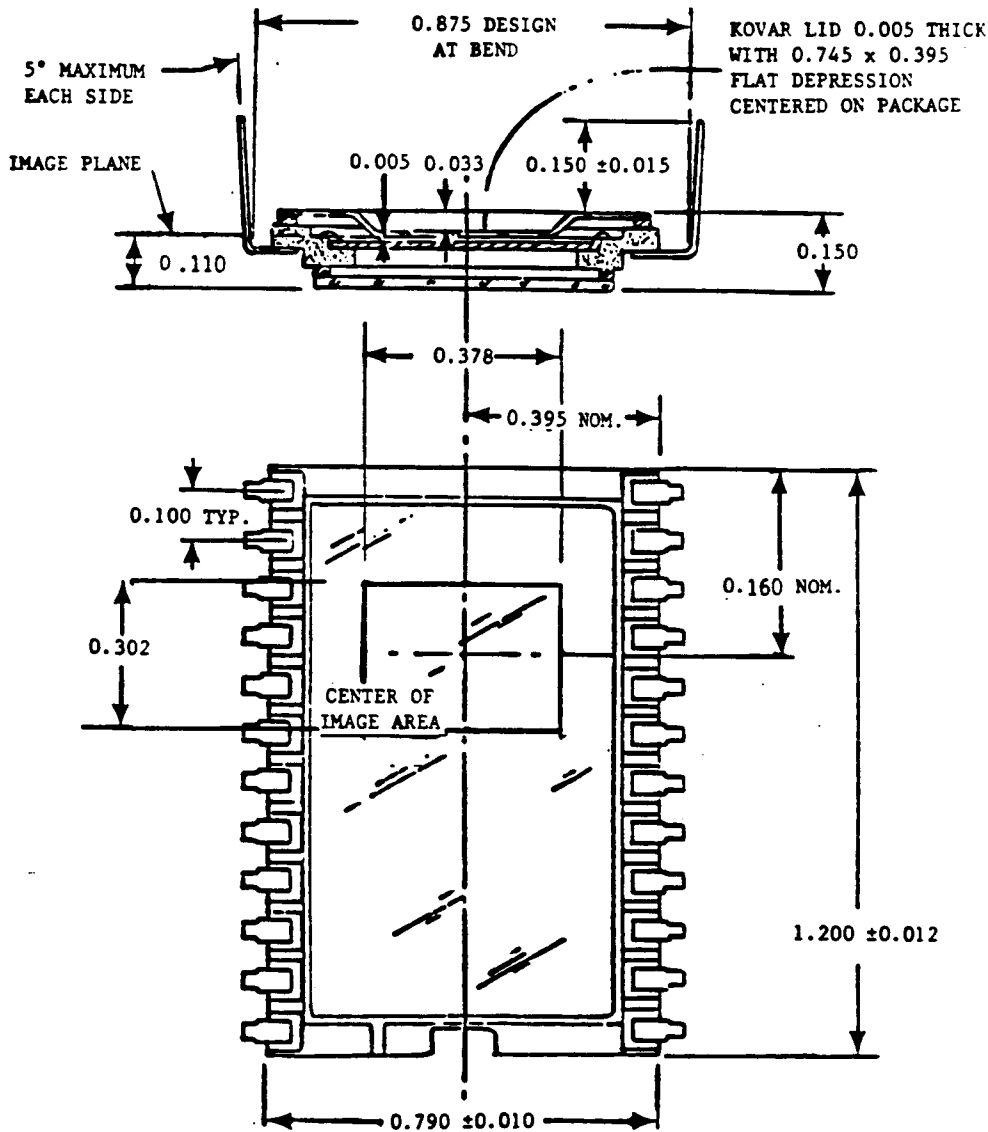
ALL DIMENSIONS IN INCHES

SID501D DIMENSIONAL OUTLINE

Figure 6.1-4

6.1.3 Performance Prediction

The threshold visual magnitude
requirement to meet the line of
sight error requirement for the
RCA SID501D area array is shown
in Figures 6.1-5 and 6.1-6. At a
bandwidth of 40 Hertz, a thres-
hold visual magnitude of 15.0 is
required to meet a line of sight
error requirement of 0.005
arcsecond. At a bandwidth of 15
Hertz a threshold visual mag-
nitude of 15.5 is required to meet
a line of sight error requirement
of 0.005 arcsecond. It is anticipated that the noise level will be 50 elec-
trons per pixel at 60 Hertz when the array is cooled to -40°C.
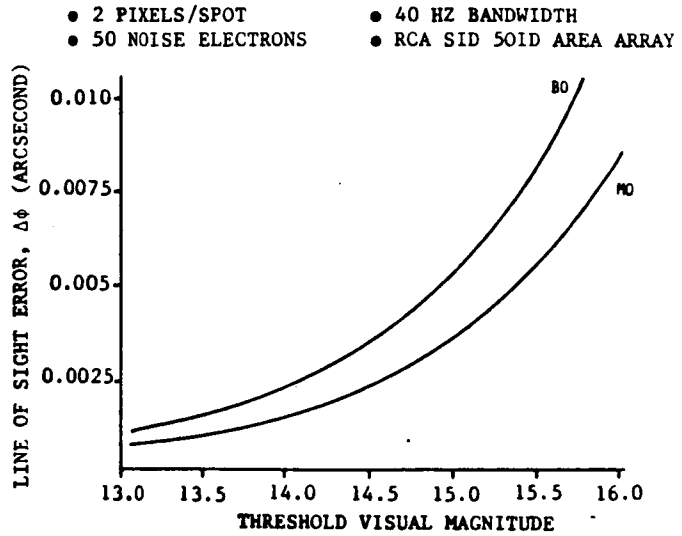
THRESHOLD VISUAL MAGNITUDE REQUIREMENT

Figure 6.1-5
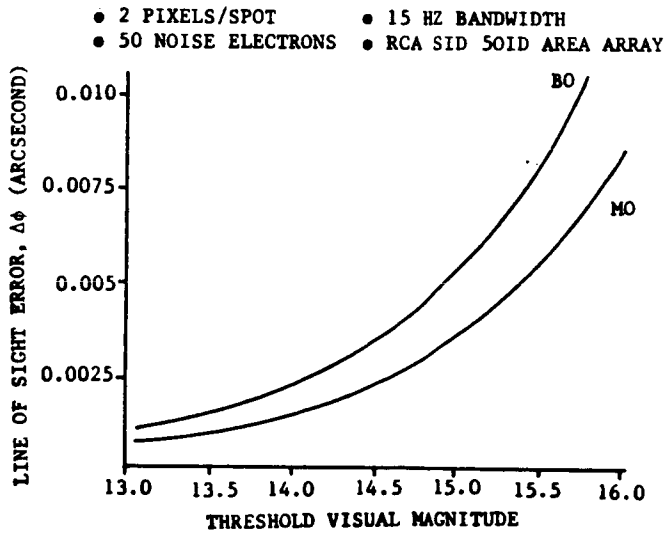
THRESHOLD VISUAL MAGNITUDE REQUIREMENT

Figure 6.1-6

The minimum guide field area required to acquire two stars with a probability of 85% is shown in Figure 6.1-7. For a threshold instrumental magnitude of 15, 33.3 square arcminutes are required. For a threshold instrumental magnitude of 15.5, 22 square arcminutes are required. The active area of the array will cover a field of view of 0.26 square arcminute. Therefore, 128 arrays are required to fill 33.3 square arcminutes or 85 arrays are required to 22 square arcminutes. Shown in Figure 6.1-8 is the required number of arrays as a function of bandwidth. The number of arrays can be reduced by decreasing the bandwidth (i.e., increasing the integration time).
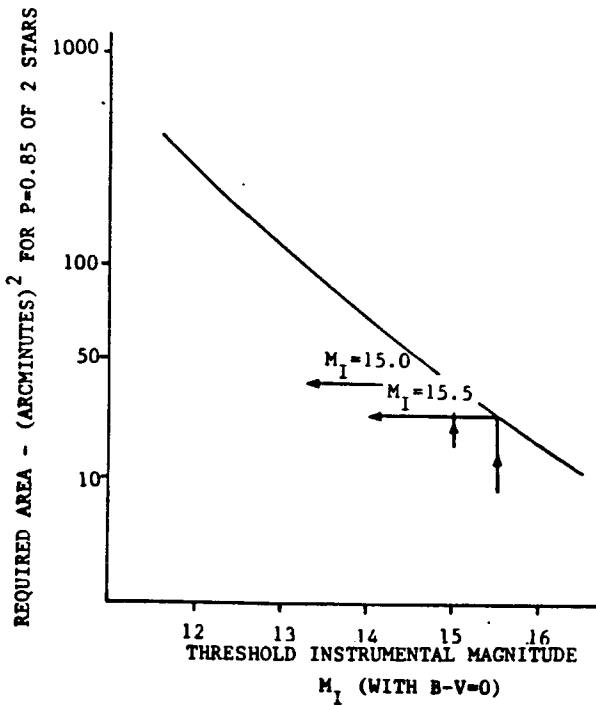
GUIDE FIELD AREA REQUIREMENT

Figure 6.1-7
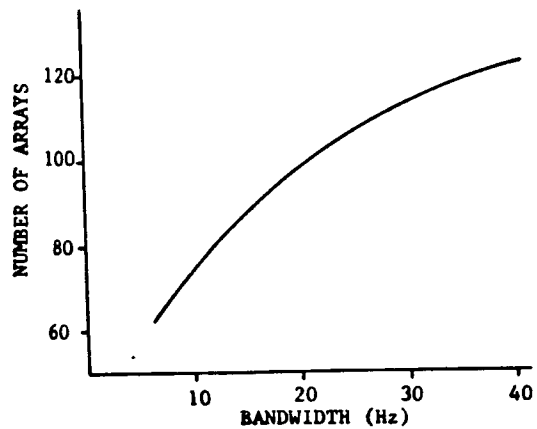
NUMBER OF AREA ARRAYS (RCA SID501D; 50 NOISE ELECTRONS)

Figure 6.1-8

As many as 140 arrays can be arranged in the current OTA annulus. Shown in Figure 6.1-9 is an arrangement in which 128 arrays are located in three annular zones within the tracking annulus.
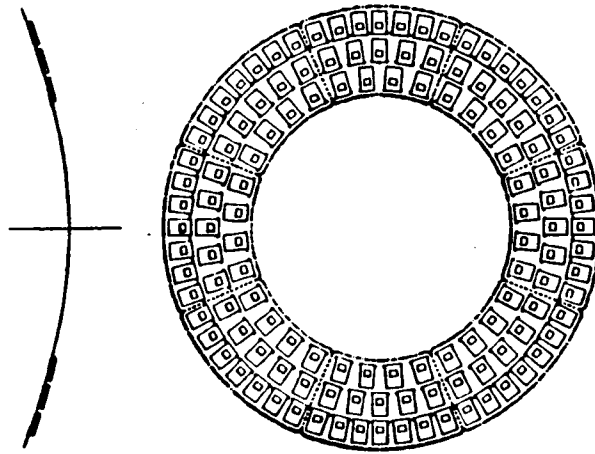
ARRANGEMENT OF AREA ARRAYS ON IMAGE SURFACE
Figure 6.1-9

Utilizing 128 arrays, the requirement will be met even at a bandwidth of 40 Hertz (integration time = 25 milliseconds).

6.1.4 Detector Processing

These arrays would be used in the frame transfer mode which provides an active area of 320 x 256 pixels. Shown in Figure 6.1-10 is a concept in which the outer annulus (289 square arcminutes) is divided into 8 sectors. Each sector contains 16 arrays. The sectors would be processed in parallel.
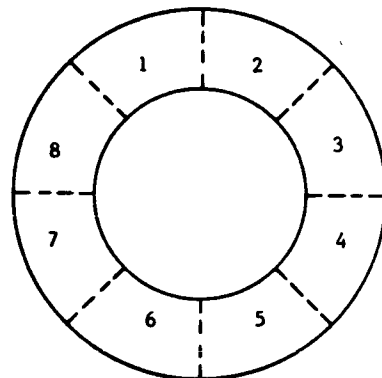
DETECTOR PROCESSING
ARCHITECTURE
Figure 6.1-10

However, the arrays in a given sector would be serially processed. The parallel sector processing allows minimization of the star acquisition time to acquire a guide star or guide stars. Once the guide star was selected the specific array of the sector would be processed with the data being sent to the guidance computer and the ground station. This configuration allows the processing of one star per sector or a maximum of eight stars simultaneously for the total fine guidance sensor. Shown in Figure 6.1-11 is a concept for processing the 16 arrays in a sector. Each array would be driven by a clock and frequency logic. This provides the proper frequency and phase to drive an array. The clock would be switched to one of the sixteen arrays. Once an

EASTMAN KODAK COMPANY · 901 ELMGROVE ROAD · ROCHESTER, NEW YORK 14650 ·

array was selected, the data from the array would be channeled through a correlated double sampler (CDS) to minimize electronic noise. The output of the CDS would then be fed through a multiplexer, a sample and hold analog to digital converter, threshold logic, first in - first out memory and, into the microprocessor. The processing would be under microprocessor control for data synchronization. The microprocessor would be redundant to provide backup capability. The output of the microprocessor would be a 5 by 5 array window around the star and/or the X,Y position of the guide star. This data is transferred to the attitude control systems and the experiment control site for further processing and/or analysis. This configuration could have redundancy built into each switching point or a backup computer could be used to process one-half of a sector. In this case a computer or logic failure would only eliminate 1/16 of the sector from being active.
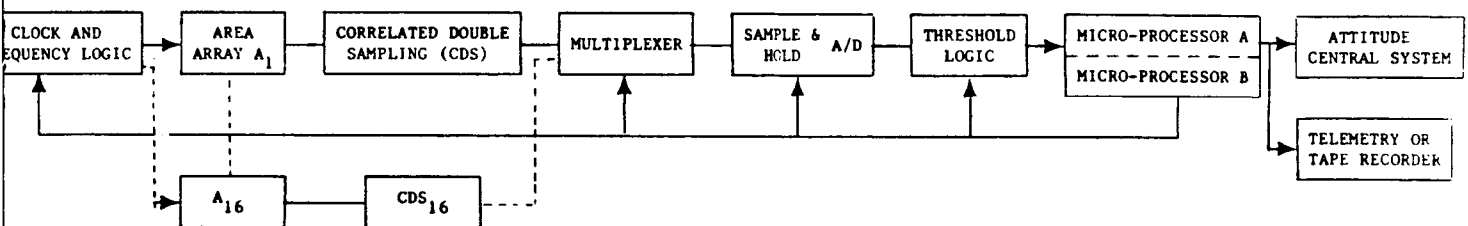
AREA ARRAY PROCESSING FLOW FOR A SECTOR
Figure 6.1-11

6.2 LINEAR ARRAY WITH OPTICAL CORRECTOR

6.2.1 Optical Subsystem

In this concept a refractive cylindrical lens is used to image the exit pupil of the OTA onto a linear array in one direction (the Y direction) so that the image matches the 2.5-millimeter height of the linear array and all the star energy to incident on the array. The image is essentially stationary on this array in the Y direction. The lens has no optical power in the orthogonal direction (the X direction) so the image will be able to move on the array. The array is placed so the astigmatic line has minimum width in the X direction (approximately 50 micrometers). This matches the array pixel width of 25 micrometers (2 pixels per spot). The total concept employs multiple units

where each unit comprises a beam splitter and two orthogonal channels. One of these channels is shown in Figure 6.2-1. In the first channel, displacement is measured along the X direction. In the second channel, displacement is measured along the Y direction since its array is placed on the focal plane corresponding to the other astigmatic focus.
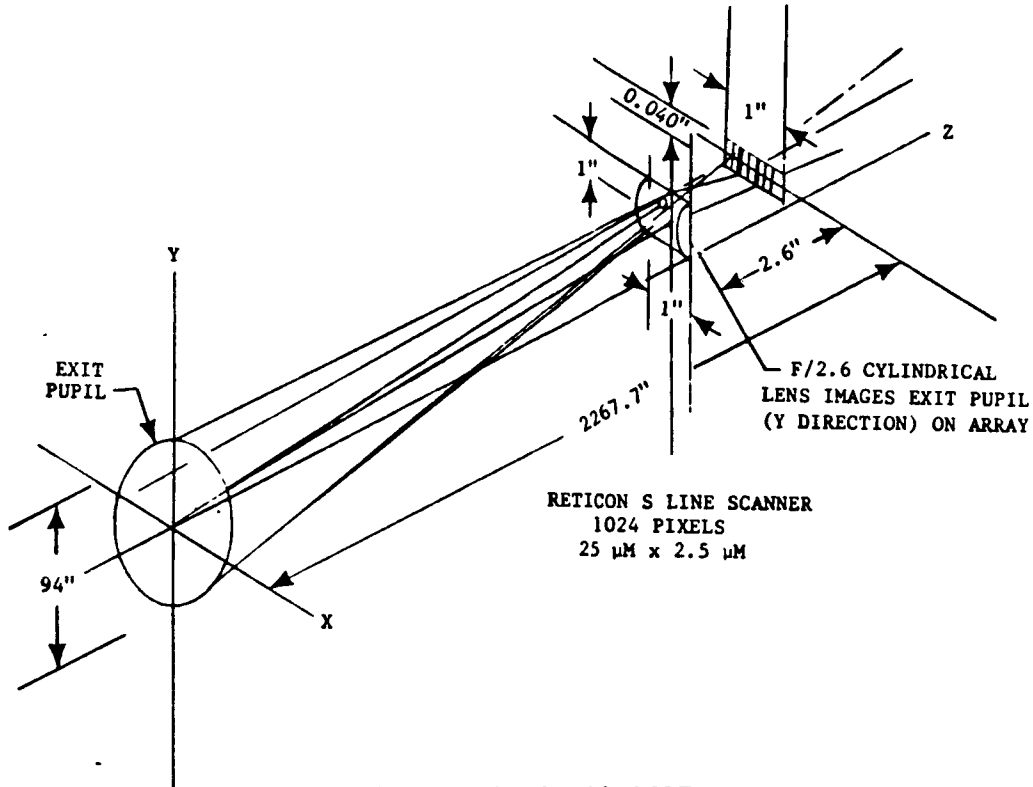
LINEAR ARRAY CONCEPT

Figure 6.2-1

The cylindrical lens forms an image of the OTA exit pupil onto the array but only in the Y direction. (Figure 6.2-2). There is theoretically no optical power in the X direction. Therefore, as the guide star moves in the field in the Y direction there is no motion. The size of the image in the Y direction is made equal to the small dimension of the array. A spectroscopic array
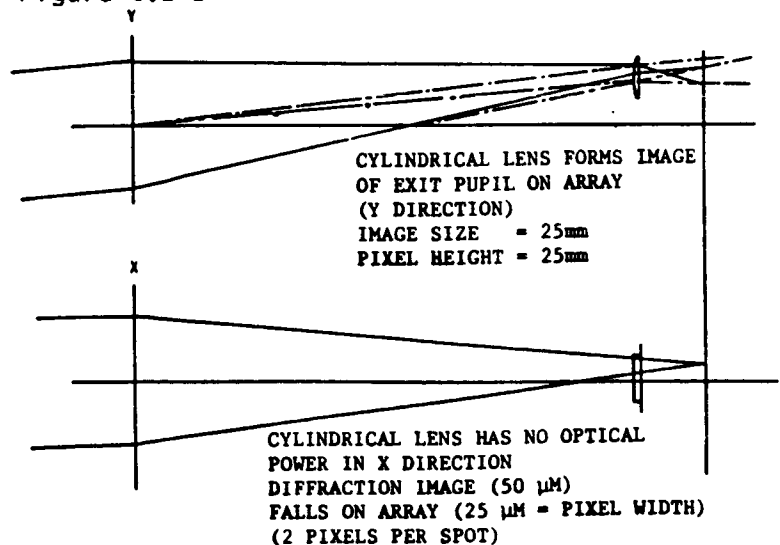
LINEAR ARRAY CONCEPT

Figure 6.2-2

was chosen due to its long length in one dimension. The array is placed at the astigmatic focus so the line width is essentially diffraction limited in the X direction. In this way, most of the star flux is incident on the array. The lens size is set to be the same as the array long dimension. This requires the focal ratio of the cylindrical lens to be f/2.6, a reasonable f-number. Another channel (not shown in the figure) has the X and Y directions reversed to sense motion in the Y direction.

6.2.2 Detector Subsystem

Potential linear arrays for star tracking applications were tabulated in Table 4.1-3. The EG&G RETICON S-SERIES linear photodiode array was selected for this analysis. Some key features of the S-SERIES devices are: 1) simultaneous integration on 128, 512, or 1024 photodiode sensor elements with 25-micrometer center-to-center spacing; 2) each sensor element has a 100:1 aspect ratio (25 micrometers x 25 micrometers); 3) integration times as short as 64 microseconds or as long as 0.3 second are possible at room temperature. Integration times of minutes or even hours can be achieved by cooling; 4) low power dissipation (less than 1 milliwatt to facilitate cooling); 5) low output capacitance for low noise.

6.2.3 Performance Prediction

A linear array module is shown in Figure 6.2-3. A module consists of two orthogonal linear arrays, two orthogonal cylindrical lenses, a beam splitter, and a fold mirror. The two arrays are mounted to a common cooled base. The distances of the arrays from the beam splitter are different since one array is placed on the sagittal surface and the second array is placed on the tangential surface.
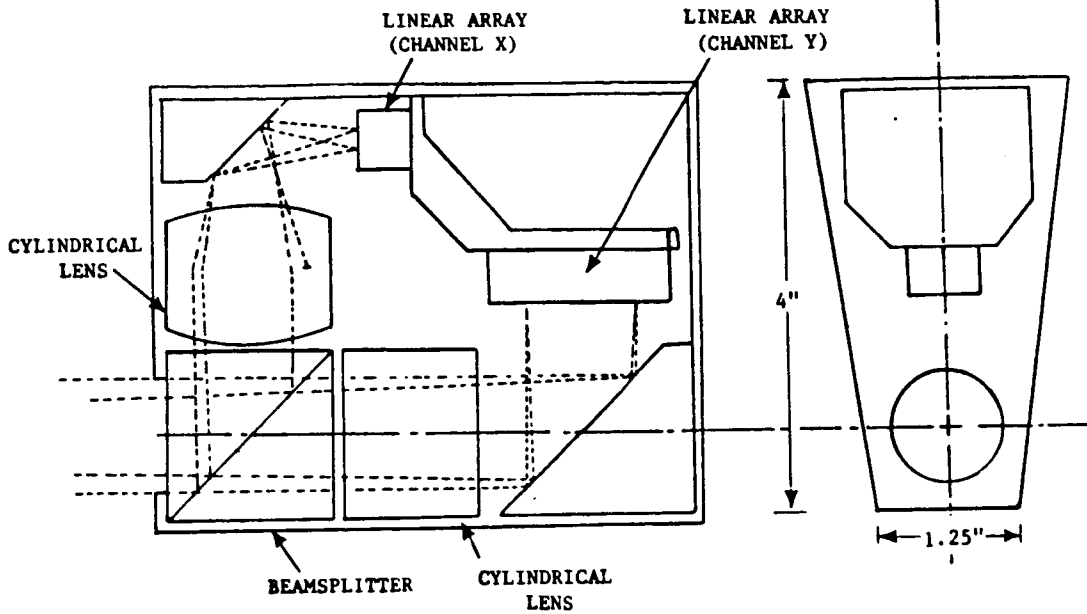
LINEAR ARRAY MODULE

Figure 6.2-3

To meet a line of sight error requirement of 0.005 arcsecond in object space requires subimage resolution of the line width to 1 part in 40.

The threshold visual magnitude requirement to meet the line of sight error requirement for the RETICON "S" spectroscopic linear array is shown in Figures 6.2-4 and 6.2-5. At a bandwidth of 40 Hertz a threshold visual magnitude of 13.8 is required to meet a line of sight error requirement of 0.005 arcsecond. At a bandwidth of 15 Hertz a threshold visual magnitude of 14.5 is required to meet a line of sight error requirement of 0.005 arcsecond.
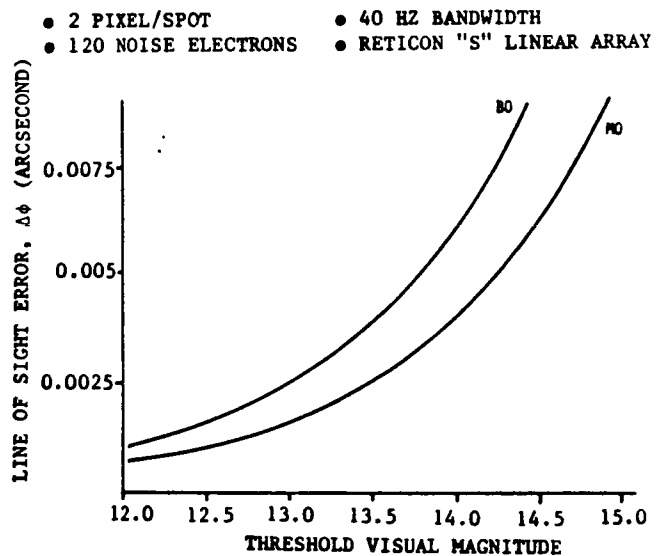
• 2 PIXEL/SPOT   • 40 HZ BANDWIDTH
• 120 NOISE ELECTRONS   • RETICON "S" LINEAR ARRAY

THRESHOLD VISUAL MAGNITUDE REQUIREMENT

Figure 6.2-4

- 2 PIXELS/SPOT
- 120 NOISE ELECTRONS
- 15 HZ BANDWIDTH
- RETICON "S" LINEAR ARRAY
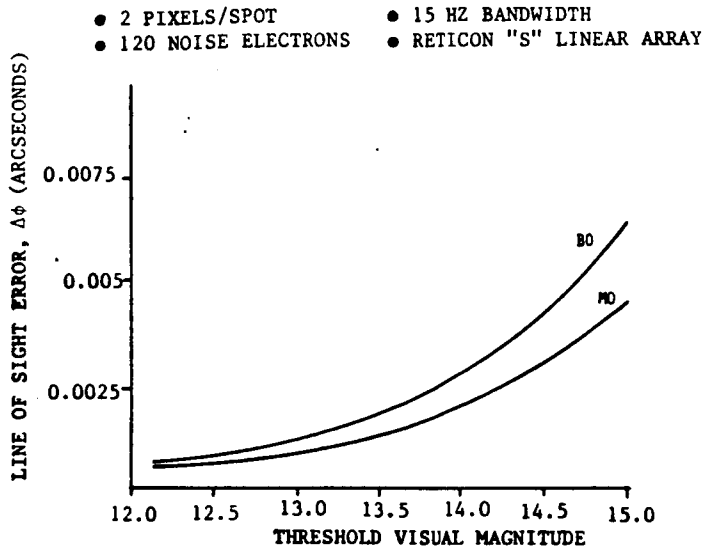
THRESHOLD VISUAL MAGNITUDE REQUIREMENT

Figure 6.2-5

The minimum guide field area required to acquire two stars with a probability of 85 percent is shown in Figure 6.2-6. For a threshold instrumental magnitude of 13.8 the required area is 70 square arcminutes. For a threshold instrumental magnitude of 14.5 the required area is 54 square arcminutes. The length of the linear array is approximately one inch. This implies that the field coverage of a module is approximately 1.8 square arcminutes in object space. Therefore 39 modules are required to fill 70 square arcminutes or 30 modules are required to fill 54 square arcminutes. Shown in Figure 6.2-7 is the required number of modules as a function of bandwidth. The number of modules can be reduced by decreasing the bandwidth (i.e., increasing the integration time). Given the current OTA annulus as a tracking area constraint, only 30 modules (60 arrays) will fit within the annulus. Shown in Figure 6.2-8 is the configuration with the active area in a single annular zone. A bandwidth of 15 Hertz (66.6 milliseconds) would be required for the arrangement. Not shown is an alternate arrangement in which the active area is increased (i.e., more modules) by "staggering" the modules in depth. This would result in multiple annular zones. However, in this latter arrangement different optical designs would be required for each annular zone.
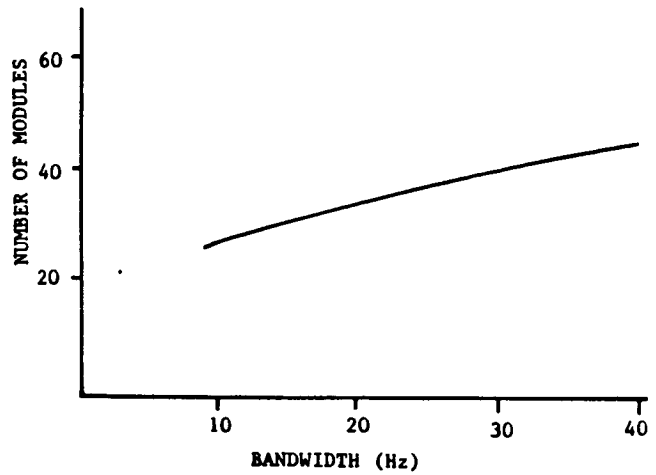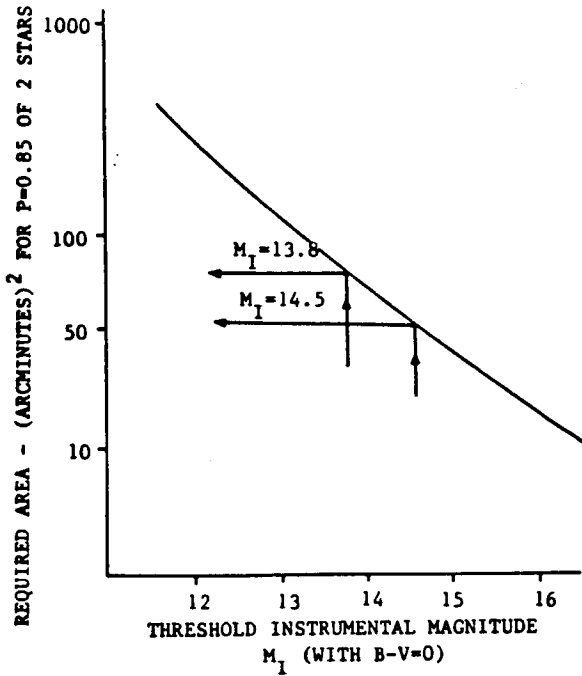
GUIDE FIELD AREA REQUIREMENT

Figure 6.2-6

NUMBER OF MODULES (RETICON "S" LINEAR
ARRAY; 120 NOISE ELECTRONS)

Figure 6.2-7
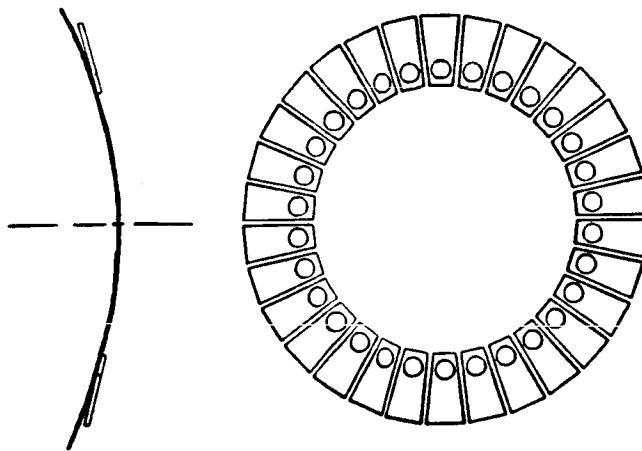
ARRANGEMENT OF LINEAR ARRAY MODULES ON IMAGE SURFACE

Figure 6.2-8

6.2.4 Detector Processing

The detector subsystem (focal plane) will require
60 arrays. The focal plane has been divided into
six sectors for processing (Figure 6.2-9). Each
sector has 10 arrays. The sectors would be pro-
cessed in parallel with each other while the
arrays in each sector would be serially processed.
The parallel processing allows the minimum star
acquisition time to acquire a guide star. Once
the guide star was selected the specific array of
each sector would be processed. This arrangement
allow the processing of one star per sector or a
maximum of 6 stars for the total focal plane.
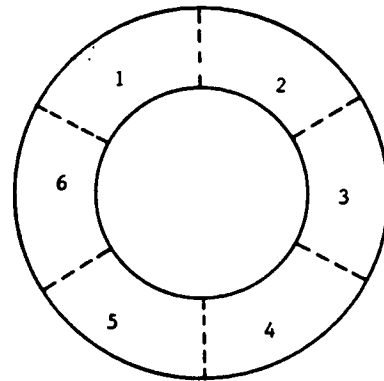
DETECTOR PROCESSING
ARCHITECTURE
Figure 6.2-9

Shown in Figure 6.2-10 is a configuration for processing ten linear arrays in
a sector.
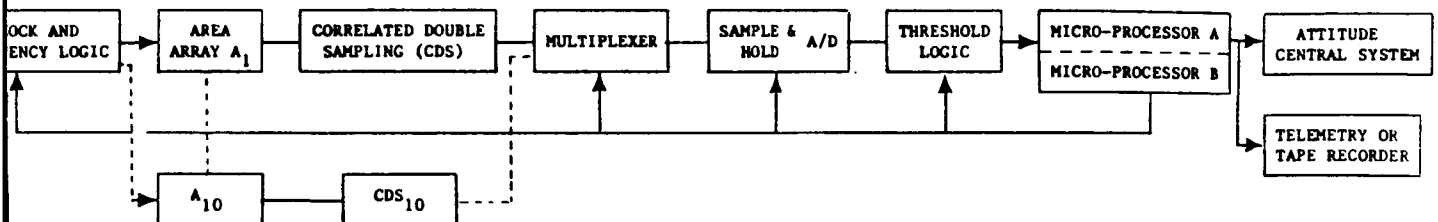
LINEAR ARRAY PROCESSING FLOW FOR A SECTOR
Figure 6.2-10

Each array is driven by a clock and frequency logic. The clock provides the
proper frequency and phase to drive an array. The clock would be switched to
one of ten arrays under computer command. After an array pair in a module is
selected the data from each array (X and Y) is channeled through a Correlated
Double Sampler (CDS) to minimize electronic noise. The output of the CDS is
fed through a multiplexer, a sample and hold/analog to digital converter,
threshold logic, and first in-first out memory.

The processing steps are under microprocessor control for data synchronization. In a hardware configuration the microprocessor would probably be redundant to provide backup capability. The output of the microprocessor is a 5 by 1 array window around the star and the X,Y position of the star. The configuration could have redundancy built into each switching point. Alternatively, the back up microprocessor could be used to process one half of each sector. In this latter case, a microprocessor or logic failure would eliminate 1/12 of the array from being active.

6.3 POINTING STABILITY

The fine guidance sensor is subject to two fundamental limits, the diffraction limit of the optical subsystem and the photon limit of the detector subsystem. This analysis, so far, has assumed degradation from the diffraction limit due to manufacturing and assembly errors in the optical subsystem and degradation from the photon limit due to noise sources (photon noise, telescope noise, electronic noise, and quantize noise). Combining these results allows for the image centroid to be determined to a fraction of the image diameter. This result yields an inherent line of sight error telescope capability (traditionally has been called the noise equivalent angle (NEA)).

The inherent line of sight error will be degraded by pointing stability errors induced by external thermal/mechanical changes. These could be due to changes in the telescope itself or the spacecraft platform. For the Space Telescope the OTA was designed so that the motion of target star images due to thermal/ mechanical effects in the OTA during observation periods will be less than 0.003 arcsecond, or approximately 33 microinches in image space in accordance with SSM/OTA IRD 3.3.4.3b. The requirement does not include any image motion due to OTA response to disturbances generated by the SSM. Control of these image motions was assumed to be a shared responsibility of the SSM and OTA contractors, and would be addressed in the interface sessions.

The OTA stability requirement, therefore, essentially defines the image motion of a target star relative to a SI aperture during an observation with the inherent NEA and its own telescope mechanical disturbances. For these conditions, there are three primary image motion error sources: (1) motion of

EASTMAN KODAK COMPANY · 901 ELMGROVE ROAD · ROCHESTER, NEW YORK 14650 ·

the target star image relative to the guide star image, (2) motion of the fine guidance sensor aperture relative to the SI mount, and (3) motion of the SI aperture relative to the SI mount. The third motion error source is internal to the SI and is thus not a direct OTA responsibility. For reference, it is limited to 0.002 arcsecond by Paragraph 3.1.2.6.2 of the SI to OTA and SSM IRD.

Therefore, the image motion error sources of concern are the motion of the target star image relative to the guide star image and the motion of the fine guidance sensor aperture relative to the SI mount. Table 6.3-1 shows an allocation of OTA pointing stability contributors. The image surface is influenced only by uncorrected focus drafts during the observational period. For the maximum focus change permitted by the focus budget (see Section 2.1.3), the spacing between an axial target star and a guide star at the edge of the guidance field changes by about 0.08 micrometer or approximately 0.0003 arcsecond in object space.

Table 6.3-1

OTA POINTING STABILITY BUDGET

| ERROR CLASS | CONTRIBUTOR | ALLOCATED ERROR* | |
		IMAGE DISPLACEMENT (MICROMETERS)	POINTING ERROR (ARCSECONDS)
MOTION OF THE TARGET STAR IMAGE RELATIVE TO THE GUIDE STAR IMAGE	FOCUS SHIFT	0.08	0.0003
MOTION OF THE FGS APERTURE RELATIVE TO THE SI MOUNT	INHERENT NEA FGS OPTICS FGS DETECTOR FGS FOCAL PLANE STRUCTURE	1.3 0.5 0.5 0.5 RSS 1.6	0.005 0.002 0.002 0.002 0.006

*Assumes SI aperture at optical axis and guide star at outside edge of FGS field

The fine guidance sensor aperture position can move relative to the SI mount if the FGS optics move; if the detector in the FGS moves relative to the FGS mounts; or if the structure between the FGS and SI mounts changes. The table shows requirements for these errors during a ten hour observation. The budget goal is to degrade the inherent NEA as little as possible by outside pointing stability error contributors. (NEA = 0.005 arcsecond $\Rightarrow \Delta\phi$ = 0.006 arcsecond.) It is apparent from the table that if moving parts (such as the plano mirrors

used in Concept VI) are used it will be extremely difficult to maintain these allocated errors. It is for this reason that concepts with no moving parts were selected in this study. Even in the case with no moving parts a high degree of dimensional stability, both short term over the observational period and long term to minimize recalibration, will be required. Dimensional stability forces the major requirement in the definition of an optical metering structure. (i.e., Is the structure just a supporting device or does it retain the optical elements in alignment to "extremely tight" tolerances?). Shown in Table 6.3-2 are the CTE's for several potential metering structure materials. Kodak with Universal Cyclops has developed a special super Invar for use with Corning's ULE™ glass. However, Invar is heavy. Based on today's technology graphite/epoxy is the preferred material for a metering structure. Metal matrix (graphite/aluminum and graphite/magnesium) and glass matrix composites show great promise but have not yet reached maturity. Shown in Figure 6.3-1 is the CTE for two Corning glasses. ULE™, for use at ambient temperatures, has a CTE of 0.0. Fused silica for use at cold temperatures has a CTE of 0.0.

Table 6.3-2

INSTANTANEOUS COEFFICIENT OF THERMAL EXPANSION FOR SEVERAL POTENTIAL METERING STRUCTURE MATERIALS

METALS	CTE (IN./IN. $\times 10^{-6}$/°F)
ALUMINUM	12.600
BERYLLIUM	6.400
MAGNESIUM	12.000
TITANIUM	4.900
STAINLESS STEEL	5.800
INVAR	0.200
COMPOSITES	
GRAPHITE/EPOXY	0.100
GRAPHITE/ALUMINUM	0.8

Corning also has developed frit bonding technology for use with Kodak designed ultra lightweight mirrors. This technology permits bonding of glass to glass. Frit's for both ULE™ and fused silica have been developed. Using this technology a glass metering structure could be developed for use with either of the concepts analyzed in this study. The dimensional instability of the contributors to motion of the FGS aperture relative to the SI mount would thereby be minimized.
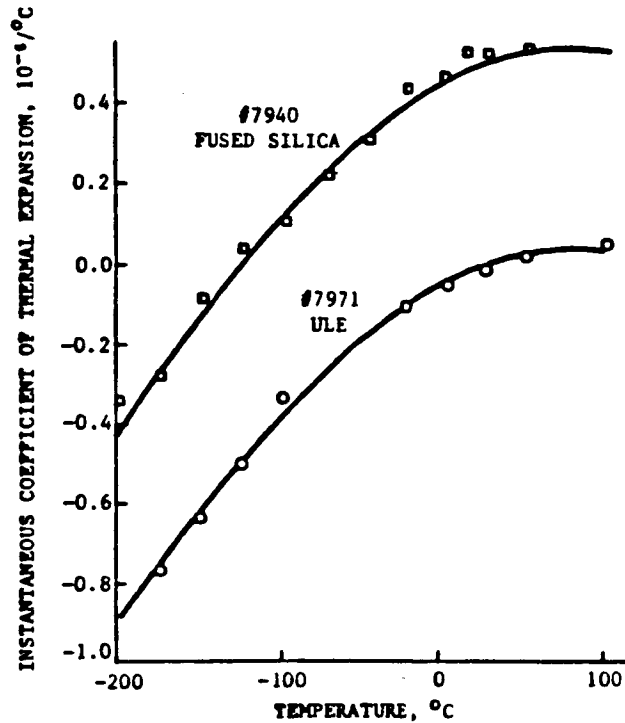
CTE OF GLASS
Figure 6.3-1

6.4 POINTING ACCURACY

For the Space Telescope on-orbit knowledge of the relative location of SI
apertures with respect to FGS guide stars must be known to ±0.01 arcsecond.
To maintain a pointing error of less than 0.010 arcsecond from the telescope
LOS, the change in the telescope focal length must be less than or known to 12
parts per million (690 micrometers) for a field point 14 arcminutes off-axis
(see Section 3.1).

A change in spacing between the primary mirror and the secondary mirror will
be used to control focus. Each time this operation is performed the system
focal length will change. This results in a plate scale factor change. To
account for this error a focal surface calibration is required.

This calibration procedure is expected to be an infrequent operation. An
initial focal surface calibration would be performed during telescope intial-
ization in orbit. The calibration would be repeated infrequently or if re-

quired, whenever an FGS or SI is replaced. A candidate focal plane calibration procedure has been devised consisting of the following two steps. First, the relative position of pixel centers on one array would be calibrated with respect to pixel centers on two other arrays. Second, the relative location of each SI aperture with respect to any pixel center would be defined.

The sequence of events required to accomplish step one is as follows:

a. From ground calibration data positions of each pixel center with respect to each FGS reference point has been calibration to ±0.001 arcsecond.

b. With two arrays operating in the fine guidance mode, the third array would perform relative astrometry on a selected, stable, multistar field. The third array would then be switched to the fine guidance mode and one of the first two arrays commanded to perform relative astrometry. This is repeated until all three arrays have performed relative astrometry.

c. The telescope performs a roll maneuver such that some of the stars on each array are displaced toward an array approximately 120 degrees away. Note that some of the stars previously measured will be retained within the same field of view, although at different locations.

d. Items b and c will be repeated until stars originally located on one array appear on the second array.

e. Ground analysis will compute the relative location of each array and its associated pixel centers in the image surface.

Step two would be accomplished as follows: two stars having a large linear separation are positioned on an array and relative astrometry is performed to established their separation. The telescope then maneuvers one star to a selected SI aperture location while retaining the second star on the array, probably at a different pixel center. Telescope maneuvers are performed to interchange the two star positions. The position of the star on the array is measured and the SI indicates when the translated star is in its aperture. The relative location of the telescope aperture relative to any FGS pixel center can not be calculated. Figure 6.4-1 presents a conceptual diagram of the major operations involved in step two.

ρ, θ STAR INITIAL
      COORDINATES

ρ′, θ′ STAR COORDINATE
        ON ARRAY WHEN
        COMPANION STAR IS
        LOCATED IN SI
        APERTURE
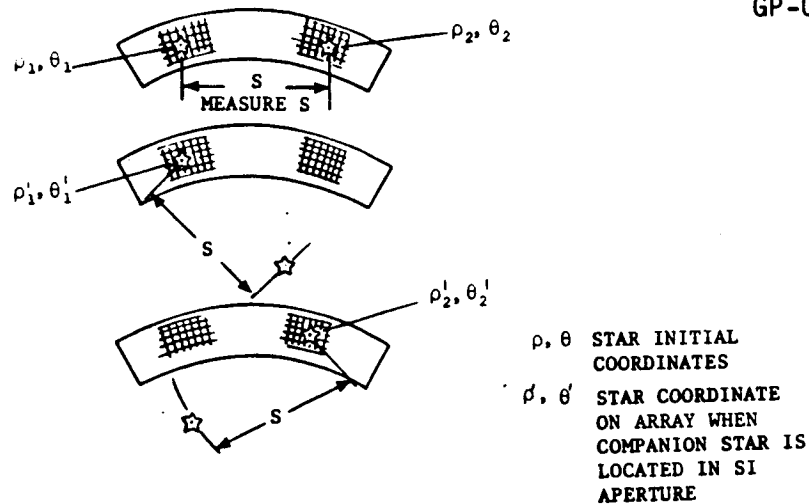
a. CONSTRUCT SPHERICAL
    TRIANGLE
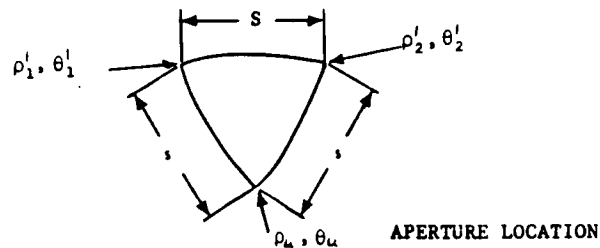
APERTURE LOCATION

b. WITH THREE SIDES KNOWN THE COSINE FORMULA OF SPHERICAL
    TRIGONOMETRY CAN BE USED TO DEFINE THE POSITION OF THE
    APERTURE RELATIVE TO THE PIXEL CENTERS.

SI APERTURE LOCATION PROCEDURE

Figure 6.4-1

6.5 SCIENCE (ASTROMETRY)

The basic astrometry requirement is to measure the relative positions of two
or more stellar object to an accuracy of ±0.002 arcsecond. This imposes a
tighter pointing accuracy requirement than on fine guidance sensing (i.e.,
±0.01 arcsecond). The minimum visual magnitude has been set at 17 in compari-
son to 14.5 for fine guidance sensing.

In the current ST concept two of the fine guidance sensors are required for ST
guidance, so only one is left free to make astrometric measurements. In the
concepts analyzed in this study, solid state sensors fill an outer annulus.
Therefore, for example, in FGS Concept No. 1 there is really only one fine
guidance sensor consisting of 21 million pixels (128 arrays with 512 x 320

pixels per array). Once the two stars required for fine guidance are "locked in" the remaining pixels are left free to make astrometric measurements.

Astrometry could be performed simultaneously with any scientific instrument operation (serendipity mode). Since these concepts utilize only electronic interrogation with no moving parts there would be no possibility of compromising the scientific instrument observation. Therefore as a by-product these concepts would have great potential for use in the science of Astrometry.

To maintain a pointing error of less than 0.002 arcsecond from the telescope LOS, the change in the telescope focal length must be less than, or know to, 95 micrometers for a field point 14 micrometers off-axis (see Section 3.1). In order to perform relative astrometry a periodic recalibration of the focal plane is required. The current ST astrometric calibration approach is as follows: First, a calibration field (for which groundbased observations are available) will be measured with the FGS for zero-order plate scale and field distortion effects. Because no field is known which contain relative star positions accurate to 0.002 arcsecond over 18 arcminutes, overlapping plate techniques will be used to determine the field distortions to within a scale factor. Then a moving target, such as an asteroid, will be used to determine the scale to within the measuring accuracy of the FGS. Finally, a sample of multiple and suspected single stars will be scanned with the FGS to determine transfer functions and brightness distributions. An approach to focal plane calibration for the concepts analyzed in this study is described in Section 6.4.

The threshold visual magnitude requirements for Concepts No. 1 and No. 2 are shown in Figures 6.5-1 and 6.5-2. As can be seen from these figures at a bandwidth of 40 hertz the threshold visual magnitude and the line of sight error requirements are not compatible. What are the options available to meet these requirements? The guide field area was set for the fine guidance sensing mode, therefore the only option is the increase integration time.

Shown in Table 6.5-1 is a comparison of Concepts No. 1 and No. 2 in the astrometry mode. Either concept will theoretically meet the astrometry requirements.
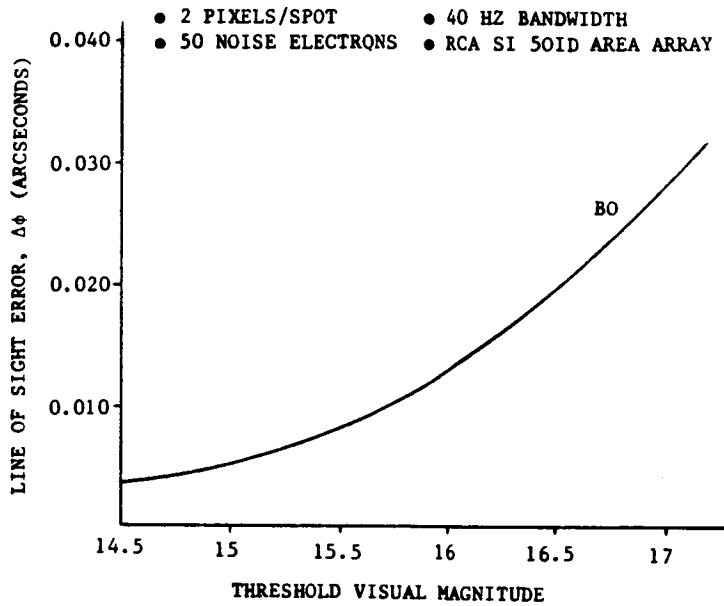
- 2 PIXELS/SPOT
- 50 NOISE ELECTRONS
- 40 HZ BANDWIDTH
- RCA SI 50ID AREA ARRAY

THRESHOLD VISUAL MAGNITUDE REQUIREMENT

Figure 6.5-1

- 2 PIXELS/SPOT
- 120 NOISE ELECTRONS
- 40 HZ BANDWIDTH
- RETICON "S" LINEAR ARRAY
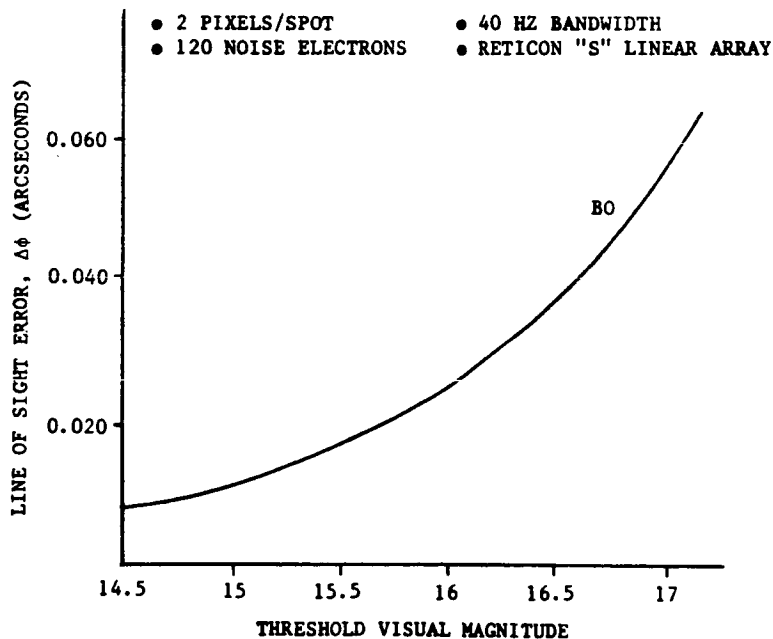
THRESHOLD VISUAL MAGNITUDE REQUIREMENT

Figure 6.5-2

Table 6.5-1 CONCEPT COMPARISON (ASTROMETRY MODE)	CONCEPT NO. 1 AREA ARRAYS WITH OPTICAL CORRECTORS	CONCEPT NO. 2 LINEAR ARRAYS WITH OPTICAL CORRECTOR
SYSTEM REQUIREMENTS		
• POINTING ACCURACY $\leq$0.002 ARCSECOND	0.002	0.002
• THRESHOLD VISUAL MAGNITUDE $\leq$17.0	17.0	17.0
• INTEGRATION TIME $\leq$10 MINUTES	<1 MINUTE	<1 MINUTE

7.0 CONCLUSIONS AND RECOMMENDATIONS

Solid State Sensors (CCD's' CID's; PDA's) have become increasingly attractive for astronomical imaging. This is due to low readout noise, high quantum efficiency, high dynamic range, linearity, and stability. The predominance of red stars near the galactic pole (poorest star density region) when combined with a solid state sensor leads to more available stars for a given threshold magnitude than with either the eye or a photomultiplier tube as a detector. Technical improvements and availablility (yield) make solid state sensors ready for serious consideration in a 1980's fine guidance sensor.

In the optimum fine guidance sensor, the detectors would be installed directly onto the focal surface presented by the optics. This would maximize through-put and minimize pointing stability error by not incorporating any additional optical elements. However, in a highly astigmatic optical system such as the OTA this forces the image centroiding requirement (as small as 1/166) to be well past the state-of-the-art (considered to be approximately 1/50).

To meet the above goal two concepts requiring additional optical elements (--however, no moving parts) were analyzed. Both concepts utilize solid state sensing technology. Implementation of these concepts are summarized in Tables 7.0-1 and 7.0-2. Concept No. 1 will meet the study requirements. Concept No. 2 requires a shorter bandwidth (longer integration time) than currently required. This is considered a minor difference. Further analysis is needed to select one concept over the other.

The following tasks are suggested for future work:

● Develop final lens designs for FGS Concepts No. 1 and No. 2.

● Revise image centroiding algorithms----in this study a Gaussian PSF was assumed.

● Reevaluate FGS Concepts No. 1 and No. 2 using different detectors.

- Use test data from selected detectors to predict NEA for real system conditions (cooling, array calibration, scan speed, etc.)

- Investigate FGS Concepts No. 1 and No. 2 for ST retrofit compatibility.

- Develop metering structure approaches for Concepts No. 1 and No. 2.

- Develop a hardware concept(s) which could be tested in the ST-FGS test facility. Build proof-of-concept prototype.

Table 7.0-1

UPRATED FINE GUIDANCE SENSOR CONCEPT NO. 1

- FEATURES

    - ZERO POWER REFRACTIVE CORRECTORS
    - 128 RCA SID 501D CCD AREA ARRAYS
    - GUIDE FIELD AREA = 33.3 $\widehat{\text{MIN}}^2$
    - IMAGE CENTROIDING = 1/43

MISSION REQUIREMENT	CONCEPT NO. 1
• NOISE EQUIVALENT ANGLE ≤0.005 $\widehat{\text{SEC}}$	0.005 $\widehat{\text{SEC}}$

SYSTEM REQUIREMENTS	
• THRESHOLD VISUAL MAGNITUDE ≤14.5	15.0
• BANDWIDTH = 40 HZ (INTEGRATION TIME = 25 MILLISECONDS)	40 HZ

GOALS	
• NO MOVING PARTS	NONE
• HIGH THROUGHPUT EFFICIENCY	YES
• MODULARITY	YES

Table 7.0-2

UPRATED FINE GUIDANCE SENSOR CONCEPT NO. 2

- FEATURES

  - TWO CHANNEL CYLINDRICAL REFRACTIVE CORRECTORS
  - 30 DETECTOR MODULES
  - 60 RETICON "S" SERIES LINEAR ARRAYS
  - GUIDE FIELD AREA = 54 MIN^2
  - IMAGE CENTROIDING = 1/40

MISSION REQUIREMENT	CONCEPT NO. 2
• NOISE EQUIVALENT ANGLE ≤ 0.005 SEC	0.005 SEC

SYSTEM REQUIREMENTS

• THRESHOLD VISUAL MAGNITUDE ≤ 14.5	14.5
• BANDWIDTH = 40 HZ (INTEGRATION TIME = 25 MILLISECONDS)	15 HZ

GOALS

• NO MOVING PARTS	NONE
• HIGH THROUGHPUT EFFICIENCY	YES
• MODULARITY	YES